TAMU-T-71-005 C.3

Sea Grant Depository

INTERACTION OF A TRAIN OF REGULAR WAVES WITH A RIGID SUBMERGED ELLIPSOID

Prepared by

V. SEETHARAMA RAO and C. J. GARRISON

Coastal and Ocean Engineering Division

Texas A&M University

MAY 1971

TAMU-SG-71-209

C. O. E. Report No. 142

TEXAS A&M UNIVERSITY SEA GRANT PROGRAM

CIRCULATING COPY
Sea Grant Depository

INTERACTION OF A TRAIN OF REGULAR WAVES WITH A RIGID SUBMERGED ELLIPSOID

by

V. Seetharama Rao and C. J. Garrison
Coastal and Ocean Engineering Division
Texas A&M University

Partially supported by the National Science Foundation
Sea Grant Program
Institutional Grant GH-59 to
Texas A&M University

Sea Grant Publication No. TAMU-SG-71-209
Coastal and Ocean Engineering Division
Report No. 142 - C.O.E.

May 1971

PREFACE

This report was primarily written by V. Seetharama Rao and represents the work done by him for a Ph.D. dissertation at Texas A&M University under the direction of Dr. C. J. Garrison.

With the increasing interest in construction offshore of large structures such as oil storage tanks, there is an urgent need for information about wave forces, moments, etc. on such structures. It is hoped that this report will serve as a beginning in our understanding of the basic problem of interaction of surface gravity waves with large submerged objects.

ABSTRACT

This report presents the practical and rigorous solution of the potential flow problem associated with the interaction of a train of regular surface gravity waves with a fixed rigid submerged half spheroid resting on the bottom.

The linearized boundary-value problem is first formulated for a fixed semiellipsoid. The radiation problem of a rigid semiellipsoid oscillating in its various degrees of freedom, one degree at a time, in otherwise still water is also formulated simultaneously, so as to use its results to check the results of the first problem by Haskind's relations. In each case the solution is obtained by the Green's function approach. In this method the velocity potential is obtained by distributing "unit wave sources" over the surface of the object. The Green's function which represents the velocity potential for a unit wave source is chosen such that it satisfies all the conditions of the problem except the normal boundary condition on the surface of the object. When this condition is applied, the result is a Fredholm integral equation of the second kind which must be solved for the distribution function. In the numerical procedure the integral equation is replaced by a matrix equation which is solved on a digital computer. The numerical procedure is outlined in detail for the semiellipsoid and finally, numerical results are obtained for a half spheroid.

The numerical results obtained include amplitudes and phase shifts of the dynamic pressures, horizontal and vertical force and moment coefficients and the phase shifts of the forces and moment. The results are complete in the sense that they include all the data necessary for practical engineering design. Several checks are made on the numerical results. These include the Haskind's relations check, an energy check for the radiation problem, and comparisons with an asymptotic solution and experimental results for a hemisphere. All these checks and comparisons are successful and it appears that the numerical method employed yields valid and accurate results.

ACKNOWLEDGMENTS

Appreciation is extended to the members of Seetharama Rao's doctoral committee, Professor R. O. Reid, Dr. D. R. Basco, Dr. W. P. Jones, Dr. W. D. Nowlin, Jr., and Dr. R. M. Sorensen for their suggestions.

The major portion of the computer time was made available by the Department of Civil Engineering.

Most of the numerical results for oblate spheroids were obtained on the computer of the Pittsburgh - Des Moines Steel Company, Pittsburgh, to whom the authors are grateful.

Partial financial support of the National Science Foundation Sea Grant Program Institutional Grant GH-59 made to Texas A&M University is acknowledged.

TABLE OF CONTENTS

LIST OF TABLES

LIST OF FIGURES

LIST OF SYMBOLS

$\bar{a}$	characteristic length of object of arbitrary shape
$\bar{a},\bar{b},\bar{c}$	semi-axes of ellipsoid in $\bar{x}$, $\bar{y}$ and $\bar{z}$ directions
a	relative size parameter, $a = 2\pi\bar{a}/\bar{L}$, dimensionless
b,c	semi-axes of ellipsoid, dimensionless
$d\bar{S}$	elementary dimensional surface area
f_j,f	distribution function, dimensionless
f_x	horizontal force coefficient, dimensionless
f_y	vertical force coefficient, dimensionless
f'_i	wave force or moment coefficient for a force or moment in the i-th direction, dimensionless
g	acceleration due to gravity
$\bar{h}$	depth of water
h	relative depth of water, dimensionless
$\bar{h}_j$	functions connected with the normal boundary condition on S, defined by (2.15)
h_j	functions defined by (2.26), dimensionless
k	wave number, $k = 2\pi/\bar{L}$
$m_{z'}$	moment coefficient, dimensionless
$\bar{n}$	normal coordinate directed into the fluid
$\hat{n}$	unit normal vector directed into the fluid
n'	normal coordinate directed away from the fluid, dimensionless
$\hat{n}'$	unit normal vector directed away from the fluid
n_x,n_y,n_z	components of the unit normal vector $\hat{n}$
p	pressure amplitude coefficient, dimensionless

$\bar{r}$	plane polar coordinate
r	plane polar coordinate, dimensionless
$\vec{\bar{r}}$	position vector of a point on surface S from O'
r_1	horizontal distance between points (x,y,z) and (ξ,η,ζ), dimensionless
s	size of the grid element, $s = \pi/2N$
t	time
u_j, u	velocity potentials for radiation and scatter problems, dimensionless
u_0	velocity potential for incident wave, dimensionless
$\bar{x},\bar{y},\bar{z}$	rectangular Cartesian coordinates with origin at O
x,y,z	coordinates, dimensionless
$\bar{x}',\bar{y}',\bar{z}'$	rectangular Cartesian coordinates with origin at O'
x',y',z'	coordinates, dimensionless
C_d	drag coefficient
C_m	added mass coefficient
C_p, D_q	Simpson's numerical coefficients
E_i	energy transmitted over one period
$\vec{\bar{F}}_j$	dynamic force (vector) due to the j-th mode of oscillation
$\bar{F}_i'$	dynamic force or moment component in the i-th direction on the fixed object
F_i'	dimensionless force or moment component in the i-th direction on the fixed object
F_{ij}	the i-th component of the dynamic force or moment due to the j-th mode of oscillation
G	Green's function

$\vec{G}_j$	dynamic moment (vector) due to the j-th mode of oscillation
H	height of the incident wave
H_j, H	functions connected with the normal boundary condition on S, dimensionless
J_0, J_1	Bessel functions of the first kind of order zero and one, respectively
$\bar{L}$	wavelength
$\bar{M}_{ij}$	added mass (or added moment of inertia) coefficient
M_{ij}	added mass (or added moment of inertia) coefficient, dimensionless
$\bar{N}_{ij}$	damping coefficient
N_{ij}	damping coefficient, dimensionless
N	grid size parameter
R	distance between points (x,y,z) and (ξ,η,ζ), dimensionless
R'	distance defined by (3.21), dimensionless
S	function describing the surface of the object
T	period
T	a function
V_0	velocity potential for incident wave
V_j	velocity potentials for radiation problem or scatter problem
$\forall$	displaced volume of object
$\bar{X}_j$	linear displacement of the object
$\bar{X}_j^o$	amplitude of linear displacement
X_j^o	amplitude of linear or angular displacement, dimensionless

α, ϕ ellipsoidal polar coordinates

β, ψ ellipsoidal polar coordinates

δ Dirac delta function

δ_i phase shift of the force or moment on the fixed object in the i-th direction

δ_m phase shift of the moment on the fixed ellipsoid

δ_p phase shift of pressure on the fixed object

δ_x phase shift of the horizontal force (in the x-direction) on the fixed ellipsoid

δ_y phase shift of the vertical force on the fixed ellipsoid

$\delta_{k\ell}$ Kronecker delta

ξ, η, ζ rectangular Cartesian coordinates

$\bar{\eta}_j$ elevation of the surface disturbance due to oscillations of the body or scatter

$\bar{\eta}^o_j$ amplitude of surface disturbance due to oscillation of body or scatter

$\bar{\eta}_w$ free surface elevation of the incident wave, above mean water level

$\bar{\eta}^o$ amplitude of incident wave

η^o amplitude of incident wave, dimensionless

θ plane polar coordinate

θ_j angular displacement of oscillating object

θ^o_j amplitude of angular displacement

κ dummy variable

$\nu = \sigma^2 \bar{a}/g = a \tanh ah$

ρ mass density of fluid

$\rho_1 = (\xi^2+\zeta^2)^{1/2}$

σ angular frequency, $\sigma = 2\pi/T$

τ polar coordinate in (β,ψ)-plane

$\bar{\Pi}_j$ dynamic pressure due to j-th mode of oscillation

Π_j dynamic pressure due to j-th mode of oscillation, dimensionless

$\bar{\Pi}'$ dynamic pressure on the fixed object

Π' dynamic pressure on the fixed object, dimensionless

Φ_0 velocity potential for incident wave

Φ_j velocity potential for oscillation of object or scatter

Φ' total velocity potential for diffraction problem

Subscripts:

i,j used to denote either the mode of oscillation (or scatter) or the direction of a force or moment component, depending on the context

k,ℓ correspond to the nodal points (α,ϕ) and (β,ψ), respectively

1. INTRODUCTION

Recent years have witnessed the emergence of two significant trends which may well mark an important turn in human history. On one hand, the population of the earth has expanded beyond all previous estimates placing ever increasing demands on the natural resources available to man. Yet, on the other hand, since the resources available on land are limited, they continue to dwindle. Therefore, it is but natural that caught between these opposing trends man should turn to the oceans (especially their coastal waters) for a solution to his dilemma. The exploitation of the natural resources of the coastal waters requires, among other things, the design and construction of large scale structures offshore. This in turn necessitates a better understanding of the interaction of surface gravity waves with structures such as large submerged oil storage tanks. It is the aim of this dissertation to contribute towards such an understanding by taking a basic approach to the problem of wave interaction with submerged objects. More specifically, the problem of interaction of a train of plane regular waves with a rigid fixed submerged semiellipsoid will be studied by potential flow theory and numerical results obtained for a half spheroid. Although the

shape considered is somewhat idealized, it is representative of practical shapes and the results provide some insight and understanding into the fundamental problem.

Before going into the details of the particular problem of this dissertation, we shall first consider briefly the various aspects of the general problem of wave forces on submerged objects. Such a review will provide a perspective on how the present problem fits into the overall picture. Next we shall review briefly the theory and the available literature on wave/structure interaction.

A Review of the General Problem of Wave Forces on Submerged Objects

Wave forces acting on such objects as piles, submerged pipelines, and small spheres have been studied extensively over the last two decades. Significant contributors include Morison, et al. (1950)*, Beckmann and Thibodeaux (1962), and Grace and Casciano (1969), to name only a few. In all these studies, the size of the object is small relative to the length of the incident wave. This condition occurs in many practical situations. It simplifies the general problem of wave/structure interaction by allowing one to assume that the object does not disturb the incident wave in any way. As far as the forces on the object are

---

*References are arranged alphabetically by author at the end of the dissertation.

concerned, one can assume that the flow field existing at the center of the object at any instant due to the incident wave extends to infinity. Further, the wave force acting on the object can be considered to be the sum of two components, drag and inertia. The drag force is proportional to the product of a drag coefficient, C_d, and the square of the fluid velocity. The inertia force is proportional to the product of an inertia coefficient, $(1 + C_m)$, where C_m is the added mass coefficient, and the local acceleration of the fluid. Normally the empirical coefficients, C_d and C_m, have to be found by practical testing. Morison, et al. (1950) first applied an expression of the above type to the wave forces on piles. Hence, it is commonly known as the "Morison equation."

As the size of the object increases relative to the length of the incident wave, two effects take place. Firstly the incident wave is scattered due to the presence of the object. Secondly, since the object is not deeply submerged, there is an effect due to the proximity of the free surface. This is the situation that occurs in the case of structures such as submerged oil storage tanks, whose dimensions may be of the order of the wave length and water depth. Both the effects mentioned are commonly known as "diffraction effects." However, it is often convenient for purposes of discussion to classify them as the relative size effect and the relative depth effect (or the free surface effect),

respectively. In view of these effects, the simplifying assumptions on which the Morison equation is based are no longer valid. Hence the Morison equation must be replaced in this range by an altogether different approach. Such a theory which accounts for the relative size of the object and the free surface effect is commonly known as "diffraction theory." In this approach separation and viscous effects are neglected and the problem is set up in terms of a velocity potential and the velocity potential which satisfies the necessary conditions is sought. Once it is found, the dynamic pressure distribution on the surface of the object is determined by Bernoulli's equation and the forces and moments are obtained from the pressure distribution by surface integration.

At this stage it is imperative to know under what conditions separation and viscous effects become negligible and diffraction theory can be expected to yield results that are practically valid. Viscous effects are accounted for in the Morison equation by the drag force term. They are mainly dependent on the ratio of the displacement of fluid particles near the object to the size of the object. For small values of the relative displacement, the flow near the object remains attached and viscous effects can be neglected. For example, for the case of a fluid starting from rest and flowing with constant acceleration past a circular cylinder, the results of Sarpkaya and Garrison (1963) have shown

that at the beginning of motion, the added mass and drag coefficients are equal to the inviscid flow values of unity and zero respectively. In the case of wave/structure interaction, if linear wave theory is assumed, then for a given wavelength and water depth, the relative displacement of fluid particles is linearly proportional to $H/2\bar{a}$, where H is the height of the incident wave and $\bar{a}$ is a characteristic length of the object. In the case of large structures, such as oil storage tanks, the parameter $H/2\bar{a}$ is usually small so that viscous effects can be neglected and potential flow theory yields valid results. This is an advantage from the theoretical point of view. On the other hand, for small objects such as piles, $H/2\bar{a}$ is generally large and viscous effects become quite significant.

In the preceding discussion on the general problem of wave/structure interaction, we have identified three dimensionless parameters as being relevant. There is first of all the relative size parameter, $\bar{a}/\bar{L}$, where $\bar{L}$ is the length of the incident wave. For convenience from the theoretical point of view, it is preferable to choose $2\pi\bar{a}/\bar{L}$ instead of $\bar{a}/\bar{L}$ to represent the relative size. This parameter is significant with respect to the region of validity of the Morison type equation. Secondly, there is the relative depth parameter, $\bar{h}/\bar{a}$, where $\bar{h}$ is the water depth. This parameter reflects the free surface effect and decides the value of C_m to be used in the Morison equation. Thus for small

relative depths, the value of C_m is greater than that for infinite depth of fluid. Finally viscous effects are represented by the relative displacement parameter, $\bar{H}/2\bar{a}$. Following Garrison, Seetharama Rao and Snider (1970), the general features of the wave/structure interaction problem can be qualitatively shown, for a given $\bar{h}/\bar{a}$, on a diagram such as figure 1. For small values of $2\pi\bar{a}/\bar{L}$ and all values of $H/2\bar{a}$, the Morison equation is valid and diffraction effects due to relative size are negligible. On the other hand for small values of $H/2\bar{a}$ and the entire range of $2\pi\bar{a}/\bar{L}$, viscous effects are negligible and diffraction theory is generally applicable. There is a region of overlap between the two approaches when both $2\pi\bar{a}/\bar{L}$ and $H/2\bar{a}$ are small. In this region, C_d in the Morison equation tends to zero and C_m approaches its potential flow value which depends on the shape of the object and the relative depth, $\bar{h}/\bar{a}$.

Having considered the broad features of the wave/structure interaction problem in general, we shall hereafter confine our remarks to the region where diffraction theory is applicable. Thus it shall be assumed in the following discussion that the height of the incident wave is small relative to the size of the object so that viscous effects can be neglected. This is true for most large structures. At this point it must be mentioned that while much work, especially of an experimental nature, has been done so far on submerged objects in the range of small values

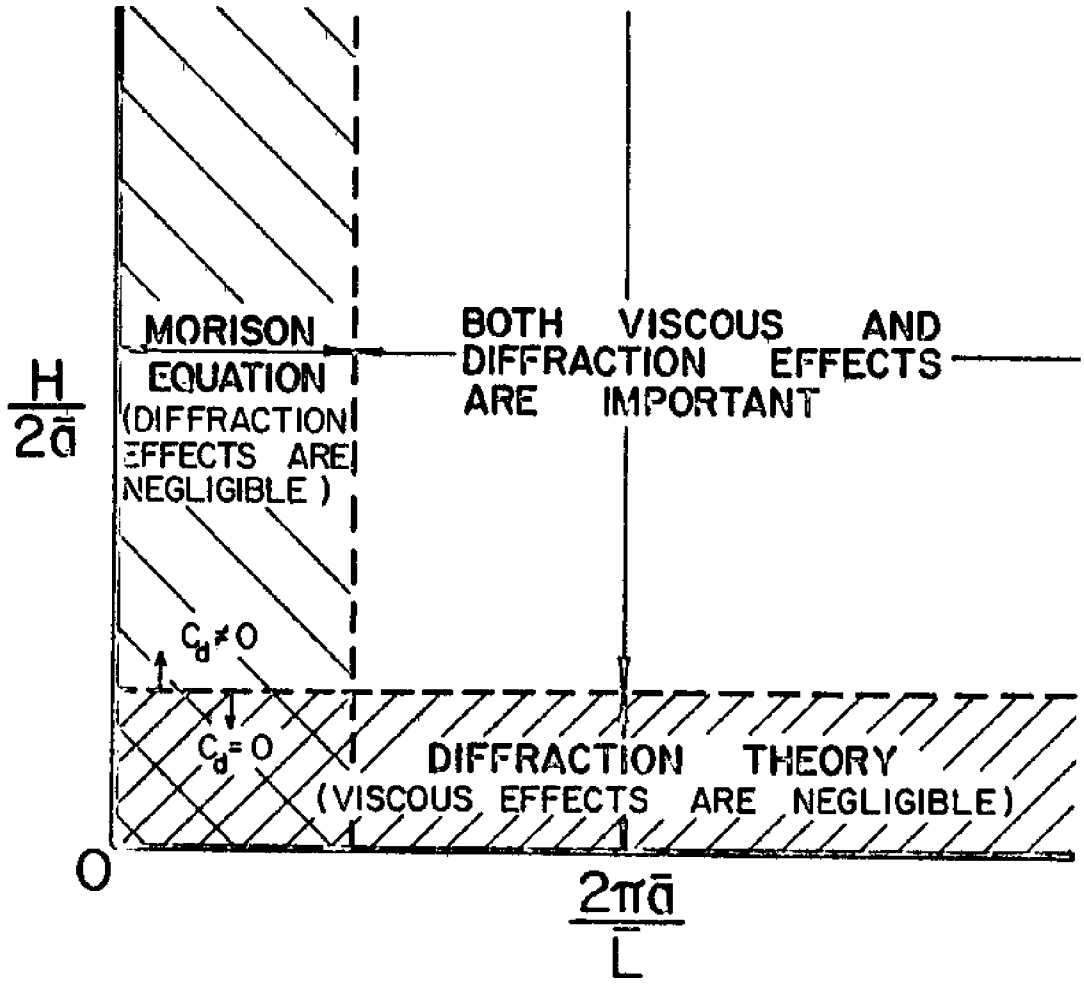

Figure 1. Regions of applicability

(after Garrison, Seetharama Rao and Snider (1970)).

of $2\pi\bar{a}/\bar{L}$, little has been accomplished in the range of higher values of the same parameter where the Morison equation becomes invalid and a diffraction theory must be employed. Part of the reason for the paucity of experimental data is that in this range testing has to be done in three-dimensional wave tanks and is both difficult and expensive. The experimental data collected, if any, appear to be proprietory and so have not appeared in the literature. This points to the need for theoretical work in this area.

A Review of the Theoretical Approach and Literature on the Problem of Wave/Structure Interaction

A review of the available literature on the application of potential flow methods to the problem of wave/structure interaction reveals that there are almost no publications devoted to the problem of wave forces on objects submerged in water of finite depth and resting on the bottom. One well-known exception is the case of vertical cylindrical piles for which MacCamy and Fuchs (1954) have developed a diffraction theory the results of which reduce to those given by the inertia term in the Morison equation, for the limiting case of $2\pi\bar{a}/\bar{L} \to 0$. On the other hand, much theoretical work has been done on the problem of objects located at the free surface in water of infinite depth, primarily because of interest in the motion of ships and breakwaters. Because the theoretical approach and many of the techniques of the latter

problem are directly applicable to the former problem, we shall review the literature available on objects located at the free surface.

There are two types of problems generally dealt with by potential flow methods. On one hand, there is the problem of a train of incident waves acting on a fixed rigid object. This is commonly known as the "diffraction problem." The main results of interest here are the forces and moments, and in the case of two-dimensional problems the reflection and transmission coefficients. The problem of this dissertation falls under this category. On the other hand, there is the problem of a rigid object executing forced harmonic oscillations of small amplitude, in otherwise still water, in its various degrees of freedom. This is commonly called the "radiation problem." The parameters of interest here are the added mass and added moment of inertia coefficients, and the damping coefficients. For the two-dimensional problem, the ratio of the wave amplitude at infinity to the amplitude of displacement of the object, known as the "wave-height ratio", is also of interest. The diffraction and radiation problems, while often studied independently, are still related as we shall see presently. Moreover, for many practical cases such as ship motions, floating breakwaters etc., the two problems have to be worked together in conjunction with the equations of motion.

Theoretical approaches. As far as the theory for the wave/structure interaction problem is concerned, there are two basic approaches. John (1949, 1950) showed that the velocity potential for the problem can be obtained by a suitable distribution of unit wave sources over the surface of the object. The potential for the unit sources, which is also called the "Green's function" for the problem, must satisfy all the conditions of the problem except the normal boundary condition on the surface of the object. When the latter condition is applied, an integral equation is obtained the solution of which specifies the manner in which the unit sources are to be distributed. In general the equations are quite complex and therefore it is difficult to obtain solutions in a closed form, so that numerical methods must be used. In an alternate approach, Ursell (1949a,b) obtained the velocity potential for the radiation problem for a circular cylinder by combining a series of wave potentials with undetermined coefficients and a potential with a multivalued singularity at the origin. The wave potentials have to satisfy certain conditions of the problem. They are superposed to satisfy the normal velocity condition on the surface of the object. This gives an infinite number of equations in an infinite number of unknown coefficients. For numerical calculations, only a finite number of wave potentials are chosen. The equations are solved by relaxation techniques to obtain the coefficients for the wave potentials. The source at

the origin is required in this scheme to satisfy the conditions at infinity. With this method Ursell treated the problem of a heaving and rolling semisubmerged circular cylinder at the free surface in water of infinite depth.

Two-dimensional problems. We shall now review briefly the literature on two-dimensional problems. Dean and Ursell (1959) considered the interaction of a train of regular waves with a fixed semi-immersed circular cylinder at the free surface in infinite depth of fluid from theoretical as well as experimental point of view. They obtained reflection and transmission coefficients, and horizontal and vertical force coefficients. Their work complements Ursell's earlier work on the radiation problem. Yu and Ursell (1961) extended Ursell's work on the heaving circular cylinder to the case of finite depth of fluid. They also presented experimental results for this case. Their theoretical results compare favorably with the experimental data. Porter (1960) extended Ursell's method to elliptic and other rather general two-dimensional shapes. Kim (1965) applied the Green's function approach to the problem of an elliptic cylinder oscillating at the free surface in infinite depth of water and obtained numerical results for the physical quantities of interest.

Three-dimensional problems. As for three-dimensional problems, Havelock (1955) treated the problem of a sphere floating half-immersed in water and describing heaving oscillations. Using

a method similar to Ursell's, he obtained approximate results for the added mass and damping coefficients. Macagno and Landweber (1958), and Landweber and Macagno (1960) considered the problem of a rigid spheroid oscillating in a free surface and obtained results for the added mass coefficients for horizontal and vertical oscillations, respectively. Barakat (1962) studied the problem of heave of a freely floating sphere under the action of regular incident waves. He solved the radiation and diffraction problems separately using Ursell's approach. The added mass and damping coefficients and the wave-height ratio in the former problem and the force on the fixed sphere in the latter problem were obtained. The results were combined via the equations of motion to solve the complete problem of a freely floating sphere in waves.

In a work that is of greater interest to the present study, Kim (1964a) formulated the complete problem of an oscillating ship, in the form of a half-ellipsoid, in waves and presented a method of solving it by the Green's function approach. Later, Kim (1964b, 1965) solved the radiation problem of an oscillating ship at the free surface in otherwise still water. The three-dimensional problem of an ellipsoid was considered. The ship was assumed to oscillate in all possible degrees of freedom. The depth of fluid was assumed infinite. Numerical results were obtained for the added mass and added moment of inertia and damping

coefficients. They were compared with results from previous investigators. Monacella (1966) considered the problem of a slender ship free to oscillate on the surface of a fluid of finite depth and subjected to oblique waves. Only the asymptotic approximation to the velocity potential valid in the "far field" was considered and used to compute the hydrodynamic pressure on the bottom of the fluid for the case of a ship in the form of a spheroid.

At this juncture one important point needs to be stressed. As mentioned previously, there are definite relations between the diffraction and the radiation problems. These are commonly known as "Haskind's relations." According to Newman (1962), in 1957 Haskind related the forces and moments on a fixed body due to a given incident wave to the asymptotic velocity potential valid at large distances from the body for the corresponding radiation problem. Thus the vertical force on a fixed object is related to the potential at an infinite distance for the same object heaving in otherwise still water, and so on. In 1962 Newman applied these relations to calculate wave forces on a submerged ellipsoid and a floating elliptic cylinder. Moreover, he showed that in the case of the radiation problem, because of conservation of energy, the damping coefficients can be related to the velocity potentials at infinity. Hence Newman related the wave forces in the diffraction problem for the ellipsoid to the damping coefficients in the corresponding radiation problem. In the case of

the elliptic cylinder, he related the wave forces to the wave-height ratios instead.

Statement of the Dissertation Problem

The problem under investigation in the present dissertation may be considered now. It is obvious, from the brief literature survey, that not much work has been done so far on the problem of wave forces on large objects completely submerged in water of finite depth and resting on the bottom, which is the case of primary interest to coastal and ocean engineers. In view of the apparent and pressing need for information about wave forces on such structures as submerged oil tanks, the research reported in this dissertation has been undertaken. More specifically the diffraction problem of a fixed rigid submerged semiellipsoid resting on the bottom and acted on by a train of regular waves is considered. Besides the assumption that the semiellipsoid is always completely submerged, there are two basic limiting assumptions to the theory. Firstly, the parameter $H/2\bar{a}$, where $\bar{a}$ is the semiaxis of the ellipsoid in the direction of advance of the incident waves, is considered small so that viscous effects may be neglected. Secondly, the wave height H is assumed small in comparison to the wave length $\bar{L}$ and the fluid depth $\bar{h}$, so that linearized wave theory can be employed. The scatter velocity potential is obtained by a distribution of unit wave sources on

the surface of the ellipsoid. On applying the normal boundary condition on the surface of the object, a Fredholm integral equation of the second kind is obtained. Its solution, by numerical methods, indicates the manner in which the sources are to be distributed. To reduce the computer time required, the problem is restricted to the case of a spheroid. Both oblate and prolate spheroids are considered. The problem considered here is quite similar to the one dealt with by Kim (1965) and in a sense complements it, since Kim considered only the radiation problem and the case of infinite depth whereas the diffraction problem and the case of finite depth are considered here. The Green's function used in this dissertation is the same one used by Monacella as a starting point, though he was able to simplify it considerably because of his assumptions. Some of the analytical and numerical techniques of both these investigators are borrowed freely in the present work, where required.

The radiation problem for the case of a submerged spheroid does not involve much work beyond the diffraction problem considered here, since the only difference between the two is in the normal boundary condition on the spheroid. The Green's function is the same. Yet the radiation problem is not studied in detail in the present work, since not much use is foreseen for it by way of practical applications. However, the problem is set up and solved and its results are used in the Haskind's relations in a

few cases as a check on the results obtained for the diffraction problem. Some other checks, including comparison with experimental results, are made to assure the validity of the results given here. All of these checks are successful and on the basis of this, it appears that the results are valid at least over the range of parameters tested.

The work described in this dissertation is of a basic theoretical nature. So no attempt will be made to list all possible areas of application. As already mentioned, one application which motivated this research is in connection with large oil storage tanks currently being built near offshore drilling sites. The present work may be useful for design of underwater habitats also.

2. FORMULATION OF THE PROBLEM

In this section the radiation and diffraction problems are formulated simultaneously, using a common notation. Thus essentially seven different problems are dealt with, simultaneously. These correspond respectively to the fluid motion produced by an object oscillating in its six degrees of freedom, one degree at a time, and the scattering of incident waves due to a fixed object.

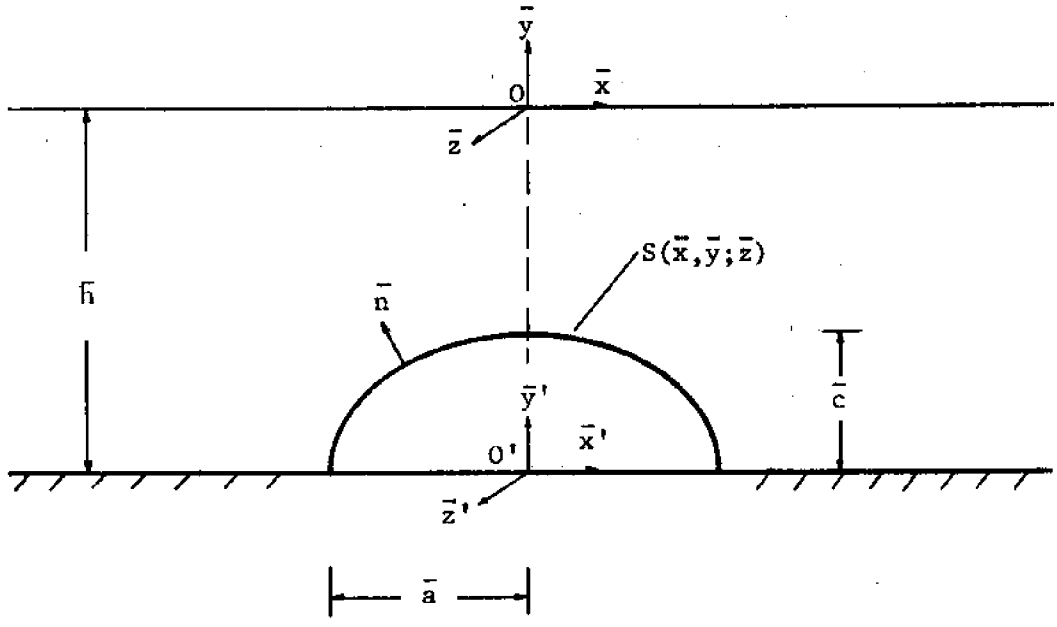

Figure 2. Schematic for the problem.

Consider a rigid semiellipsoid submerged in an inviscid, incompressible liquid of finite depth $\bar{h}$ and resting on the bottom, as shown in figure 2. Let a rectangular Cartesian coordinate

scheme $0\bar{x}\bar{y}\bar{z}$ be chosen such that the $(\bar{x},\bar{z})$-plane coincides with the undisturbed free surface. The surface S of the semiellipsoid with center $(0,-\bar{h},0)$ and semiaxes of length $\bar{a}$, $\bar{c}$ and $\bar{b}$ is given by

$$\frac{\bar{x}^2}{\bar{a}^2} + \frac{(\bar{y}+\bar{h})^2}{\bar{c}^2} + \frac{\bar{z}^2}{\bar{b}^2} = 1. \tag{2.1}$$

For convenience another coordinate scheme $0'\bar{x}'\bar{y}'\bar{z}'$ is also chosen such that its origin is at the center 0' of the semiellipsoid and its axes are respectively parallel to those of the first scheme, as shown in figure 2.

If the body now executes linear or angular oscillations of small amplitude with an angular frequency, $\sigma=2\pi/T$ about its undisturbed position, where T is the period of the oscillations, then the surface disturbances created by the motion travel outward as waves in all directions. The motion of the rigid object oscillating in its six degrees of freedom may be described by

$$\bar{X}_j(t) = Re[\bar{X}_j^o\, e^{-i\sigma t}], \quad j=1,2,3 \tag{a}$$

and (2.2)

$$\theta_j(t) = Re[\theta_j^o\, e^{-i\sigma t}], \quad j=4,5,6 \tag{b}$$

where $\bar{X}_j^o$ and θ_j^o denote the amplitudes of the linear and angular displacements, respectively, and Re denotes the real part of a

complex expression. Here $\bar{X}_1$, $\bar{X}_2$ and $\bar{X}_3$ denote linear oscillations in the $\bar{x}$, $\bar{y}$ and $\bar{z}$ directions and are called "surge", "heave" and "sway", respectively. Similarly θ_4, θ_5 and θ_6 represent angular oscillations about the $\bar{x}'$, $\bar{y}'$ and $\bar{z}'$ axes and are called "roll", "yaw" and "pitch", respectively. In all cases, the linear displacements of the object due to its oscillations are assumed small compared to its linear dimensions, so that the resulting waves may be assumed to be of small amplitude, and separation and viscous effects may be neglected.

Assuming the fluid motion to be irrotational and harmonic with the frequency σ when the transient motion disappears, a velocity potential Φ_j may be introduced to describe the motion. Φ_j is defined such that its gradient gives the fluid velocity. Let

$$\Phi_j(\bar{x},\bar{y},\bar{z};t) = \mathcal{R}e[V_j(\bar{x},\bar{y},\bar{z})\ e^{-i\sigma t}] \tag{2.3}$$

where V_j is a complex function of space only. Then because the fluid is incompressible, Φ_j must satisfy the Laplace equation. That is,

$$\nabla^2\Phi_j(\bar{x},\bar{y},\bar{z};t) = 0 \tag{2.4}$$

in the region R outside the body and between the free surface and the bottom, $\bar{y} = -\bar{h}$.

Let us now consider the diffraction problem. Assuming the body to be fixed in its undisturbed position, consider a train of regular progressive waves of relatively small amplitude $\bar{\eta}^o$ and of frequency σ (wave length $\bar{L}$) coming from $\bar{x} = -\infty$ and advancing in the $+\bar{x}$ direction. Let the free surface elevation of these incident waves, above the mean water level, be given by

$$\bar{\eta}_w(\bar{x},\bar{z};t) = Re[\bar{\eta}^o\, e^{i(k\bar{x}-\sigma t)}] \tag{2.5}$$

where $\bar{\eta}^o$ is assumed to be real and $k=2\pi/\bar{L}$. Note that the height, H, of the incident waves is equal to twice the amplitude $\bar{\eta}^o$.

Once the transients due to interaction between the wave and the object have disappeared, we shall assume that the resultant fluid motion is irrotational and harmonic everywhere with the frequency, σ. Moreover, since the amplitude of the incident wave system is small, the amplitude of the resulting wave system may also be assumed to be small compared to $\bar{L}$ and $\bar{h}$ so that linearized theory can be employed in what follows. Hence the velocity potential Φ' associated with wave interaction with the fixed object may be written as

$$\Phi' = \Phi_0 + \Phi_7 \tag{2.6}$$

where Φ_0 represents the velocity potential of the incident wave in the absence of the body, and Φ_7, which is called the "scatter

potential", arises due to the presence of the body. The potential Φ_0 is already known from linear wave theory. Therefore hereafter the problem is formulated in terms of the unknown scatter potential Φ_7 rather than the total potential Φ'.

Since the total potential Φ' must satisfy the Laplace equation and Φ_0 is already a solution of the same, Φ_7 must now satisfy the Laplace equation. Therefore the subscript j in (2.3) and (2.4) may be considered to range from 1 through 7, the first six values representing the various degrees of freedom, and 7 denoting scatter. Since the problem for Φ_7 is mathematically similar to that for Φ_j, j=1,2,3,...,6, they will be formulated simultaneously hereafter by using the notation j=7 to correspond to the scatter problem. In view of (2.3), (2.4) may now be rewritten as

$$\nabla^2 V_j(\bar{x},\bar{y},\bar{z}) = 0 \text{ in the region } R \text{ .} \quad j=1,2,3,\ldots,7 \tag{2.7}$$

The various boundary conditions that have to be satisfied by Φ_j, j=1,2,3,...,7, will be considered next. At the free surface, Φ_j has to satisfy two boundary conditions. The first of these, which is a dynamic condition, is obtained by linearizing the unsteady form of Bernoulli's equation. It may be written as

$$g\bar{n}_j(\bar{x},\bar{z};t) + \frac{\partial \Phi_j}{\partial t}(\bar{x},0,\bar{z};t) = 0 \tag{2.8}$$

where $\bar{\eta}_j$ represents the elevation, above the mean water level, of the surface disturbance resulting from the oscillation of the body or scatter, and g denotes the acceleration due to gravity. The second boundary condition, which is a kinematic condition, requires that particles on the free surface must always remain there. After linearization, it may be written in the form

$$\frac{\partial \Phi_j}{\partial \bar{y}}(\bar{x},0,\bar{z};t) = \frac{\partial \bar{\eta}_j}{\partial t}(\bar{x},\bar{z};t) \ . \tag{2.9}$$

Conditions (2.8) and (2.9) may be combined into one to yield the complete free surface boundary condition

$$\frac{\partial V_j}{\partial \bar{y}}(\bar{x},0,\bar{z}) - \frac{\sigma^2}{g} V_j(\bar{x},0,\bar{z}) = 0 \ . \tag{2.10}$$

However, using the well-known relation

$$\frac{\sigma^2}{g} = k \tanh k\bar{h} \tag{2.11}$$

from linear wave theory, equation (2.10) may be rewritten as

$$\frac{\partial V_j}{\partial \bar{y}}(\bar{x},0,\bar{z}) - k \tanh (k\bar{h})\ V_j(\bar{x},0,\bar{z}) = 0 \ . \tag{2.12}$$

On the rigid impermeable bottom, $\bar{y}=-\bar{h}$, Φ_j must satisfy the kinematic boundary condition that the velocity normal to the bottom be zero. Therefore

$$\frac{\partial V_j}{\partial \bar{y}}(\bar{x},-\bar{h},\bar{z}) = 0 \ . \tag{2.13}$$

In addition, Φ_j must satisfy the kinematic boundary condition on the surface of the body. For the oscillating body, this requires that the fluid velocity normal to the surface must equal the velocity of the surface normal to itself. Because of linearization, this condition is satisfied on the undisturbed position, $S(\bar{x},\bar{y},\bar{z})$, of the surface. Therefore

$$\frac{\partial V_j}{\partial \bar{n}}(\bar{x},\bar{y},\bar{z}) = \bar{h}_j(\bar{x},\bar{y},\bar{z}) \text{ on } S(\bar{x},\bar{y},\bar{z}),\ j=1,2,3,\ldots,6 \tag{2.14}$$

where $\bar{n}$ is a coordinate normal to S, as shown in figure 2, and

$$\bar{h}_1 = -i\sigma\ \bar{X}_1^o\ n_x,\quad \bar{h}_2 = -i\sigma\ \bar{X}_2^o\ n_y,\quad \bar{h}_3 = -i\sigma\ \bar{X}_3^o\ n_z$$

$$\bar{h}_4 = -i\sigma\ \theta_4^o[(\bar{y}+\bar{h})n_z - \bar{z}n_y],\ \bar{h}_5 = -i\sigma\ \theta_5^o[\bar{z}n_x - \bar{x}n_z], \tag{2.15}$$

$$\bar{h}_6 = -i\sigma\ \theta_6^o[\bar{x}n_y - (\bar{y}+\bar{h})n_x] \ .$$

Here n_x, n_y and n_z denote the components of the outward unit normal $\hat{n}$ to the surface S at any point $(\bar{x},\bar{y},\bar{z})$ on the surface. The derivation of the functions $\bar{h}_j$ is shown in Appendix A.

For the diffraction problem, the kinematic boundary condition on the surface S requires that the fluid velocity normal to the surface must be zero, or $\partial\Phi'/\partial\bar{n}=0$. In view of (2.6), this condition may be written in terms of the scatter potential Φ_7 as

$$\frac{\partial\Phi_7}{\partial\bar{n}}(\bar{x},\bar{y},\bar{z}) = -\frac{\partial\Phi_0}{\partial\bar{n}}(\bar{x},\bar{y},\bar{z}) \text{ on } S(\bar{x},\bar{y},\bar{z}) \ . \tag{2.16}$$

From linear wave theory, the velocity potential for the incident wave, Φ_0, is given by

$$\Phi_0 = Re\left[-\frac{i\bar{g}\bar{\eta}^o}{\sigma}\frac{\cosh k(\bar{h}+\bar{y})}{\cosh k\bar{h}}\, e^{i(k\bar{x}-\sigma t)}\right] \ . \tag{2.17}$$

In a manner analogous to the representation (2.3), we may define a function V_0 corresponding to the incident wave such that

$$V_0(\bar{x},\bar{y},\bar{z}) = -\frac{i\bar{g}\bar{\eta}^o}{\sigma}\frac{\cosh k(\bar{h}+\bar{y})}{\cosh k\bar{h}}\, e^{ik\bar{x}} \ . \tag{2.18}$$

Therefore (2.16) may be rewritten as

$$\frac{\partial V_7}{\partial\bar{n}}(\bar{x},\bar{y},\bar{z}) = -\frac{\partial V_0}{\partial\bar{n}}(\bar{x},\bar{y},\bar{z})$$

$$= -\frac{\bar{g}\bar{\eta}^o k}{\sigma}\left[n_x\frac{\cosh k(\bar{h}+\bar{y})}{\cosh k\bar{h}} - in_y\frac{\sinh k(\bar{h}+\bar{y})}{\cosh k\bar{h}}\right] e^{ik\bar{x}} \text{ on } S. \tag{2.19}$$

Finally, the disturbances caused by the oscillations of the object or the scattering of the incident wave must produce only outgoing progressive waves at a large distance from the object. In other words, Φ_j must, at an infinite horizontal distance from the origin, approach the velocity potential for such waves. This restriction on the asymptotic behaviour of Φ_j is known as the "radiation condition." In terms of V_j it may be written as

$$V_j(\bar{r},\theta,\bar{y}) - C_j(\theta)\ \bar{r}^{-1/2}\ \frac{\cosh k(\bar{h}+\bar{y})}{\cosh k\bar{h}}\ e^{ik\bar{r}} \to 0 \text{ as } \bar{r} \to \infty \qquad (2.20)$$

where $\bar{r}$ and θ are polar coordinates given by $\bar{r} = (\bar{x}^2+\bar{z}^2)^{1/2}$ and $\theta = \tan^{-1}(\bar{z}/\bar{x})$ and C_j is some unknown complex function of θ. For given $\bar{r}$ and θ, the factor $C_j(\theta)\ \bar{r}^{-1/2}$ is proportional to the amplitude of the waves.

Equations (2.7), (2.12), (2.13), (2.14) or (2.19) and (2.20) together constitute the boundary-value problem for V_j. However, it is more convenient to rewrite the problem in terms of dimensionless variables and to solve it in terms of dimensionless parameters, since the results will then be universally valid. As indicated in the "INTRODUCTION", the solution to the problem depends on the following dimensionless parameters:

(i) $2\pi\bar{a}/\bar{L}$, which indicates the effect of the relative size of the ellipsoid,

(ii) $\bar{h}/\bar{a}$, which is related to the proximity of the free surface, and

(iii), (iv) $\bar{b}/\bar{a}$ and $\bar{c}/\bar{a}$, which establish the geometry of the ellipsoid.

In order to show clearly the dependence of the solution on the various parameters, we shall define $a = k\bar{a}=2\pi\bar{a}/\bar{L}$ and make the rest of the space variables and amplitudes dimensionless, using $\bar{a}$. That is , let

$$h = \bar{h}/\bar{a},\ b = \bar{b}/\bar{a},\ c = \bar{c}/\bar{a},\ x = \bar{x}/\bar{a},\ y = \bar{y}/\bar{a},\ z = \bar{z}/\bar{a},$$

$$x' = \bar{x}'/\bar{a},\ y' = \bar{y}'/\bar{a},\ z' = \bar{z}'/\bar{a},\ r = \bar{r}/\bar{a},\ n = \bar{n}/\bar{a}, \qquad (2.21)$$

$$\eta^o = \bar{\eta}^o/\bar{a},\ X_j^o = \bar{X}_j^o/\bar{a},\ j = 1,2,3 \quad , \text{etc.}$$

For convenience, the following notation will also be used hereafter:

$$X_j^o = \theta_j^o \ , \ j=4,5,6. \qquad (2.22)$$

The surface $S(x,y,z)$ of the ellipsoid is now given by

$$x^2 + \frac{(y+h)^2}{c^2} + \frac{z^2}{b^2} = 1. \qquad (2.23)$$

We shall next define dimensionless potentials u_j as follows:

$$au_j(x,y,z) = i\sigma V_j(\bar{x},\bar{y},\bar{z})/g\bar{a}\, X_j^o \tanh(k\bar{h}),\ j=1,2,3,\ldots,6,$$

$$au_7(x,y,z) = -i\sigma V_7(\bar{x},\bar{y},\bar{z})/g\bar{a}\, n^o . \qquad (2.24)$$

The reasons for the particular form of definitions chosen are: (1) the normalized problems for u_j all appear similar and the normal velocity condition on S is simplified, and (2) the dimensionless dynamic pressure is linearly proportional to u_j in each case.

By using the definitions given above and the conditions previously mentioned for V_j, the boundary-value problem corresponding to the fluid motion arising from small harmonic oscillations of the rigid submerged body in its six degrees of freedom, as well as the scattering of a train of regular small amplitude waves due to the fixed object can now be written concisely in terms of u_j. Thus the dimensionless potential $u_j(x,y,z)$, $j=1,2,3,\ldots,7$, continuous in the fluid region R is sought such that

(A) $\nabla^2 u_j(x,y,z) = 0$ in region R

(B) $\dfrac{\partial u_j}{\partial y}(x,0,z) - a\tanh(ah)\, u_j(x,0,z) = 0$

(C) $\dfrac{\partial u_j}{\partial y}(x,-h,z) = 0$ outside $S(x,y,z)$ $\qquad (2.25)$

$$(D)\quad \frac{\partial u_j}{\partial n}(x,y,z) = h_j(x,y,z) \text{ on } S(x,y,z)$$

$$(E)\quad u_j(r,\theta,y) - A_j(\theta) r^{-1/2} \frac{\cosh a(h+y)}{\cosh ah} e^{iar} \to 0 \text{ as } r \to \infty ,$$

where $S(x,y,z)$ represents the immersed surface of the ellipsoid in its undisturbed position and A_j is an unknown dimensionless complex function of θ. Here $h_j(x,y,z)$ denotes a prescribed function which depends on the mode of oscillation for $j=1,2,3,\ldots,6$, and on the incident wave for $j=7$. The functions h_j are obtained from (2.15) and (2.19) as

$$h_1 = n_x,\ h_2 = n_y,\ h_3 = n_z,\ h_4 = (y+h)n_z - zn_y,$$

$$h_5 = zn_x - xn_z,\ h_6 = xn_y - (y+h)n_x , \qquad (2.26)$$

$$h_7 = \frac{e^{iax}}{\cosh ah} [n_y \sinh a(h+y) + in_x \cosh a(h+y)] .$$

It is apparent that the seven problems described by (2.25) are identical except for the functions h_j. This makes it very convenient to solve them simultaneously. The remainder of this dissertation is primarily devoted to the solution of (2.25).

3. FORMULATION OF THE SOLUTION IN TERMS OF THE GREEN'S FUNCTION

The solution to the boundary-value problem (2.25) can be obtained in terms of a Green's function. In physical terms, this approach consists of distributing a number of three-dimensional "wave sources" on the surface of the ellipsoid. The wave sources are chosen so as to satisfy all the conditions of the problem except the condition (D) on the surface of the ellipsoid. The strengths of these sources are finally adjusted so as to satisfy the condition (D). The potential for one such wave source of unit strength is called the "Green's function" for the problem.

We proceed by use of Green's reciprocal theorem, applied to the region R, as shown in figure 3. The region R is bounded by the free surface, S_f, the bottom, S_b, the cylindrical surface, S_∞ (the axis of the cylinder coinciding with the y-axis and the radius $r \to \infty$), and the surface of the ellipsoid, S.

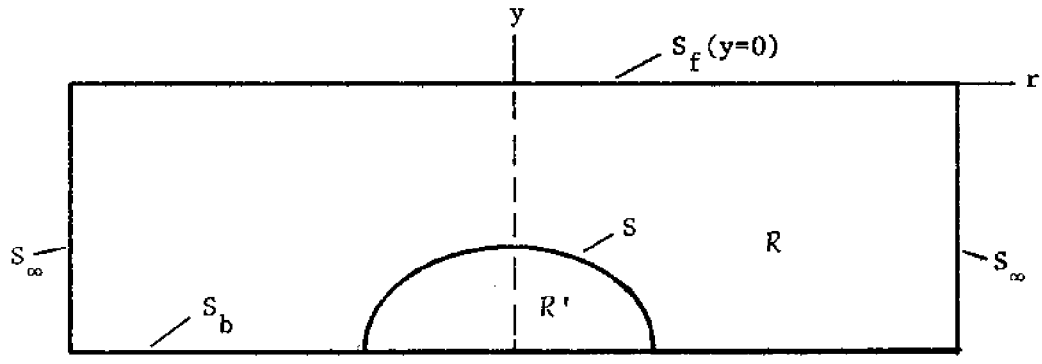

Figure 3. Region of application of Green's theorem.

Let $u_j(x,y,z)$ and the Green's function $G(x,y,z;\xi,\eta,\zeta)$ be chosen as subjects of Green's reciprocal theorem. Here (x,y,z) is any general point in the fluid region, including the boundaries, and (ξ,η,ζ) is a particular point in the interior of the region, where a unit wave source is located. $G(x,y,z;\xi,\eta,\zeta)$ is the velocity potential at the point (x,y,z) due to the unit source at (ξ,η,ζ). From Green's theorem

$$\iiint_R \left[u_j(x,y,z)\ \nabla^2 G(x,y,z;\xi,\eta,\zeta) - G(x,y,z;\xi,\eta,\zeta)\ \nabla^2 u_j(x,y,z) \right]$$

$$dx\ dy\ dz = \iint_{S_f+S_b+S_\infty+S} \left[u_j(x,y,z)\ \frac{\partial G}{\partial n'}(x,y,z;\xi,\eta,\zeta) \right.$$

$$\left. - G(x,y,z;\xi,\eta,\zeta)\ \frac{\partial u_j}{\partial n'}(x,y,z) \right] dS \ . \qquad (3.1)$$

Here the Green's function, G, is yet unknown. $\hat{n}'$ is the unit normal to any of the surfaces, outward from the fluid region. n' is used to denote a coordinate in the same direction. Since u_j satisfies the Laplace equation throughout the region R, the second part of the integral on the left hand side of (3.1) vanishes and, moreover, if $G(x,y,z;\xi,\eta,\zeta)$ is chosen such as to satisfy

$$\nabla^2 G(x,y,z;\xi,\eta,\zeta) = \delta(x-\xi)\ \delta(y-\eta)\ \delta(z-\zeta) \qquad (3.2)$$

where δ is the Dirac delta function, the left hand side of (3.1) reduces to $u_j(\xi,\eta,\zeta)$.

Next we shall consider the integral on the right hand side of (3.1) for each segment of the boundary surface. First we may write

$$\int\int_{S_f}\left[u_j \frac{\partial G}{\partial n'} - G \frac{\partial u_j}{\partial n'}\right] dS = \int\int_{S_f}\left[u_j\left[\frac{\partial G}{\partial n'} - a \tanh(ah)\, G\right] - G\left[\frac{\partial u_j}{\partial n'} - a \tanh(ah)\, u_j\right]\right] dS \ . \tag{3.3}$$

In view of (2.25-B), the integral on the right vanishes provided G is chosen to satisfy the free surface condition, i.e.

$$\frac{\partial G}{\partial y}(x,0,z;\xi,\eta,\zeta) - a \tanh(ah)\, G(x,0,z;\xi,\eta,\zeta) = 0 \ . \tag{3.4}$$

Secondly, in view of (2.25-C),

$$\int\int_{S_b}\left[u_j \frac{\partial G}{\partial n'} - G \frac{\partial u_j}{\partial n'}\right] dS = 0 \tag{3.5}$$

provided G satisfies the bottom boundary condition, i.e.

$$\frac{\partial G}{\partial n}(x,-h,z;\xi,\eta,\zeta) = \frac{\partial G}{\partial y}(x,-h,z;\xi,\eta,\zeta) = 0 \ . \tag{3.6}$$

Thirdly,

$$\int\int_{S_\infty}\left[u_j \frac{\partial G}{\partial n'} - G \frac{\partial u_j}{\partial n'}\right] dS = \int\int_{S_\infty}\left[u_j\left[\frac{\partial G}{\partial n'} - ia\, G\right] - G\left[\frac{\partial u_j}{\partial n'} - ia\, u_j\right]\right] dS \ . \tag{3.7}$$

By means of the radiation condition, (2.25-E), it can be shown that

$$\frac{\partial u_j}{\partial n'} - iau_j = 0 \text{ on } S_\infty \ . \tag{3.8}$$

Therefore if G is required to satisfy the condition

$$\frac{\partial G}{\partial n'} - iaG = 0 \text{ on } S_\infty \ , \tag{3.9}$$

the integral on the right hand side of (3.7) vanishes. Thus we obtain finally the result

$$u_j(\xi,\eta,\zeta) = \iint_S u_j(x,y,z) \frac{\partial}{\partial n'} G(x,y,z;\xi,\eta,\zeta)\ dS$$

$$- \iint_S G(x,y,z;\xi,\eta,\zeta) \frac{\partial}{\partial n'} u_j(x,y,z)\ dS \ . \tag{3.10}$$

Interchanging the roles of (x,y,z) and (ξ,η,ζ) (that is, now let (x,y,z) be a point in the region and (ξ,η,ζ) be a point on the surface S, where a source is located), and requiring that the function G be symmetric in (x,y,z) and (ξ,η,ζ), we can rewrite (3.10) as

$$u_j(x,y,z) = \iint_S u_j(\xi,\eta,\zeta) \frac{\partial}{\partial n'} G(x,y,z;\xi,\eta,\zeta)\ dS$$

$$- \iint_S G(x,y,z;\xi,\eta,\zeta) \frac{\partial}{\partial n'} u_j(\xi,\eta,\zeta)\ dS \ . \tag{3.11}$$

Now G and some other function $u_j'(x,y,z)$ are chosen such that both of them satisfy the Laplace equation in the region R' interior to the surface S and the bottom, and $\partial u_j'/\partial y$ and $\partial G/\partial y$ vanish on the bottom, $y = -h$. Applying Green's theorem once again, we have

$$\iint_S u_j' \frac{\partial G}{\partial n}\, dS = \iint_S G \frac{\partial u_j'}{\partial n}\, dS \tag{3.12}$$

where n is the coordinate normal to the surface S, as defined previously. Note that $\partial/\partial n = -\partial/\partial n'$. Hence (3.12) may be re-written as

$$0 = \iint_S u_j' \frac{\partial G}{\partial n'}\, dS + \iint_S G \frac{\partial u_j'}{\partial n}\, dS \ . \tag{3.13}$$

Subtracting (3.13) from (3.11) gives

$$u_j(x,y,z) = \iint_S (u_j - u_j') \frac{\partial G}{\partial n'}\, dS - \iint_S G \left[\frac{\partial u_j}{\partial n'} + \frac{\partial u_j'}{\partial n} \right] dS. \tag{3.14}$$

If now it is required in addition that the arbitrary function u_j' be such that $u_j' = u_j$ on the surface S, we have

$$u_j(x,y,z) = \iint_S \left[- \frac{\partial u_j}{\partial n'} - \frac{\partial u_j'}{\partial n} \right] G\, dS \ . \tag{3.15}$$

Defining a function f_j such that

$$f_j(\xi,\eta,\zeta) = -4\pi \left[\frac{\partial u_j}{\partial n'}(\xi,\eta,\zeta) + \frac{\partial u'_j}{\partial n}(\xi,\eta,\zeta) \right] \tag{3.16}$$

we can rewrite (3.15) as

$$u_j(x,y,z) = \frac{1}{4\pi} \int\int_S f_j(\xi,\eta,\zeta)\ G(x,y,z;\xi,\eta,\zeta)\ dS\ . \tag{3.17}$$

This is the representation desired. It is unique. It indicates that the velocity potential u_j may be obtained in terms of wave sources located at points (ξ,η,ζ) of the surface S. Here f_j is called the "distribution function", since it indicates the manner in which unit wave sources are to be distributed over the surface. It is a continuous complex function which has to be determined.

The next logical step in the solution is to determine the Green's function, G. In order to obtain the representation for u_j shown in (3.17), a number of conditions were imposed on G. These may be summarized to give a boundary-value problem for G as shown below:

$$\text{(A)}\quad \nabla^2 G(x,y,z;\xi,\eta,\zeta) = \delta(x-\xi)\ \delta(y-\eta)\ \delta(z-\zeta)$$

$$\text{(B)}\quad \frac{\partial G}{\partial y}(x,0,z;\xi,\eta,\zeta) - a\ \tanh(ah)\ G(x,0,z;\xi,\eta,\zeta) = 0$$

$$\text{(C)}\quad \frac{\partial G}{\partial y}(x,-h,z;\xi,\eta,\zeta) = 0 \tag{3.18}$$

$$\text{(D)}\quad \lim_{r\to\infty} \left[\frac{\partial G}{\partial r} - iaG \right] = 0\ .$$

Condition (D) may also be written in the following form:

$$(D') \quad G(r,\theta,y;\xi,\eta,\zeta) \to Br^{-1/2} \frac{\cosh a(y+h)}{\cosh ah} \cosh a(\eta+h)\, e^{iar}, \text{ as } r \to \infty$$

where B is some unknown complex constant.

The radiation condition (D) or (D') in the boundary-value problem for G makes the Green's function, which satisfies (3.18), unique.

On comparing (2.25) with (3.17) and (3.18), it is apparent that the boundary-value problem for u_j is in effect exchanged for two separate problems, namely, a boundary-value problem for the Green's function and a problem of finding the unknown distribution function f_j which satisfies (3.17). The reason for this approach is as follows. Since the Green's function does not have to satisfy the normal boundary condition on the surface S, it is easier to find than u. Once G is obtained, the distribution function, f_j, may be determined by using the normal boundary condition, (2.25-D) for u_j.

Normally the Green's function is obtained from the boundary-value problem for G by means of Fourier and Laplace transform techniques. In the present case, however, the Green's function which satisfies (3.18) is given in a dimensional form by Wehausen

and Laitone (1960) and, when made dimensionless in our variables, appears as given below (refer figure 4):

$$G(x,y,z;\xi,\eta,\zeta) = \frac{1}{R} + \frac{1}{R'} + 2PV \int_{\kappa=0}^{\infty} (\kappa+\nu)\ e^{-\kappa h}$$

$$\frac{\cosh \kappa(\eta+h)\ \cosh \kappa(y+h)}{(\kappa \sinh \kappa h - \nu \cosh \kappa h)}\ J_0(\kappa r_1)\ d\kappa$$

$$+ i\ \frac{2\pi(a^2-\nu^2)\ \cosh a(\eta+h)\ \cosh a(y+h)}{a^2h - \nu^2h + \nu}\ J_0(ar_1) \qquad (3.19)$$

where

$$R = \left[(x-\xi)^2 + (y-\eta)^2 + (z-\zeta)^2 \right]^{1/2}, \qquad (3.20)$$

$$R' = \left[(x-\xi)^2 + (y+2h+\eta)^2 + (z-\zeta)^2 \right]^{1/2}, \qquad (3.21)$$

$$r_1 = \left[(x-\xi)^2 + (z-\zeta)^2 \right]^{1/2}, \qquad (3.22)$$

and

$$\nu = \frac{\sigma^2}{g}\,\bar{a} = a \tanh ah. \qquad (3.23)$$

In (3.19) PV is used to denote the Cauchy principal value of the infinite integral and J_0 is the Bessel function of the first kind of order zero. Note that κ is a dummy variable of integration. It is necessary to take the principal value of the integral

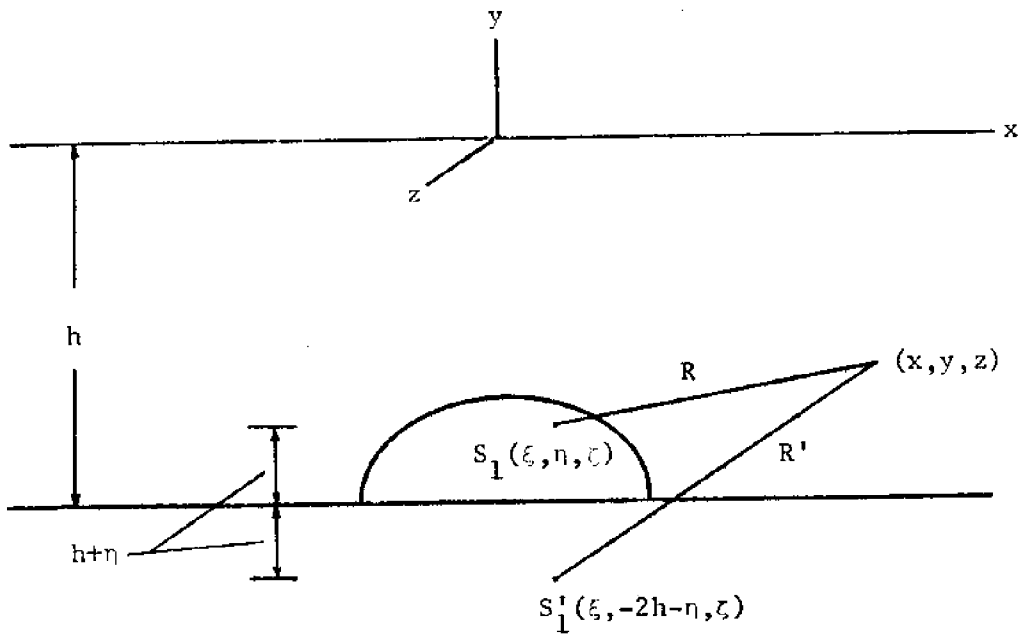

Figure 4. Definition sketch for Green's function.

because when $\kappa=a$, the denominator of the integrand goes to zero so that the integrand tends to infinity.

It is worthwhile to consider the significance of each of the terms in G separately. Normally in steady three-dimensional potential flow past an object in an infinite fluid, it is necessary to distribute only simple three-dimensional sources, such as S_1, on the surface of the object. Their potentials are of the form 1/R. However if we are interested in the flow past a half object

in a semi-infinite fluid with a rigid boundary in the plane of symmetry, then we must consider the effect at any point (x,y,z) due to the image source S_1' also. S_1' is the image of S_1 in the rigid boundary. This is to satisfy the kinematic condition on the rigid boundary. In this case, in our coordinate scheme, the potential of the image source is of the form $1/R'$. Besides the $1/R$ and $1/R'$ terms, which occur in regular potential flow problems, the infinite integral term and the imaginary term are needed in G in order to satisfy the free surface boundary condition and the radiation condition.

Before proceeding further, we note that G may be written as

$$G(x,y,z;\xi,\eta,\zeta) = \frac{1}{R} + G^*(x,y,z;\xi,\eta,\zeta) \tag{3.24}$$

where

$$G^*(x,y,z;\xi,\eta,\zeta) \equiv \frac{1}{R'} + 2\,PV \int_{\kappa=0}^{\infty} (\kappa+\nu)\, e^{-\kappa h}$$

$$\frac{\cosh \kappa(\eta+h) \cosh \kappa(y+h)}{(\kappa \sinh \kappa h - \nu \cosh \kappa h)} J_0(\kappa r_1)\, d\kappa$$

$$+ i\, \frac{2\pi(a^2-\nu^2) \cosh a(\eta+h) \cosh a(y+h)}{a^2h - \nu^2h + \nu} J_0(ar_1) \,. \tag{3.25}$$

As the general point (x,y,z) tends to the source location (ξ,η,ζ), $1/R$ tends to infinity. On the other hand G^* remains finite. Thus (3.24) splits G into two parts, one singular at (ξ,η,ζ) and the other everywhere regular.

It is to be noted that in the representation (3.17) because of the way G is chosen, u_j automatically satisfies conditions (A), (B), (C) and (E) of the boundary-value problem (2.25). So the only condition left for it to fulfill is the boundary condition (D) on the surface S(x,y,z) of the body. When the normal derivative of u_j is taken at a point (x,y,z) of the surface S, using the representation (3.17), the result is as follows.

$$\frac{\partial u_j}{\partial n}(x,y,z) = -\frac{1}{2} f_j(x,y,z) + \frac{1}{4\pi} \int\int_S f_j(\xi,\eta,\zeta) \frac{\partial G}{\partial n}(x,y,z;\xi,\eta,\zeta)\, dS \,. \tag{3.26}$$

It may be noted that on the right hand side of (3.26) there is an extra term, $-f_j(x,y,z)/2$, which is unexpected. It arises because of the effect on the point (x,y,z) due to the source located there. This is discussed in detail in Appendix B. Substitution of (3.26) in the boundary condition (2.25-D) for u_j results in the following equation which must be satisfied at all points (x,y,z) of the surface S:

$$-f_j(x,y,z) + \frac{1}{2\pi} \int\int_S f_j(\xi,\eta,\zeta) \frac{\partial G}{\partial n}(x,y,z;\xi,\eta,\zeta)\, dS = 2h_j(x,y,z) \,. \tag{3.27}$$

In (3.27), for given (x,y,z) and (ξ,η,ζ), $\partial G/\partial n$ is known since G is given by (3.19). Similarly $h_j(x,y,z)$ is known from Section 2. Hence the only unknown is the distribution function, f_j. Since f_j occurs both under the integral sign as well as outside of it, (3.27) is called an "integral equation." This particular form of equation is known as "Fredholm's integral equation of the second kind." Thus the boundary-value problem (2.25) for the velocity potential u_j is finally reduced to a problem of solving the integral equation, (3.27). Because the Green's function is quite complicated, it is not possible to solve (3.27) in a closed form. Hence numerical methods will have to be used. Once f_j is known, the potential u_j can be obtained from (3.17), and the problem is essentially solved.

At this stage, one point must be emphasized. While so far we have thought of the object as being a semiellipsoid because of our interest in obtaining physical solutions for this case eventually, nowhere in setting up the boundary-value problem (2.25), and arriving at the integral equation (3.27) did we actually use the fact that the object is a semiellipsoid. Thus the formulation presented so far is by no means restricted to a semiellipsoid, but is valid for an object of arbitrary shape, provided $\bar{a}$ is interpreted as a characteristic length of such an object and S its surface. It is only when we attempt numerical solution of the integral equation that we have to assume a specific

shape for the object in order to simplify calculations. In tune with this procedure, we shall next consider how to obtain physical quantities such as forces and moments in the case of an object of arbitrary shape, and postpone discussion of the numerical scheme to a later section.

4. PHYSICAL QUANTITIES

In this section we shall consider how to obtain the dynamic pressures, forces and moments, once the integral equation (3.27) is solved numerically and the velocity potentials u_j are determined.

In all cases, the hydrodynamic pressure is obtained from the corresponding velocity potential by applying Bernoulli's equation. The forces and moments caused by the action of the dynamic pressure on the immersed surface of the object are obtained by integration over the surface. In the case of an oscillating rigid object, the forces and moments are resolved into components in phase with the acceleration and other components in phase with the velocity of the object. The former components are characterized by dimensionless added mass or added moment of inertia coefficients, whereas the latter components may be described in terms of dimensionless linear or angular damping coefficients. When a three-dimensional rigid submerged object of arbitrary shape is held fixed and subjected to the action of a train of regular waves, three possible components of force and three possible components of moment arise. These are simply referred to as "wave forces and moments" and their amplitudes are usually expressed in terms of dimensionless force and moment coefficients. In the case of both the radiation and diffraction problems, the final results in the form of dimensionless

coefficients depend on the parameters a, h and other parameters characterizing the geometry, which, for a semiellipsoid, are given by b and c.

The hydrodynamic pressure $\bar{\Pi}(\bar{x},\bar{y},\bar{z};t)$ at any point $(\bar{x},\bar{y},\bar{z})$ in the fluid region may be obtained from the linearized form of Bernoulli's equation as

$$\bar{\Pi}(\bar{x},\bar{y},\bar{z};t) = -\rho\frac{\partial\Phi}{\partial t}(\bar{x},\bar{y},\bar{z};t) \tag{4.1}$$

where ρ is the fluid density and Φ is the velocity potential for the particular problem under consideration. Therefore for oscillation of the object in its various degrees of freedom, the dynamic pressure is given by

$$\bar{\Pi}_j(\bar{x},\bar{y},\bar{z};t) = \rho g\bar{a}\ Re[X_j^o\ a u_j(x,y,z)\ \tanh(ah)\ e^{-i\sigma t}]\ ,$$

$$j=1,2,3,\ldots,6. \tag{4.2}$$

For the case of wave interaction with the fixed object, the dynamic pressure $\bar{\Pi}'(\bar{x},\bar{y},\bar{z};t)$ is given by

$$\bar{\Pi}'(\bar{x},\bar{y},\bar{z};t) = -\rho g\bar{a}\ Re\left[\ \eta^o\ a[u_7(x,y,z) + u_0(x,y,z)]\ e^{-i\sigma t}\ \right] \tag{4.3}$$

where the dimensionless potential u_0 for the incident wave is defined, analogous to u_7, by

$$au_0(x,y,z) = -i\sigma V_0(\bar{x},\bar{y},\bar{z})/g\bar{a}\,\eta^o = -\frac{\cosh a(h+y)}{\cosh ah}\,e^{iax} \quad . \qquad (4.4)$$

We now define dimensionless dynamic pressures as

$$\Pi_j(x,y,z;t) = \bar{\Pi}_j(\bar{x},\bar{y},\bar{z};t)/\rho g\bar{a}\,X_j^o \quad , \quad j=1,2,3,\ldots,6, \quad (a)$$

$$\Pi'(x,y,z;t) = \bar{\Pi}'(\bar{x},\bar{y},\bar{z};t)/\rho g\bar{a}\,\eta^o \quad . \qquad (b) \qquad (4.5)$$

In this dissertation, the main interest is in the dimensionless pressure, Π'. The pressure Π' has a simple physical interpretation. It is the ratio of the pressure head in feet of liquid to the amplitude of the incident wave in feet. Since Π' is harmonic with time, we shall use $p(x,y,z)$ to denote the amplitude of the same and δ_p to denote its phase shift with respect to the phase of the incident wave at the origin O. Thus, by definition,

$$\Pi'(x,y,z;t) = Re[p(x,y,z)\,e^{i\delta_p}\,e^{-i\sigma t}] \qquad (4.6)$$

where

$$p(x,y,z) = |a[u_7(x,y,z) + u_0(x,y,z)]| \qquad (4.7)$$

and

$$\delta_p(x,y,z) = arg\left[\,-a[u_7(x,y,z) + u_0(x,y,z)]\,\right] \quad . \qquad (4.8)$$

Here *arg* is used to denote the argument of a complex variable. To avoid confusion when discussing the diffraction problem, $\Pi'(x,y,z;t)$ will be called the "dimensionless pressure" or "pressure coefficient", $p(x,y,z)$ the "pressure amplitude coefficient", and δ_p the "phase shift of pressure."

The dynamic forces $\vec{F}_j$ and moments $\vec{G}_j$ due to the j-th mode of oscillation of the object are obtained from the pressure distribution as

$$\vec{F}_j(t) = -\int\int_S \bar{\Pi}_j(\bar{x},\bar{y},\bar{z};t)\, \hat{n}\, d\bar{S},\quad j=1,2,3,\ldots,6, \tag{4.9}$$

and

$$\vec{G}_j(t) = -\int\int_S \bar{\Pi}_j(\bar{x},\bar{y},\bar{z};t)\, (\vec{\bar{r}} \times \hat{n})\, d\bar{S},\quad j=1,2,3,\ldots,6. \tag{4.10}$$

where $\vec{\bar{r}}$ represents the dimensional position vector from the point O' to a point on the surface S, and $d\bar{S}$ the dimensional surface area.

The i-th component of the dynamic force (or moment) which arises due to the j-th mode of oscillation of the object may then be obtained from (4.9) and (4.10), after simplification, as

$$F_{ij}(t) = -(1 \text{ or } \bar{a}) \int\int_S \bar{\Pi}_j(\bar{x},\bar{y},\bar{z};t)\, h_i(x,y,z)\, d\bar{S}$$

$$= -(1 \text{ or } \bar{a})\, \rho g \bar{a}^3\, X_j^o\, a \tanh(ah)$$

$$\mathrm{Re}\left[\int\int_S u_j(x,y,z)\, h_i(x,y,z)\, dS\, e^{-i\sigma t}\right],$$

$$i,j=1,2,3,\ldots,6\ , \tag{4.11}$$

on substituting for $\bar{\Pi}_j$ from (4.2). In (4.11), for i=1,2,3, F_{ij} represents a force and the coefficient 1 should be chosen, whereas for i=4,5,6, F_{ij} represents a moment and the coefficient $\bar{a}$ should be chosen. The subscripts i=1,2 and 3 in F_{ij} represent force components in the x,y and z directions, respectively, and the subscripts i=4,5 and 6 in F_{ij} represent moment components about the x', y' and z' axes, respectively.

The forces (or moments) on the body in the case of the radiation problem may each be expressed as the sum of two components, one in phase with the acceleration and the other in phase with the velocity of the body, in the form

$$F_{ij}(t) = -\bar{M}_{ij}\,\bar{a}\,\ddot{X}_j(t) - \bar{N}_{ij}\,\bar{a}\,\dot{X}_j(t),\quad i,j=1,2,3,\ldots,6, \tag{4.12}$$

where $\bar{M}_{ij}$ and $\bar{N}_{ij}$ represent added mass (or added moment of inertia) and linear (or angular) damping coefficients, respectively. We must emphasize that the term "damping" in the present context does not bear any relation to viscous damping, but is related to energy transport. The negative signs are introduced in (4.12) to account for the fact that by definition the forces and moments

oppose the motion of the body. Substituting for X_j from (2.2) and comparing (4.12) with (4.11), we may write the following expressions for the dimensionless added mass (or added moment of inertia) and damping coefficients:

$$M_{ij} = -\,Re\left[\iint_S u_j(x,y,z)\; h_i(x,y,z)\; dS\right],\quad i,j=1,2,3,\ldots,6, \tag{4.13}$$

$$N_{ij} = -\,Im\left[\iint_S u_j(x,y,z)\; h_i(x,y,z)\; dS\right],\quad i,j=1,2,3,\ldots,6. \tag{4.14}$$

Here *Im* is used to denote the imaginary part of a complex expression and the dimensionless added mass and linear damping coefficients are defined by

$$M_{ij} = \frac{\bar{M}_{ij}}{\rho a^3}, \qquad N_{ij} = \frac{\bar{N}_{ij}}{\rho\sigma a^3}, \qquad \begin{matrix} i=1,2,3 \\ j=1,2,3,\ldots,6, \end{matrix} \tag{4.15}$$

and the dimensionless added moment of inertia and angular damping coefficients are defined by

$$M_{ij} = \frac{\bar{M}_{ij}}{\rho a^4}, \qquad N_{ij} = \frac{\bar{N}_{ij}}{\rho\sigma a^4}, \qquad \begin{matrix} i=4,5,6 \\ j=1,2,3,\ldots,6. \end{matrix} \tag{4.16}$$

As previously mentioned, the first subscript i indicates the direction of the force (or moment) involved and the second subscript j denotes the particular mode of oscillation. For a three-dimensional body of arbitrary shape, the two sets of coefficients

M_{ij} and N_{ij} may each be arranged in a 6 x 6 matrix. The dimensionless coefficients M_{ij} and N_{ij} characterize the solution to the radiation problem.

The dynamic forces and moments due to the action of a train of regular incident waves on the fixed rigid object may be obtained in a similar manner from the pressure distribution as

$$\bar{F}_i'(t) = - (1 \text{ or } \bar{a}) \int\int_S \bar{\Pi}'(\bar{x},\bar{y},\bar{z};t)\, h_i(x,y,z)\, d\bar{S},$$

$$i=1,2,3,\ldots,6, \tag{4.17}$$

where again the coefficient 1 is chosen for the case of a force, i.e., when i=1,2,3 and the coefficient $\bar{a}$ is chosen for the case of a moment, i.e., when i=4,5,6. Substituting for $\bar{\Pi}'$ from (4.3) and simplifying, we may write the dimensionless force and moment components as

$$F_i'(t) = Re\left[\int\int_S a \left[u_7(x,y,z) + u_0(x,y,z) \right] n_i(x,y,z)\, dS\, e^{-i\sigma t} \right], \quad i=1,2,3,\ldots,6, \tag{4.18}$$

where, by definition

$$F_i'(t) = \frac{\bar{F}_i'(t)}{(1 \text{ or } \bar{a})\, \rho g \bar{a}^3\, \eta_o}, \quad i=1,2,3,\ldots,6. \tag{4.19}$$

In (4.19) the coefficient 1 applies for i=1,2,3 and the coefficient $\bar{a}$ for i=4,5,6.

We shall for convenience rewrite (4.18) as

$$F_i'(t) = Re[f_i' e^{i\delta_i} e^{-i\sigma t}], \quad i=1,2,3,\ldots,6 , \tag{4.20}$$

where f_i' represents the amplitude of F_i' and δ_i its phase shift with respect to the phase of the incident wave at the origin 0. Thus

$$f_i' = \left| \int\int_S a[u_7(x,y,z) + u_0(x,y,z)]\, h_i(x,y,z)\, dS \right|$$

$$i=1,2,3,\ldots,6 , \tag{4.21}$$

and

$$\delta_i = arg\left[\int\int_S a[u_7(x,y,z) + u_0(x,y,z)]\, h_i(x,y,z)\, dS \right] ,$$

$$i=1,2,3,\ldots,6 . \tag{4.22}$$

In general f_i' may be called the wave force or moment coefficient and δ_i the phase shift of the wave force or moment, as the case may be. The coefficients f_i' together with the phase shifts δ_i completely characterize the forces and moments acting on a fixed object of arbitrary shape.

For a fixed semiellipsoid, because of symmetry, the only non-zero force coefficients are f_1' and f_2' which correspond to forces

in the x and y directions respectively. In this dissertation, for easy identification, these will be denoted by f_x and f_y and called the "horizontal and vertical force coefficients", respectively. Similarly, the only non-zero moment coefficient is f_6' which corresponds to a moment about the z'-axis. Therefore it will be denoted by m_z, and simply called the "moment coefficient." The phase shifts δ_1, δ_2 and δ_6 will be denoted by δ_x, δ_y and δ_m and called the "phase shifts for the horizontal force, vertical force and moment", respectively. Summing up, we use the notation hereafter that

$$f_x = f_1', \qquad f_y = f_2', \qquad m_z' = f_6', \qquad \text{(a)}$$

$$\delta_x = \delta_1, \qquad \delta_y = \delta_2, \text{ and } \delta_m = \delta_6 . \qquad \text{(b)} \tag{4.23}$$

In view of the fact that for a fixed semiellipsoid f_x, f_y and m_z, are the only non-zero force and moment coefficients, we shall, for applying Haskind's relations, concern ourselves hereafter mainly with the cases j=1,2, and 6, i.e., surge, heave and pitch for an oscillating ellipsoid.

Haskind's relations as well as the energy check are developed in Appendix C.

5. TRANSFORMATION OF COORDINATES

The body under consideration in this dissertation is in the form of an ellipsoid. It is therefore convenient to work the problem in terms of ellipsoidal polar coordinates which conform to the shape of the body. These coordinates are defined on the surface of the body as follows:

$$\begin{aligned} x &= \cos\alpha \sin\phi, \quad y + h = c\cos\phi, \quad z = b \sin\alpha \sin\phi \\ \xi &= \cos\beta \sin\psi, \quad \eta + h = c\cos\psi, \quad \zeta = b \sin\beta \sin\psi \ . \end{aligned} \tag{5.1}$$

Thus on the surface S, we associate the new coordinates (α,ϕ) with the point (x,y,z) and (β,ψ) with the point (ξ,η,ζ). The coordinates α and β represent azimuth angles while ϕ and ψ represent vertical angles, as shown in figure 5.

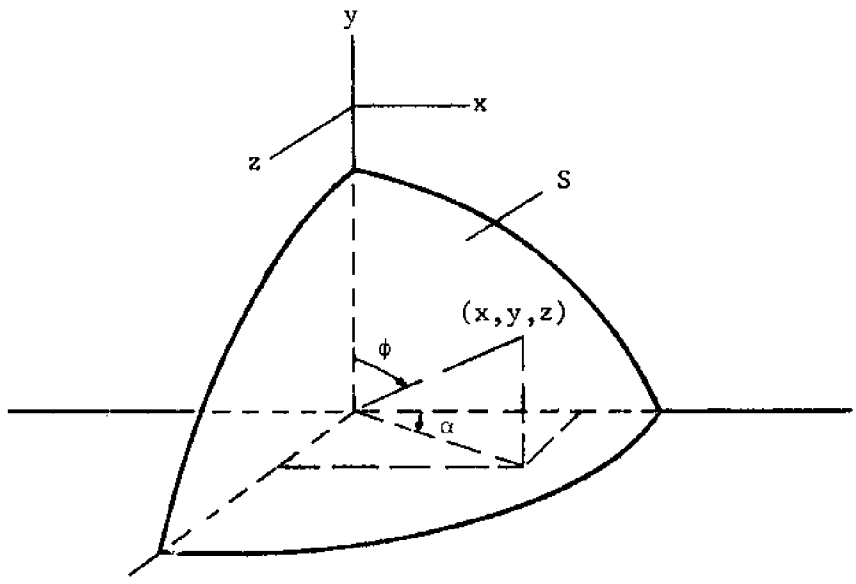

Figure 5. Transformation of coordinates.

Since the equation of the surface of the ellipsoid is given by

$$S(x,y,z) = x^2 + \frac{(y+h)^2}{c^2} + \frac{z^2}{b^2} - 1 = 0 \ , \tag{5.2}$$

the unit normal vector $\hat{n}$ is given by

$$\hat{n} = \frac{\nabla S}{|\nabla S|} = \frac{\hat{i}x + \hat{j}\,(\frac{y+h}{c^2}) + \hat{k}\,\frac{z}{b^2}}{[x^2 + \frac{(y+h)^2}{c^4} + \frac{z^2}{b^4}]^{1/2}} \ . \tag{5.3}$$

An expression is derived next for the area of an elemental surface dS of the ellipsoid in terms of the new coordinates. Suppose the elemental strip dS is so chosen that its projection dS_x on the (y,z)-plane is a rectangular strip with sides dy and dz, as shown in figure 6. Then

$$dS_x = dy\ dz = dS\ (\hat{n}\cdot\hat{i}) \tag{5.4}$$

so that

$$dS = \frac{dy\ dz}{x}\left[\ x^2 + \frac{(y+h)^2}{c^4} + \frac{z^2}{b^4}\ \right]^{1/2} \ . \tag{5.5}$$

Note that dy and dz are increments in the coordinates obtained by moving along the surface. Therefore if z were held fixed and y alone varied, then from (5.1)

$$dy = -c \sin\phi\ d\phi \quad . \tag{5.6}$$

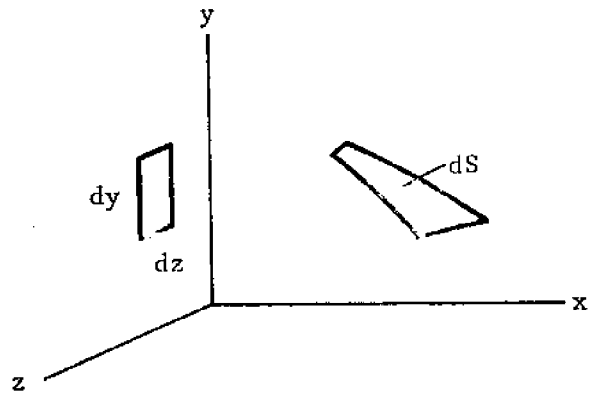

Figure 6. Determination of dS.

Similarly if y were held fixed and z alone varied,

$$dz = b \cos \alpha \sin \phi \, d\alpha \quad . \tag{5.7}$$

Therefore, on substitution into (5.5), and simplification, we have

$$dS = - bc \sin \phi \, T(\alpha,\phi) \, d\phi \, d\alpha \tag{5.8}$$

where

$$T(\alpha,\phi) = \left[\left(\cos^2\alpha + \frac{\sin^2\alpha}{b^2}\right) \sin^2\phi + \frac{\cos^2\phi}{c^2} \right]^{1/2} \quad . \tag{5.9}$$

Since we are using the convention that (α,ϕ) is a particular point, and (β,ψ) any general point, on the surface S, the coordinates α and ϕ will be replaced by β and ψ, respectively, in the expression for dS to yield

$$dS = -bc \sin \psi \, T(\beta,\psi) \, d\psi \, d\beta \quad . \tag{5.8'}$$

The integral equation (3.27) can now be transformed, using the new coordinates, as

$$-f_j(\alpha,\phi) + \frac{bc}{2\pi} \int_{\beta=0}^{2\pi} \int_{\psi=0}^{\pi/2} f_j(\beta,\psi) \frac{\partial G}{\partial n}(\alpha,\phi;\beta,\psi)\, T(\beta,\psi) \sin\psi \, d\psi \, d\beta$$

$$= 2\, H_j(\alpha,\phi) \qquad (5.10)$$

where the functions $H_j(\alpha,\phi)$ are to be obtained from the functions $h_j(x,y,z)$ given in (2.26) by transformation of coordinates. The new notation is introduced to avoid confusion with the relative depth h when the subscript j is dropped in subsequent sections.

From (5.3), in terms of the new coordinates,

$$\hat{n} = \frac{1}{T(\alpha,\phi)} \left[i \cos\alpha \sin\phi + \hat{j} \frac{\cos\phi}{c} + \hat{k} \frac{\sin\alpha \sin\phi}{b} \right] . \qquad (5.11)$$

Therefore the functions $h_j(x,y,z)$ given in (2.26) transform as follows:

$$H_1(\alpha,\phi) = \frac{\cos\alpha \sin\phi}{T(\alpha,\phi)} , \quad H_2(\alpha,\phi) = \frac{\cos\phi}{c\, T(\alpha,\phi)}$$

$$H_3(\alpha,\phi) = \frac{\sin\alpha \sin\phi}{b\, T(\alpha,\phi)} , \quad H_4(\alpha,\phi) = \frac{c^2-b^2}{bc} \frac{\sin\alpha \sin\phi \cos\phi}{T(\alpha,\phi)} \qquad (5.12)$$

$$H_5(\alpha,\phi) = \frac{b^2-1}{b} \frac{\sin\alpha \cos\alpha \sin^2\phi}{T(\alpha,\phi)} , \quad H_6(\alpha,\phi) = \frac{1-c^2}{c} \frac{\cos\alpha \sin\phi \cos\phi}{T(\alpha,\phi)}$$

$$H_7(\alpha,\phi) = \frac{e^{ia \cos\alpha \sin\phi}}{T(\alpha,\phi) \cosh ah} \left[\frac{\cos\phi}{c} \sinh(ac \cos\phi) \right.$$

$$\left. + i \cos\alpha \sin\phi \cosh(ac \cos\phi) \right] .$$

6. NUMERICAL PROCEDURE FOR A SEMIELLIPSOID

In this section the numerical procedure for a semiellipsoid is first outlined briefly and then details of the procedure are given. Since additional subscripts are introduced in this section, the subscript j, which corresponds to the mode of oscillation or scatter, is dropped from u_j, f_j and H_j in this section and Section 7. Note that the procedures given hereafter are applied only to the four problems corresponding to surge, heave, pitch and scatter (j=1,2,6 and 7, respectively).

Outline of the Procedure

The approach to the numerical solution of the integral equation (5.10) mainly consists of replacing the integral equation by a finite set of linear equations. Since only two ellipsoidal coordinates are needed to represent a point on the surface S, we may imagine a two-dimensional surface $S(\beta,\psi)$ on the (β,ψ)-plane corresponding to the three-dimensional surface $S(\xi,\eta,\zeta)$ (refer figure 7). The surface $S(\beta,\psi)$ is actually a rectangle with sides of length 2π and $\pi/2$ respectively. It is next divided into a grid of $4N^2$ squares with sides of length $s=\pi/2N$, parallel to the β and ψ axes respectively, where N is a suitably chosen positive integer. Thus N characterizes the grid size, a smaller N indicating a coarser grid and a larger N, a finer grid. The centers of the various squares are called "nodal" or "pivotal points." We attempt

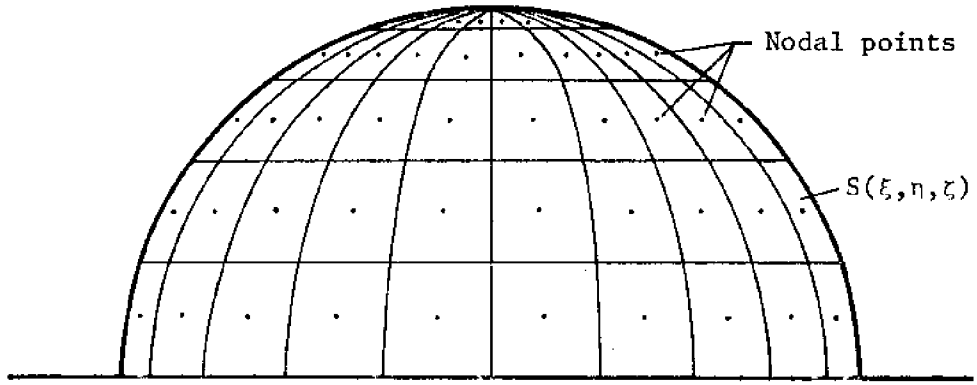

(a) Numerical grid in three dimensions.

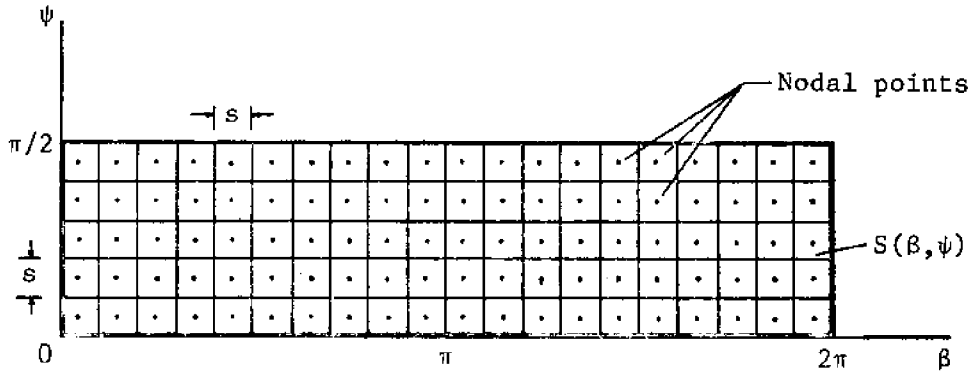

(b) Numerical grid in (β,ψ)-plane.

Figure 7. Numerical grid for N=5.

to satisfy the integral equation at only the $4N^2$ nodal points instead of all the points of the surface of the semiellipsoid. A unique index k is associated with any particular nodal point (α,ϕ) and the square element surrounding it, and another index ℓ with any general nodal point (β,ψ) and the square element surrounding it.

For example, the coordinates of the nodal point k are denoted by α_k and ϕ_k, and those for the nodal point ℓ by β_ℓ and ψ_ℓ, respectively. While k and ℓ may assume integer values from 1 to $4N^2$, α_k and β_ℓ may each assume only 4N unique values. Similarly, ϕ_k and ψ_ℓ may each assume only N unique values.

Since the distribution function $f(\beta,\psi)$ is well-behaved, we may assume that its average value over each square element is approximately equal to the value at the nodal point of the element. Thus the integral equation (5.10) is now rewritten as a set of $4N^2$ linear equations as follows:

$$-f_k + \sum_{\ell=1}^{4N^2} f_\ell \, K_{k\ell} = 2H_k \quad , \quad k=1,2,3,\ldots,4N^2 \quad , \tag{6.1}$$

where

$$f_k = f(\alpha_k,\phi_k) \quad , \qquad \text{(a)} \tag{6.2}$$

$$f_\ell = f(\beta_\ell,\psi_\ell) \quad , \qquad \text{(b)}$$

$$K_{k\ell} = \frac{bc}{2\pi} \int_{\beta_\ell - \frac{s}{2}}^{\beta_\ell + \frac{s}{2}} \int_{\psi_\ell - \frac{s}{2}}^{\psi_\ell + \frac{s}{2}} \frac{\partial G}{\partial n}(\alpha_k,\phi_k;\beta,\psi)\; T(\beta,\psi) \sin\psi \; d\psi \; d\beta \quad , \tag{6.3}$$

and

$$H_k = H(\alpha_k,\phi_k) \quad . \tag{6.4}$$

Equation (6.1) may now be set up as a matrix equation. Thus

$$[K_{k\ell} - \delta_{k\ell}]\ [f_\ell] = [2H_k] \tag{6.5}$$

where $\delta_{k\ell}$ is the Kronecker delta function defined such that

$$\begin{aligned} \delta_{k\ell} &= 1 \text{ for } k = \ell \\ &= 0 \text{ for } k \neq \ell. \end{aligned} \tag{6.6}$$

Note that the first matrix on the left hand side of (6.5) is a square matrix. Its elements may be computed numerically from (6.3) since G is known from (3.19). The other two matrices in the equation are column matrices. Of these, the elements of $[2H_k]$ can be computed from (5.12) so that $[f_\ell]$ is the only unknown. On solving (6.5) by a special computer subroutine for the unknown distribution function, we obtain the values of f at the nodal points as

$$[f_\ell] = [K_{k\ell} - \delta_{k\ell}]^{-1}\ [2H_k]\ . \tag{6.7}$$

Once the distribution function is known, the velocity potential u may be obtained from the representation (3.17), which may be written in ellipsoidal coordinates as

$$u(\alpha,\phi) = \frac{bc}{4\pi} \int_{\beta=0}^{2\pi} \int_{\psi=0}^{\pi/2} f(\beta,\psi)\ G(\alpha,\phi;\beta,\psi)\ T(\beta,\psi)\ \sin\psi\ d\psi\ d\beta\ . \tag{6.8}$$

As far as the determination of the pressures, forces, etc., is concerned, we saw in Section 4 that it is necessary to know the velocity potential u only on the surface of the ellipsoid. In the numerical procedure u is determined at only the nodal points of the surface instead of all the points. Following the same indicial notation as before, we write (6,8) as

$$u_k = \sum_{\ell=1}^{4N^2} f_\ell \, M_{k\ell} \ , \quad k=1,2,3,\ldots,4N^2 \ , \tag{6.9}$$

where

$$u_k = u(\alpha_k, \phi_k) \ , \tag{6.10}$$

and

$$M_{k\ell} = \frac{bc}{4\pi} \int_{\beta_\ell - \frac{s}{2}}^{\beta_\ell + \frac{s}{2}} \int_{\psi_\ell - \frac{s}{2}}^{\psi_\ell + \frac{s}{2}} G(\alpha_k, \phi_k; \beta, \psi) \ T(\beta, \psi) \sin\psi \, d\psi \, d\beta \ . \tag{6.11}$$

Equation (6.9) may be rewritten as a matrix equation. Thus

$$[u_k] = [M_{k\ell}] \ [f_\ell] \ . \tag{6.12}$$

The elements of the square matrix $M_{k\ell}$ may be computed numerically from (6.11) since G is known from (3.19). The column matrix f_ℓ is already given by (6,7). Therefore the velocity potential, u, corresponding to the nodal points is obtained from (6.12) as a

column matrix, by matrix multiplication. Once u is known, the physical quantities of interest such as pressures, forces, etc., may be obtained numerically, using the relations given in Section 4.

The numerical procedure for the problem, applied in a straightforward manner, has been explained so far. In practice this procedure is somewhat modified. For a semiellipsoid, the distribution function f is symmetric about the (x,y)-plane in all four cases. Even greater symmetry exists for f in the case of the three radiation problems, but is not utilized in this dissertation since the radiation and scatter problems are solved simultaneously, using a common numerical procedure. In view of the symmetry of f, it is necessary to solve the integral equation over only half of the surface S. The resulting modifications in the numerical procedure are explained later on.

The rest of this section is devoted mainly to the numerical evaluation of the matrix elements $K_{k\ell}$ and $M_{k\ell}$ which involve $\partial G/\partial n$ and G, respectively. Because $\partial G/\partial n$ and G are quite similar, we consider them simultaneously, where necessary.

Matrix Elements $M_{k\ell}$

We use for G the form (3.19) which is rewritten here, for convenience, as

$$G(x,y,z;\xi,\eta,\zeta) = \frac{1}{R} + \frac{1}{R'} + G^{**}(x,y,z;\xi,\eta,\zeta) \qquad (6.13)$$

where

$$G^{**}(x,y,z;\xi,\eta,\zeta) \equiv 2\ PV \int_{\kappa=0}^{\infty} \frac{(\kappa+\nu)\ e^{-\kappa h} \cosh \kappa(\eta+h)}{(\kappa \sinh \kappa h-\nu \cosh \kappa h)}$$

$$\cosh \kappa(y+h)\ J_0(\kappa r_1)\ d\kappa$$

$$+ i\ \frac{2\pi(a^2-\nu^2) \cosh a(\eta+h) \cosh a(y+h)}{a^2h - \nu^2h + \nu} J_0(ar_1) \ . \qquad (6.14)$$

As mentioned previously, 1/R becomes singular as the point (ξ,η,ζ) approaches (x,y,z) and, in general, varies rapidly in the neighbourhood of (x,y,z). On the other hand, 1/R' and G** are both regular everywhere. However, the former varies rapidly whereas the latter varies slowly. In view of these features the three parts of the Green's function in (6.13) are integrated separately, using different methods. We take up these three integrals, one by one, next.

In terms of the ellipsoidal coordinates, R may be written from (3.20) as

$$R(\alpha,\phi;\beta,\psi) = [(\cos \alpha \sin \phi-\cos \beta \sin \psi)^2 + c^2(\cos \phi-\cos\psi)^2$$

$$+ b^2(\sin \alpha \sin \phi-\sin \beta \sin \psi)^2]^{1/2} \ . \qquad (6.15)$$

Because of the rapidly varying nature of 1/R, for purposes of accuracy, a nine point Simpson's method is used to integrate 1/R

over all the elements ℓ except the element $\ell=k$. Thus we approximate the surface integral over the element ℓ as

$$\frac{bc}{4\pi}\int_{\beta_\ell-\frac{s}{2}}^{\beta_\ell+\frac{s}{2}}\int_{\psi_\ell-\frac{s}{2}}^{\psi_\ell+\frac{s}{2}} \frac{1}{R(\alpha_k,\phi_k;\beta,\psi)}\,T(\beta,\psi)\,\sin\psi\,d\psi\,d\beta$$

$$\approx \frac{bcs^2}{144\pi}\sum_{p=1}^{3}\sum_{q=1}^{3}\frac{C_p\,D_q}{R(\alpha_k,\phi_k;\beta_p,\psi_q)}\,T(\beta_p,\psi_q)\,\sin\psi_q$$

(valid for $\ell \neq k$) (6.16)

where β_p and ψ_q are defined for the ℓ-th element as

$$\beta_p = \beta_\ell + (p-2)\frac{s}{3}, \quad p=1,2,3, \quad \text{(a)}$$

$$\psi_q = \psi_\ell + (q-2)\frac{s}{3}, \quad q=1,2,3, \quad \text{(b)} \qquad (6.17)$$

and the Simpson's numerical coefficients C_p and D_q are given by

$$C_1 = C_3 = D_1 = D_3 = 1, \text{ and}$$

$$C_2 = D_2 = 4\ . \qquad (6.18)$$

The numerical method given above breaks down for the singular element (case $\ell=k$) since, close to the singularity, the 1/R term tends to infinity. Therefore a different scheme has to be used for evaluating the surface integral on the left hand side of (6.16)

for such cases. Such a scheme is described in a subsequent paragraph.

As for the second integral in $M_{k\ell}$, since $1/R'$ varies rapidly, we evaluate its surface integral also, by a nine point Simpson's method, in a manner similar to that given in (6.16). Note that in ellipsoidal coordinates R' is given from (3.21) as

$$R'(\alpha,\phi;\beta,\psi) = [(\cos\alpha \sin\phi - \cos\beta \sin\psi)^2 + c^2(\cos\phi+\cos\psi)^2 + b^2(\sin\alpha \sin\phi - \sin\beta \sin\psi)^2]^{1/2} \quad (6.19)$$

and that since $1/R'$ is regular everywhere, the Simpson's method is valid for all ℓ.

As for the third integral in $M_{k\ell}$, since G^{**} is not only regular everywhere, but also varies slowly, its surface integral over any element ℓ is approximated by multiplying the value of the integrand at the nodal point (β_ℓ,ψ_ℓ) by the area of the element. Thus

$$\frac{bc}{4\pi}\int_{\beta_\ell-\frac{s}{2}}^{\beta_\ell+\frac{s}{2}}\int_{\psi_\ell-\frac{s}{2}}^{\psi_\ell+\frac{s}{2}} G^{**}(\alpha_k,\phi_k;\beta,\psi)\, T(\beta,\psi) \sin\psi \, d\psi \, d\beta$$

$$\simeq \frac{bcs^2}{4\pi} G^{**}(\alpha_k,\phi_k;\beta_\ell,\psi_\ell)\, T(\beta_\ell,\psi_\ell) \sin\psi_\ell,$$

(valid for all ℓ) (6.20)

where in terms of the new coordinates

$$G^{**}(\alpha,\phi;\beta,\psi) = 2\,PV \int_{\kappa=0}^{\infty} \frac{(\kappa+\nu)\, e^{-\kappa h} \cosh(\kappa c \cos\psi)}{(\kappa \sinh \kappa h - \nu \cosh \kappa h)}$$

$$\cosh(\kappa c \cos\phi)\, J_0(\kappa r_1)\, d\kappa$$

$$+ i\, \frac{2\pi(a^2-\nu^2) \cosh(ac\cos\psi) \cosh(ac\cos\phi)}{a^2h-\nu^2h+\nu} J_0(ar_1) \qquad (6.21)$$

and r_1 is obtained from (3.22) as

$$r_1(\alpha,\phi;\beta,\psi) = [(\cos\alpha \sin\phi - \cos\beta \sin\psi)^2$$

$$+ b^2(\sin\alpha \sin\phi - \sin\beta \sin\psi)^2]^{1/2} . \qquad (6.22)$$

We note here that the numerical integration of the infinite integral in (6.21) poses certain problems. These are discussed in a subsequent paragraph.

Matrix Elements $K_{k\ell}$

Following a procedure similar to that used for G, we rewrite $\partial G/\partial n$ occurring in (6.3) as

$$\frac{\partial G}{\partial n} = \frac{\partial}{\partial n}\left(\frac{1}{R}\right) + \frac{\partial}{\partial n}\left(\frac{1}{R'}\right) + \frac{\partial}{\partial n} G^{**} . \qquad (6.23)$$

The three terms on the right will be integrated separately. Noting that the normal derivative is taken at the point (α,ϕ), it may be

shown from the expression for R given in (3.20), after considerable simplification, that

$$\frac{\partial}{\partial n}\left(\frac{1}{R}\right)(\alpha,\phi;\beta,\psi) = -\frac{1}{R^3\, T(\alpha,\phi)}\,[1-\cos(\alpha-\beta)\,\sin\beta\,\sin\psi$$

$$-\cos\phi\,\cos\psi]\ . \qquad (6.24)$$

Since $1/R^3$ varies rapidly, we use the nine point Simpson's method for numerical integration of $\partial(1/R)/\partial n$ for all elements ℓ except $\ell=k$. In the latter case, an alternate numerical scheme is used. It is described in a subsequent paragraph.

From (3.21) the normal derivative of $1/R'$ at any point (α,ϕ) can be shown to be given by

$$\frac{\partial}{\partial n}\left(\frac{1}{R'}\right)(\alpha,\phi;\beta,\psi) = -\frac{1}{R'^3\, T(\alpha,\phi)}\,[1-\cos(\alpha-\beta)\,\sin\beta\,\sin\psi$$

$$+\cos\phi\,\cos\psi]\ . \qquad (6.25)$$

Note that the expression on the right is regular everywhere. Moreover, since $1/R'^3$ varies rapidly, we use the nine point Simpson's method for integration of $\partial(1/R')/\partial n$ for all elements ℓ.

In terms of ellipsoidal coordinates, $\partial G^{**}/\partial n$ at any point (α,ϕ) is given by

$$\frac{\partial G^{**}}{\partial n}(\alpha,\phi;\beta,\psi) = -2\,PV\int_{\kappa=0}^{\infty} \frac{\kappa(\kappa+\nu)\,e^{-\kappa h}\cosh(\kappa c\cos\psi)}{(\kappa\sinh\kappa h-\nu\cosh\kappa h)\,T(\alpha,\phi)}$$

$$\left[\{\sin^2\phi - \cos(\alpha-\beta)\sin\phi\sin\psi\}\cosh(\kappa c\cos\phi)\,\frac{J_1(\kappa r_1)}{r_1}\right.$$

$$\left. -\frac{\cos\phi}{c}\sinh(\kappa c\cos\phi)\,J_0(\kappa r_1)\right]d\kappa$$

$$-i\,\frac{2\pi a(a^2-\nu^2)\cosh(ac\cos\psi)}{(a^2h-\nu^2h+\nu)\,T(\alpha,\phi)}\left[\{\sin^2\phi\right.$$

$$\left. -\cos(\alpha-\beta)\sin\phi\sin\psi\}\cosh(ac\cos\phi)\,\frac{J_1(ar_1)}{r_1}\right.$$

$$\left. -\frac{\cos\phi}{c}\sinh(ac\cos\phi)\,J_0(ar_1)\right]. \qquad (6.26)$$

Since $\partial G^{**}/\partial n$ is, like G^{**}, regular everywhere and varies slowly, we approximate the surface integral corresponding to it, over any element ℓ, by the product of the surface area of the element and the value of the integrand at the nodal point (β_ℓ,ψ_ℓ). For the case $\ell=k$, note that as $r_1 \to 0$, $J_1(\kappa r_1)/r_1$ and $J_1(ar_1)/r_1$ tend to $\kappa/2$ and $a/2$ respectively, whereas $J_0(\kappa r_1)$ and $J_0(ar_1)$ tend to unity. Also, the integral in (6.26) poses numerical problems similar to those for the integral in (6.21). So the two integrals are evaluated by using the same methods.

Special Scheme for Integrating 1/R and $\partial(1/R)/\partial n$ over the Singular Element (case $\ell=k$)

It was indicated previously that Simpson's method cannot be used for the singular element containing the nodal point (α_k,ϕ_k), i.e. for the case, $\ell=k$. This is because even though the integrals are finite, the 1/R and $\partial(1/R)/\partial n$ terms become singular as (β,ψ) approaches (α_k,ϕ_k) and pose problems in numerical integration. The integrals in these cases are "improper" and have to be treated by a special scheme. Kim (1964a; Appendix) has given in detail a method for treating such integrals. Therefore only the idea behind the scheme and the final results are indicated here briefly.

For each of the integrals mentioned, by using Taylor's series expansion around the singular point (α_k,ϕ_k) and binomial expansion, we can show that the integrand consists mainly of three parts: (i) a singular part which varies as $1/\delta$ where δ is the distance in the (β,ψ)-plane between the points (β,ψ) and (α_k,ϕ_k), (ii) an indeterminate part which depends on the angle of approach from (β,ψ) to (α_k,ϕ_k), i.e. on $(\psi-\phi_k)/(\beta-\alpha_k)$, and (iii) terms of higher order. One of the reasons for the complexity of the problem is that the surface S(x,y,z) of the object is curved and not plane in the neighborhood of the singularity. In order to overcome the numerical problems and obtain good accuracy, parts (i) and (ii) are integrated by using a special scheme of plane polar coordinates

valid around the singularity. The higher order terms, on the other hand, are separated and integrated using Simpson's nine point method, noting that they vanish when $(\beta,\psi) = (\alpha_k,\phi_k)$.

The final results of the special scheme are given as follows. The integral of (1/R) for the case $\ell=k$ is evaluated as

$$I_1 = \frac{bc}{4\pi} \int_{\alpha_k - \frac{s}{2}}^{\alpha_k + \frac{s}{2}} \int_{\phi_k - \frac{s}{2}}^{\phi_k + \frac{s}{2}} \frac{1}{R(\alpha_k,\phi_k;\beta,\psi)}\, T(\beta,\psi)\, \sin\psi\, d\psi\, d\beta$$

$$\approx \frac{bcs^2}{16\pi} \left\{ \frac{4}{s} \sin\phi_k\, T(\alpha_k,\phi_k) \right.$$

$$\left[\int_{-\pi/4}^{\pi/4} \frac{|\sec\tau|\, d\tau}{[E(\cos\tau, \sin\tau)+c^2 \sin^2\tau \sin^2\phi_k]^{1/2}} \right.$$

$$\left. + \int_{\pi/4}^{3\pi/4} \frac{|\csc\tau|\, d\tau}{[E(\cos\tau, \sin\tau)+c^2 \sin^2\tau \sin^2\phi_k]^{1/2}} \right]$$

$$+ \sum_{p=1}^{3} \sum_{q=1}^{3} \frac{C_p D_q}{9} \left[\frac{1}{R(\alpha_k,\phi_k;\beta_p,\psi_q)} \right.$$

$$\left. - \frac{1}{[E(\beta_p-\alpha_k,\psi_q-\phi_k)+c^2 (\psi_q-\phi_k)^2 \sin^2\phi_k]^{1/2}} \right]$$

$$\left. T(\beta_p,\psi_q) \sin\psi_q \right\} \qquad (6.27)$$

where

$$E(\Delta\alpha,\Delta\phi) \equiv (\Delta\alpha \sin\alpha \sin\phi - \Delta\phi \cos\alpha \cos\phi)^2$$

$$+ b^2(\Delta\alpha \cos\alpha \sin\phi + \Delta\phi \sin\alpha \cos\phi)^2 \ . \qquad (6.28)$$

Equation (6.27) is the counterpart of (6.16), valid for the case $\ell=k$.

Similarly, the integral of $\partial(1/R)/\partial n$ for the case $\ell=k$ is evaluated as

$$I_2 = \frac{bc}{2\pi} \int_{\alpha_k - \frac{s}{2}}^{\alpha_k + \frac{s}{2}} \int_{\phi_k - \frac{s}{2}}^{\phi_k + \frac{s}{2}} \frac{\partial}{\partial n}\left(\frac{1}{R}\right) T(\beta,\psi) \sin\psi \, d\psi \, d\beta$$

$$\approx -\frac{bcs^2}{8\pi} \left\{ \frac{2}{s} \sin\phi_k \right.$$

$$\left[\int_{-\pi/4}^{\pi/4} \frac{|\sec\tau| \ (\cos^2\tau \sin^2\phi_k + \sin^2\tau) \, d\tau}{[E(\cos\tau, \sin\tau) + c^2 \sin^2\tau \sin^2\phi_k]^{3/2}} \right.$$

$$\left. \left. + \int_{\pi/4}^{3\pi/4} \frac{|\csc\tau| \ (\cos^2\tau \sin^2\phi_k + \sin^2\tau) \, d\tau}{[E(\cos\tau, \sin\tau) + c^2 \sin^2\tau \sin^2\phi_k]^{3/2}} \right] \right.$$

$$+ \sum_{p=1}^{3} \sum_{q=1}^{3} \frac{C_p D_q}{9} \left[\frac{1}{[R(\alpha_k,\phi_k;\beta_p,\psi_q)]^3} \right.$$

$$[1-\cos(\alpha_k-\beta_p)\ \sin\phi_k\ \sin\psi_q - \cos\phi_k\ \cos\psi_q]$$

$$-\frac{1}{2}\frac{(\beta_p-\alpha_k)^2\ \sin^2\phi_k + (\psi_q-\phi_k)^2}{[E(\beta_p-\alpha_k,\psi_q-\phi_k)+c^2\ (\psi_q-\phi_k)^2\ \sin^2\phi_k]^{3/2}}\Bigg]$$

$$\frac{T(\beta_p,\psi_q)}{T(\alpha_k,\phi_k)}\ \sin\psi_q\Bigg\}\ . \qquad (6.29)$$

Note that corresponding to p = q = 2, the integrand in the Simpson's formula is set to zero, in the numerical procedure.

In (6.27) and (6.29), for the integrals involving τ, the integrands become indeterminate at the midpoint of each integration range and pose a problem in numerical evaluation, even though the integrals are finite. To avoid this, the τ-integration is carried out to within 1% accuracy, using Simpson's three-eighths rule. Details of this method are given in connection with the infinite integrals.

Numerical Evaluation of the Infinite Integrals in G** and $\partial G^{**}/\partial n$

As indicated previously, the infinite integrals in G** and $\partial G^{**}/\partial n$ pose certain numerical problems. In each case, the denominator of the integrand tends to zero when $\kappa \to \kappa_0$ where κ_0 is the solution of the equation

$$\kappa \tanh(\kappa h) - \nu = 0. \tag{6.30}$$

(Since $\nu = a \tanh(ah)$, note that κ_0 is equal to a.) In view of this, the principal value of the integral must be taken. Moreover, the upper limit of the integral is infinite, so that for numerical purposes it has to be replaced by a suitably large number such that convergence is assured. The procedures used in overcoming these problems are described briefly next. They are taken directly from Monacella (1966).

The singularity $\kappa = \kappa_0$. The basic idea of the procedure consists in recognizing that the integrands are singular like $1/(\kappa-\kappa_0)$, subtracting out the singularity $1/(\kappa-\kappa_0)$ and then integrating the singularity analytically and the rest of the integral numerically. Consider first the integral in G**. If it is denoted by I_3, then from (6.21)

$$I_3 = PV \int_{\kappa=0}^{\infty} \frac{(\kappa+\nu)\, e^{-\kappa h} \cosh(\kappa c \cos\psi) \cosh(\kappa c \cos\phi)}{(\kappa \sinh \kappa h - \nu \cosh \kappa h)} J_0(\kappa r_1)\, d\kappa \quad . \tag{6.31}$$

Note that as far as the integration is concerned, the integrands are functions of κ only since everything else is fixed. Therefore, for convenience, we define

$$P_1(\kappa) = (\kappa+\nu)\ e^{-\kappa h}\ \cosh(\kappa c \cos\psi)\ \frac{\cosh(\kappa c \cos\phi)}{\cosh(\kappa h)}\ J_0(\kappa r_1)\ , \quad (6.32)$$

and

$$Q_1(\kappa) = \frac{P_1(\kappa)\ (\kappa-\kappa_0)}{\kappa\ \tanh(\kappa h)-\nu}\ . \quad (6.33)$$

The integral I_3 may now be rewritten as

$$I_3 = PV \int_{\kappa=0}^{\infty} \frac{Q_1(\kappa)}{\kappa-\kappa_0}\ d\kappa$$

$$= \int_0^{2\kappa_0} \frac{Q_1(\kappa)-Q_1(\kappa_0)}{\kappa-\kappa_0}\ d\kappa + Q_1(\kappa_0)\left[\ PV \int_{\kappa=0}^{2\kappa_0} \frac{d\kappa}{\kappa-\kappa_0}\ \right]$$

$$+ \int_{2\kappa_0}^{\infty} \frac{Q_1(\kappa)}{\kappa-\kappa_0}\ d\kappa\ . \quad (6.34)$$

As $\kappa \to \kappa_0$, both the numerator and the denominator of the first integral on the right vanish so that it becomes indeterminate, but not singular. It is finite and its value can be established by l'Hospital's rule, if necessary. The integrand of the second integral becomes singular at this point and therefore the principal value of the integral has to be taken. As for the third integral, since the singularity $\kappa=\kappa_0$ is outside the integration range, there is no problem involved in numerical evaluation.

Let us now consider the second integral. By definition,

$$PV \int_{\kappa=0}^{2\kappa_0} \frac{d\kappa}{\kappa-\kappa_0} = \lim_{\varepsilon\to 0} \left[\int_0^{\kappa_0-\varepsilon} \frac{d\kappa}{\kappa-\kappa_0} + \int_{\kappa_0+\varepsilon}^{2\kappa_0} \frac{d\kappa}{\kappa-\kappa_0} \right] . \qquad (6.35)$$

On carrying out the integrations, setting the limits, and simplifying, we have the result

$$PV \int_{\kappa=0}^{2\kappa_0} \frac{d\kappa}{\kappa-\kappa_0} = 0 . \qquad (6.36)$$

Therefore

$$I_3 = \int_{\kappa=0}^{2\kappa_0} \frac{Q_1(\kappa)-Q_1(\kappa_0)}{\kappa-\kappa_0} d\kappa + \int_{2\kappa_0}^{\infty} \frac{Q_1(\kappa)}{\kappa-\kappa_0} d\kappa . \qquad (6.37)$$

Thus the singularity $\kappa=\kappa_0$ is removed and both the remaining integrals are well-behaved, and can be numerically evaluated.

We next determine $Q_1(\kappa_0)$ by using l'Hospital's rule as

$$Q_1(\kappa_0) = \lim_{\kappa\to\kappa_0} \frac{P_1(\kappa)\ (\kappa-\kappa_0)}{\kappa\ \tanh(\kappa h)-\nu}$$

$$= \frac{P_1(\kappa_0)\ \kappa_0}{h[\kappa_0^2-\nu^2+\nu]} . \qquad (6.38)$$

If the infinite integral in $\partial G^{**}/\partial n$ is denoted by I_4, then by following a procedure similar to that for I_3, we may obtain for I_4 the final result

$$I_4 = \int_{\kappa=0}^{2\kappa_0} \frac{Q_2(\kappa)-Q_2(\kappa_0)}{\kappa-\kappa_0} d\kappa + \int_{2\kappa_0}^{\infty} \frac{Q_2(\kappa)}{\kappa-\kappa_0} d\kappa \qquad (6.39)$$

where

$$Q_2(\kappa) = \frac{P_2(\kappa)\ (\kappa-\kappa_0)}{\kappa\ \tanh(\kappa h)-\nu} \quad , \tag{6.40}$$

$$P_2(\kappa) = \frac{\kappa(\kappa+\nu)\ e^{-\kappa h}}{T(\alpha,\phi)} \frac{\cosh(\kappa c \cos\ \psi)}{\cosh\ (\kappa h)} \left[\{\sin^2\phi \right.$$

$$- \cos(\alpha-\beta)\ \sin\ \phi\ \sin\ \psi\}\ \cosh(\kappa c \cos\ \phi)\ \frac{J_1(\kappa r_1)}{r_1}$$

$$\left. - \frac{\cos\ \phi}{c}\ \sinh(\kappa c \cos\ \phi)\ J_0(\kappa r_1) \right] \quad , \tag{6.41}$$

and

$$Q_2(\kappa_0) = \frac{P_2(\kappa_0)\ \kappa_0}{h[\kappa_0^{\ 2}-\nu^2+\nu]} \quad . \tag{6.42}$$

Numerical integration of the integrals, I_3 and I_4. We first consider the integration of the finite integral in (6.37) and (6.39) and then pass on to the infinite integral. Since the integrals I_3 and I_4 are similar in form, the procedure is given for I_3 only.

The integrand in the finite integral in (6.37) becomes indeterminate as $\kappa \to \kappa_0$, even though the value of the integral is finite. This poses a problem in numerical integration. In order to overcome the same, Simpson's three-eighths rule is used. In this procedure, it is not necessary to evaluate the integrand at $\kappa=\kappa_0$, because the ordinate there is never used in the integration.

The integration range (0 to $2\kappa_0$) is divided into 6n+3 equal intervals where n is a suitably chosen positive integer, usually 1 to start with. The integrand is evaluated at the ends of each interval and the integral is determined from the weighted average of the 6n+4 ordinates. The number of intervals are next increased by 6, the calculation is repeated and the final result is compared with that obtained previously, to see if the two results are sufficiently close, as determined by a suitably chosen convergence criterion. If they are, the process is stopped and the second result is assumed to be the value of the integral. If not, the iteration process is continued until the results at the beginning and end of an iteration satisfy the convergence criterion. Then the result at the end of the last iteration is assumed to be the value of the integral. In either case, the interval $\Delta\kappa=\Delta\kappa_0$ that provides convergence is stored for future use in connection with the infinite integral.

The main problem with the integral with an infinite upper limit is to carry out the numerical integration up to a suitably large number (as an upper limit) such that convergence is ensured. For this purpose the following scheme is adopted. The integral is written in the form

$$\int_{2\kappa_0}^{\infty} \frac{Q_1(\kappa)}{\kappa \tanh \kappa h - \nu} d\kappa = \sum_{n=1}^{\infty} I_n \qquad (6.43)$$

where

$$I_n = \int_{\kappa_n}^{\kappa_{n+1}} \frac{Q_1(\kappa)}{\kappa \tanh \kappa h - \nu} \, d\kappa \quad , \tag{6.44}$$

and

$$\kappa_1 = 2\kappa_0 \text{ and } \kappa_{n+1} = \kappa_n + \mu, \quad n=1,2,3,\ldots$$

μ is chosen as follows. If $1 \leq 2\Delta\kappa_0$, μ is chosen to be $2\Delta\kappa_0$. If $1 > 2\Delta\kappa_0$, μ is chosen to be the highest integral multiple of $2\Delta\kappa_0$ that is less than one. Here $\Delta\kappa_0$ is the mesh size that has given convergence for the finite integral. Each of the integrals I_n is evaluated by the usual Simpson's one-third rule using the mesh size $\Delta\kappa_0$. The partial sum $S_M = \sum_{n=1}^{M} I_n$ is assumed to be the value of the infinite integral, where M is chosen such that the ratio $|I_M/S_{M-1}|$ is less than a suitably chosen convergence criterion.

The actual convergence criteria used in obtaining the results are as follows. In the case of the finite integrals between the limits $\kappa=0$ and $2\kappa_0$, if the value of the integral obtained by using 6n+4 ordinates is denoted by I(n), the convergence criterion used is that

$$\left|\frac{I(n+1)-I(n)}{I(n)}\right| \leq 1\% \; . \tag{6.45}$$

Similarly in the case of the infinite integrals, the criterion used is that

$$\left|\frac{I_M}{S_{M-1}}\right| \leq 1\% \tag{6.46}$$

with the notation previously defined. Since these criteria are arbitrary, to determine their effect on convergence, the accuracy was changed in a few cases to 0.5% and the final results were compared. Negligible differences were found in the final results due to the change. Thus we are assured of the convergence of the integrals as well as the accuracy of the results obtained with the criteria given in (6.45) and (6.46).

Symmetry in the Case of a Semiellipsoid

As previously mentioned, the distribution function f is symmetric about the (ξ,η)-plane for the four problems being considered. This symmetry may be expressed as

$$f(\beta,\psi) = f(-\beta,\psi) \ . \tag{6.47}$$

As a result, it is necessary to find the distribution function f over only one half of the surface $S(\beta,\psi)$, say, the half for which $0 \leq \beta \leq \pi$. Therefore in the numerical scheme for finding f we have to consider only $2N^2$ linear equations instead of $4N^2$ equations.

Since $T(\beta,\psi)$ is even in β, we may, using (6.47), write

$$\frac{bc}{2\pi}\int_{\beta=0}^{2\pi}\int_{\psi=0}^{\pi/2} f(\beta,\psi)\,\frac{\partial G}{\partial n}(\alpha,\phi;\beta,\psi)\,T(\beta,\psi)\,\sin\psi\,d\psi\,d\beta$$

$$= \frac{bc}{2\pi}\int_{\beta=0}^{\pi}\int_{\psi=0}^{\pi/2} f(\beta,\psi)\left[\frac{\partial G}{\partial n}(\alpha,\phi;\beta,\psi) + \frac{\partial G}{\partial n}(\alpha,\phi;-\beta,\psi)\right]$$

$$T(\beta,\psi)\,\sin\psi\,d\psi\,d\beta\,. \qquad (6.48)$$

The physical interpretation of (6.48) is that at any point (α,ϕ) the effects of a source at (β,ψ) and another source at $(-\beta,\psi)$ are considered simultaneously. The second source is the mirror image of the first in the (ξ,η)-plane.

Similarly, the representation (6.8) for the velocity potential at (α,ϕ) may be rewritten as

$$u(\alpha,\phi) = \frac{bc}{4\pi}\int_{\beta=0}^{\pi}\int_{\psi=0}^{\pi/2} f(\beta,\psi)\,[G(\alpha,\phi;\beta,\psi) + G(\alpha,\phi;-\beta,\psi)]$$

$$T(\beta,\psi)\,\sin\psi\,d\psi\,d\beta\,. \qquad (6.49)$$

In view of the preceding, equations (6.1), (6.5), (6.7), (6.9) and (6.12) are modified as

$$-f_k + \sum_{\ell=1}^{2N^2} f_\ell\,[K_{k\ell} + K'_{k\ell}] = 2H_k \quad , \; k=1,2,3,\ldots,2N^2\,, \qquad (6.1')$$

$$[(K_{k\ell} + K'_{k\ell}) - \delta_{k\ell}]\,[f_\ell] = [2\,H_k] \tag{6.5'}$$

$$[f_\ell] = [(K_{k\ell} + K'_{k\ell}) - \delta_{k\ell}]^{-1}\,[2\,H_k] \tag{6.7'}$$

$$u_k = \sum_{\ell=1}^{2N^2} f_\ell (M_{k\ell} + M'_{k\ell}) \quad , \quad k=1,2,3,\ldots,2N^2 \ , \tag{6.9'}$$

and

$$[u_k] = [M_{k\ell} + M'_{k\ell}]\,[f_\ell] \quad , \tag{6.12'}$$

where $K'_{k\ell}$ is obtained by replacing the argument β of $\partial G/\partial n$ in (6.3) by $-\beta$. Similarly $M'_{k\ell}$ is obtained by replacing the argument β of G in (6.11) by $-\beta$.

The matrix elements $K'_{k\ell}$ and $M'_{k\ell}$ are evaluated numerically using the same methods employed for $K_{k\ell}$ and $M_{k\ell}$, respectively. There is however one important difference. The $\partial(1/R)/\partial n$ term in $K'_{k\ell}$ and the $(1/R)$ term in $M'_{k\ell}$ never become singular. This is because the image singularity $(-\beta,\psi)$ can never coincide with the particular point (α_k,ϕ_k), as they are on opposite sides of the (ξ,η)-plane. Therefore the numerical integration of the terms mentioned can be done using the nine point Simpson's method for all elements ℓ. No special scheme is necessary for the case $\ell=k$.

7. SIMPLIFICATION OF CALCULATIONS FOR A HALF SPHEROID

The numerical scheme presented in Section 6 involves, for a semiellipsoid, much computational work, even after the symmetry of the distribution function, f, is utilized. For example, for N=5, which is the grid size used in obtaining most of the data presented in this dissertation, the matrices corresponding to the Green's function and its derivative are each of size 50 x 50. Thus 2500 elements of each of the matrices $[K_{k\ell}]$, $[K'_{k\ell}]$, $[M_{k\ell}]$ and $[M'_{k\ell}]$ have to be evaluated. The singular cases of $[K_{k\ell}]$ and $[M_{k\ell}]$ have to be calculated by using a special scheme. Moreover, for each element, the numerical evaluation of the infinite integral takes considerable computer time because it involves iteration. In addition, the integrals involve Bessel functions which themselves have to be calculated by a series approach. In view of these factors, the time and cost involved in solving numerically the diffraction problem for a semiellipsoid, for a given set of parameters a, h, b and c, become prohibitive even on a high speed digital computer such as the IBM 360/65 system used, at least for the particular form of Green's function chosen. Hence it was decided to restrict the numerical computations to a half spheroid, axisymmetric about the vertical axis (case b=1), so that by utilizing the axisymmetric nature of the object most of the numerical calculations could be kept to the barest minimum, and

the results stored and used over and again. Thus repetition of the same calculations was avoided and the computer time was reduced to only a fraction of what it would have been otherwise.

In what follows, only the basic ideas behind the simplifications are given. For the sake of brevity, the details are kept to a minimum. Since much of the computational time is spent on the evaluation of the infinite integrals, it was decided to concentrate on all possible ways of reducing the computations connected with them.

Consider, for example, the infinite integral part in I_4. From (6.40) and (6.41) it may be written in the form

$$\int_{2\kappa_0}^{\infty} \frac{Q_2(\kappa)}{\kappa-\kappa_0}\, d\kappa = \frac{\{\sin^2\phi-\cos(\alpha-\beta)\ \sin\ \phi\ \sin\ \psi\}}{T(\alpha,\phi)\ r_1}$$

$$\int_{2\kappa_0}^{\infty} \left[\frac{\kappa(\kappa+\nu)\ e^{-\kappa h}}{\kappa\ \tanh\ \kappa h-\nu} \frac{\cosh(\kappa c\ \cos\ \phi)}{\cosh\ \kappa h} \cosh(\kappa c\ \cos\ \psi) \right.$$

$$\left. J_1(\kappa r_1) \right] d\kappa \ - \frac{\cos\ \phi}{cT(\alpha,\phi)} \int_{2\kappa_0}^{\infty} \left[\frac{\kappa(\kappa+\nu)\ e^{-\kappa h}}{\kappa\ \tanh\ \kappa h-\nu} \right.$$

$$\left. \frac{\sinh(\kappa c\ \cos\ \phi)}{\cosh\ \kappa h} \cosh(\kappa c\ \cos\ \psi)\ J_0(\kappa r_1) \right] d\kappa\ . \qquad (7.1)$$

The procedure used consisted of evaluating the two integrals on the right separately, storing the results and when necessary, multiplying them with the other factors, which are functions only of the coordinates, and using them. If the coordinates were not involved

in the hyperbolic and Bessel functions, the integrals could have been calculated once for all. As it is, the integration had to be carried out for each set of coordinates. Note that, for b=1, the expression for r_1 simplifies to

$$r_1(\alpha,\phi;\beta,\psi) = [\sin^2\phi+\sin^2\psi-2 \sin \phi \sin \psi \cos(\alpha-\beta)]^{1/2} . \qquad (7.2)$$

Thus, r_1 is a function of only ϕ, ψ and $|\alpha-\beta|$ rather than all the four variables ϕ, ψ, α and β. Therefore the two integrands are functions of ϕ, ψ and $|\alpha-\beta|$, besides κ. Once the integration with respect to κ is carried out, the results are functions of ϕ, ψ and $|\alpha-\beta|$ only. Further, since in the numerical procedure only the nodal points are considered, each of the integrals is a function of ϕ_k, ψ_ℓ and $|\alpha_k-\beta_\ell|$. Suppose we carry out the integration of the first integral for all possible combinations of these three variables. Then we may imagine the results to be stored in a three-dimensional matrix of size N x N x 2N corresponding to the unique values of ϕ_k, ψ_ℓ, and $|\alpha_k-\beta_\ell|$. However, since the first integral is symmetric in ϕ and ψ, it is necessary to evaluate the diagonal elements and only half of the remaining elements. Thus for N=5, instead of the integral being computed 2500 times by going in a straightforward manner, it was evaluated only 150 times, by understanding its functional dependence. As far as the second integral is concerned, since it is not symmetric in ϕ and ψ,

all the 250 elements of the corresponding matrix had to be evaluated.

The approach just described was used also in connection with the finite integral part in I_4 and the two integrals in I_3. As far as the infinite integrals in matrix elements $K'_{k\ell}$ and $M'_{k\ell}$ are concerned, note that if we consider the complete half spheroid, there is no basic difference between $r_1(\alpha_k,\phi_k,\beta_\ell,\psi_\ell)$ and $r_1(\alpha_k,\phi_k;-\beta_\ell,\psi_\ell)$ since they both represent the horizontal distance between any two nodal points.

It may be shown similarly that for the half spheroid R is a function only of ϕ, ψ and $|\alpha-\beta|$ and is symmetric in ϕ and ψ, and that there is no basic difference between R and R' if the complete spheroid were considered. Similar ideas can be applied to $\partial(1/R)/\partial n$ and $\partial(1/R')/\partial n$. To reduce computation time, functions such as r_1, R, $J_0(ar_1)$, $J_1(ar_1)$, etc., were computed once for all at the beginning and stored in the form of three-dimensional matrices. Several other ideas were also used to reduce computation time, wherever possible.

The description of the numerical evaluation and integration of $\partial G/\partial n$ and G is now complete. We note that the solution of the matrix equation (6.5') on the computer was done by using a special computer subroutine, valid for solution of matrix equations involving complex matrices. This subroutine called "COMAT" was originally prepared by Mrs. Sharon Good of the David Taylor Model Basin staff.

It can be applied for sizes of $[(K_{k\ell} + K'_{k\ell}) - \delta_{k\ell}]$ upto 100 x 100. This limits the grid size parameter N to a maximum value of 7. However, because of storage limitations of the IBM 360/65 system employed, the maximum value of N that could be used with the present program was 6.

Once the velocity potentials u are obtained as a column matrix corresponding to the nodal points on one half of the surface S, the physical parameters of interest are determined from the expressions given in Section 4. It is to be noted that the pressure distribution is symmetric about the (x,y)-plane for all the four problems considered. This fact is utilized in the calculation of the various other physical parameters. The forces and moments and their phase shifts for the diffraction problem, and the damping and added mass coefficients for the radiation problem are determined from the velocity potentials by using straightforward numerical integration. Thus the value of any surface integral over a grid element is approximated by the product of the area of the element and the value of the integrand at the nodal point.

8. ASYMPTOTIC SOLUTION AND EXPERIMENTS FOR A HEMISPHERE

Asymptotic Solution for a Hemisphere

From the theoretical point of view it is of interest to develop analytically an asymptotic solution for the diffraction problem for a half spheroid, valid at least over certain ranges of the parameters h, a and c. Such a solution will serve as a check on the more detailed numerical solution in the range over which the asymptotic solution is valid. From the engineering point of view, while the detailed numerical solution is exact, it takes considerable computer time. So it is advantageous to have a simpler closed form solution to the problem and know over what range of the relevant parameters, the simpler solution yields practically valid results. Such an asymptotic solution has been developed by Garrison for a hemisphere (c = 1.0). The details are given in Garrison and Seetharama Rao (1971). So only the assumptions and the final results are given here.

For $a \to 0$, the boundary-value problem simplifies somewhat and the free surface behaves as a rigid plane boundary. If in addition, the relative depth, $h = h/\bar{a}$, is large, the free surface boundary condition may be neglected and the problem reduces to that of unsteady motion of a hemisphere in a semi-infinite fluid. The velocity potential for this case is well-known from potential flow theory. The pressure coefficient is obtained from the velocity potential as

$$\Pi'(x,y,z;t) = \frac{1}{\cosh ah}\left[\cosh[a(h+y)] \cos ax \cos \sigma t \right.$$

$$\left. + \{\cosh[a(h+y)] \sin ax + \frac{ax}{2}\} \sin \sigma t \right] . \qquad (8.1)$$

Hence $p(x,y,z)$, f_x and f_y are determined as

$$p(x,y,z) = \frac{1}{\cosh ah}\left[\cosh^2[a(h+y)] \cos^2 ax \right.$$

$$\left. + \{\cosh[a(h+y)] \sin ax + \frac{ax}{2}\}^2 \right]^{1/2} \qquad (8.2)$$

$$f_x = \frac{\pi a}{\cosh ah} \qquad (8.3)$$

and

$$f_y = 2\pi\left[\frac{a \sinh a - \cosh a + 1}{a^2 \cosh ah} \right] . \qquad (8.4)$$

Note that m_z, = 0 for a hemisphere. We can expect the above expressions to be valid for small a. Note that in the limit as $a \to 0$, f_x tends to πa and f_y to π.

An equivalent form of (8.3) may be obtained by assuming the horizontal force to be the sum of two components: (i) the buoyancy force due to the pressure gradient, and (ii) the added mass force. If $\forall$ is the displaced volume of the object, the result is

$$f_x = \frac{\forall}{\frac{4}{3}\pi a^3} \frac{a(1+C_m)}{\cosh ah} . \qquad (8.5)$$

Since for a sphere in an infinite fluid the added mass coefficient C_m is 0.5, for a hemisphere the expression for f_x given in (8.5) reduces to that in (8.3).

Experiments for a Hemisphere

Some experimental results on the horizontal and vertical force coefficients for a hemisphere, obtained at Texas A&M University, are also presented in this dissertation for a comparison with the diffraction theory. Details of the experiments are given by Garrison and Snider (1970). So only a brief description will be given here.

The experiments were conducted in a 2 ft wide by 3 ft deep by 125 ft long wave channel. A 7 in. O.D. plastic hemispherical model was suspended vertically by fine wires from small cantilever beams equipped with strain gages. The model was suspended with a clearance of approximately 1/16 in. off the channel floor so that it was supported only by the beams. The pressure inside the model fluctuated because the model was off the channel floor. Therefore the internal pressure of the model was recorded, by using a pressure transducer, simultaneously with the strain gage readings for the vertical force and the latter were corrected suitably to account for the varying internal pressure. Horizontal forces on the model were also measured by strain gages. The wave height was measured by a resistance type wave gage.

Because the experiments were conducted in a "two-dimensional" wave tank, they were restricted to large relative depths ($h = 2, 3$ and 4) and small values of the relative size parameter ($a<1.0$).

9. DISCUSSION OF RESULTS

Accuracy of Numerical Results and Effect of Grid Size

As previously indicated, the numerical results presented in this dissertation were obtained with the grid size parameter N set equal to 5. Since the accuracy obviously depends on the grid size, the question naturally arises as to what constitutes a proper grid size. Some ideas on this question have been given by previous investigators such as Kim (1965), Garrison (1969), etc. As the parameter a increases, the fineness of the grid size must be increased in order to obtain the same degree of accuracy in the final results. This is because some of the terms of the kernel, $\partial G/\partial n$, of the integral equation and the Green's function, G, oscillate in r_1 with a wave length proportional to $2\pi/a$. Thus in order for the numerical integrations to be accurate, the subdivisions $\Delta\beta=\Delta\psi=s$ must be kept small in comparison to $2\pi/a$. That is

$$s = \frac{\pi}{2N} << \frac{2\pi}{a} .$$

Therefore for each grid size parameter N there is a value of a above which the numerical results become inaccurate. Increasing the grid size merely increases this value of a. However this process cannot be continued indefinitely. The numerical scheme eventually breaks down.

Obviously the computer time and the cost of computation increase with N. So, in order to check the effect of grid size, the parameter N was changed to N = 4 and N = 6, respectively and numerical results were obtained in a few cases over a range of a, keeping h and c constant. A comparison of the final results is shown in Table 1. Using the results from the finest grid as the standard, the percentage deviations from it in the other two cases are also shown.

The comparison shows that for values of a up to 3.39, all but one of the results obtained with the coarser grid of N = 5 are within 1% of those given by the grid of N = 6. The exception is the vertical force coefficient, f_y, which deviates less than 3.5% for a = 3.39. Even the results obtained with the coarsest grid of N = 4 are within 2.5%, for values of a up to 2.29. In general the vertical force coefficient f_y is more sensitive to grid size variation than the horizontal force coefficient or moment coefficient. This is natural since some of the errors tend to cancel out in the case of f_x and $m_{z'}$, whereas they all add up for f_y. The comparison shown in Table 1 is for the relative depth, h = 1.25. In general we may expect the effect of grid size variation to decrease as the relative depth h increases, since diffraction effects become smaller. In view of the preceding it may be concluded that the results obtained in this dissertation with a grid size of N = 5 are of accuracy approximately comparable to those obtained with a

Table 1. Effect of Grid Size on Accuracy of Results

c = 0.75 h = 1.25

a	N	f_x	δ_x	f_y	δ_y	m_z,	δ_m
0.34	6	0.73809	-1.5451	2.95345	-3.1396	0.16546	-1.5451
	5	0.73802	-1.5451	2.96902	-3.1395	0.16627	-1.5451
		-0.01%*		0.53%		0.49%	
	4	0.73780	-1.5450	2.99799	-3.1391	0.16776	-1.5450
		-0.04%		1.51%		1.39%	
0.60	6	1.08270	-1.5016	2.56686	-3.1273	0.24747	-1.5016
	5	1.08260	-1.5016	2.58108	-3.1266	0.24862	-1.5016
		-0.01%		0.55%		0.46%	
	4	1.08222	-1.5015	2.60708	-3.1254	0.25070	-1.5015
		-0.04%		1.57%		1.31%	
1.07	6	1.12268	-1.4367	1.72583	-3.0527	0.27072	-1.4367
	5	1.12265	-1.4367	1.73548	-3.0505	0.27176	-1.4367
		0%		0.56%		0.38%	
	4	1.12244	-1.4367	1.75319	-3.0466	0.27365	-1.4367
		-0.02%		1.59%		1.08%	
2.29	6	0.39523	-1.4539	0.36547	-2.9602	0.12442	-1.4539
	5	0.39546	-1.4544	0.36847	-2.9569	0.12453	-1.4544
		0.06%		0.82%		0.09%	
	4	0.39564	-1.4557	0.37373	-2.9497	0.12461	-1.4557
		0.10%		2.26%		0.15%	
3.39	6	0.10050	-1.5028	0.09031	-3.0488	0.04579	-1.5028
	5	0.10079	-1.5035	0.09325	-3.0457	0.04577	-1.5035
		0.29%		3.26%		-0.04%	
	4	0.10128	-1.5060	0.09839	-3.0378	0.04561	-1.5060
		0.78%		8.95%		-0.39%	
4.52	6	0.01768	-1.5401	0.02088	-3.1011	0.01382	-1.5401
	5	0.01796	-1.5410	0.02352	-3.0983	0.01383	-1.5410
		1.58%		12.64%		0.07%	

*Results for N = 6 are taken as the standard in computing the percentage deviations.

finer grid size of N = 6 for values of a upto 3.39. Even the coarse grid of N = 4 appears to furnish results that are of the same order of accuracy, for values of a upto 2.29, which might suffice for engineering purposes. Finally, it is noted that Kim (1965), using a similar numerical procedure, obtained quite accurate results for an ellipsoid for values of a upto 4, with a grid size of N = 6.

The majority of the numerical results presented in this dissertation were obtained on the IBM 360/65 computer system of Texas A&M University. The total computer time required for one run (i.e., for given values of h, c and a) for the diffraction problem for the grid size of N = 5 increased as the relative size a decreased. This is because of the numerical procedure used in computing the infinite integrals. It was also observed that the computer time varied depending on the relative depth h, being greater for smaller values of h. The time was of the order of 3 to 6 minutes for a = 3.39 and 8 to 20 minutes for a = 0.19.

The computations were in general performed setting a = 0.19, 0.34, 0.60, 1.07, 1.91 and 3.39. The reason for the choice was that the points were logarithmically spaced. Additional points were added as necessary in the ranges where the results varied rapidly. The data extended over the range of a values up to 4 and in some cases even up to higher a, which is the range of practical engineering interest. Four different geometries were considered. These included the hemisphere (c = 1.0), two oblate spheroids

(c = 0.5 and 0.75) and one prolate spheroid (c = 2.0). Because of limitations on available computer time, the hemisphere was tested over a wide range of h, from 1.25 to 4. Results were obtained for the oblate spheroids for h = 1, 1.25 and 1.5 only, and for the prolate spheroid for h = 2.5, 3 and 4 only. These cover the range of practical interest.

Haskind's Relations and Energy Check

As previously indicated, important checks on the numerical technique and the final results can be made by using Haskind's relations and the energy check which are developed in Appendix C. The former verifies the solution for the diffraction problem and the latter the solution for the radiation problem itself. These checks were applied over a range of values of a, for given conditions of c and h. The results are shown in Tables 2 and 3, respectively.

The comparison in Table 2 shows that the results obtained directly from the numerical solution of the diffraction problem do not differ by more than 0.5% in most cases from those obtained indirectly from the solution of the radiation problem, by using Haskind's relations. The only exceptions are the results corresponding to f_y for large a. These may be explained in terms of what was noted earlier about f_y. The general agreement is gratifying, since the diffraction and radiation problems are solved separately,

Table 2. Haskind's Relations Check

c = 0.5 h=1.25

a	$\|F_1'\| = f_x$			$\|F_2'\| = f_y$			$\|F_6'\| = m_{z'}$		
	Direct Soln.	Haskind's Rel.	%* Dev.	Direct Soln.	Haskind's Rel.	% Dev.	Direct Soln.	Haskind's Rel.	% Dev.
0.19	0.26092	0.26037	-0.02	3.10606	3.11528	0.30	0.14974	0.14998	0.16
0.34	0.43959	0.43894	-0.15	2.92628	2.93175	0.19	0.25320	0.25329	0.04
0.60	0.63903	0.63906	0	2.46555	2.47017	0.19	0.37256	0.37315	0.16
1.07	0.66011	0.65950	-0.09	1.53660	1.53899	0.16	0.39882	0.39919	0.09
2.29	0.21834	0.21775	-0.27	0.27898	0.27688	-0.75	0.16086	0.16067	-0.12
3.39	0.04476	0.04456	-0.45	0.05183	0.04978	-3.96	0.04700	0.04694	-0.13

*Results from the direct solution are taken as the standard in computing the percentage deviations.

Table 3. Energy Check for Damping Coefficients

c=0.5 h=1.25

a	N_{11}			N_{22}			N_{66}		
	Near Field Soln.	Far Field Soln.	%** Dev.	Near Field Soln.	Far Field Soln.	% Dev.	Near Field Soln.	Far Field Soln.	% Dev.
0.60	0.05659	0.05659	0	1.69095	1.69738	0.38	0.01929	0.01936	0.36
2.29	0.02636	0.02624	-0.46	0.08525	0.08404	-1.42	0.01435	0.01433	-0.14

**Results from the near field solution are taken as the standard in computing the percentage deviations.

and the accuracy of the numerical results in general is expected to be no better than $\pm$ 1%.

Table 3 shows that for the radiation problem the damping coefficients obtained directly from the near field solution do not differ by more than 0.5% from those obtained from the far field solution by using the energy check. The only exception is the damping coefficient N_{22} (for heave) for a = 2.29. This is in keeping with the trends observed previously for f_y. The comparison of Table 3 is especially encouraging and provides confidence in the numerical scheme used, since the far field solution was obtained by using an asymptotic form of the Green's function and not that used for the near field.

Pressure Distribution

For design purposes, it is important to know the pressure distribution on the body for various phase angles of the incident wave. The computer program gives the pressure amplitude coefficient p and the phase shift δ_p at various nodal points. With these data, the instantaneous pressure distribution over the body can be easily calculated corresponding to any instant of time during the wave cycle.

Since the body is three-dimensional, there is no convenient way of representing the values of p and δ_p obtained from the program. Even presentation of the data in the form of tables takes

considerable space. Therefore it was decided to give here only a sampling of the pressure data and indicate briefly the trends.

As part of the computer program, the instantaneous pressure coefficients, $\Pi'(x,y,z;t)$, were calculated at the nodal points corresponding to the instants of maximum horizontal force and maximum vertical force, respectively. Using this information, contours of equal values of $\Pi'(x,y,z;t)$ were plotted, showing the body in plan view. Such contours are shown in figures 8-11 for the case of a hemisphere ($c = 1.0$) for $h = 1.5$. The first two figures correspond to the condition of maximum horizontal force and the next two to the condition of maximum vertical force. The radial straight lines and the circles represent ellipsoidal polar coordinates, as shown in figure 8, the former corresponding to azimuth angles α and the latter to vertical angles ϕ. Note that the x-axis represents the direction of advance of the incident wave.

Before going into the details of the results obtained from diffraction theory for the case of maximum horizontal force, it is interesting to consider the effect of the incident wave alone, disregarding scatter, since it is quite instructive. The maximum horizontal force due to the incident wave occurs when the horizontal particle acceleration in the x-direction is maximum at the center of the object, i.e., when $\sigma t = -\pi/2$ according to the notation of (2.5). Corresponding to this condition, the crest portion of the wave is overhead of that half of the object for

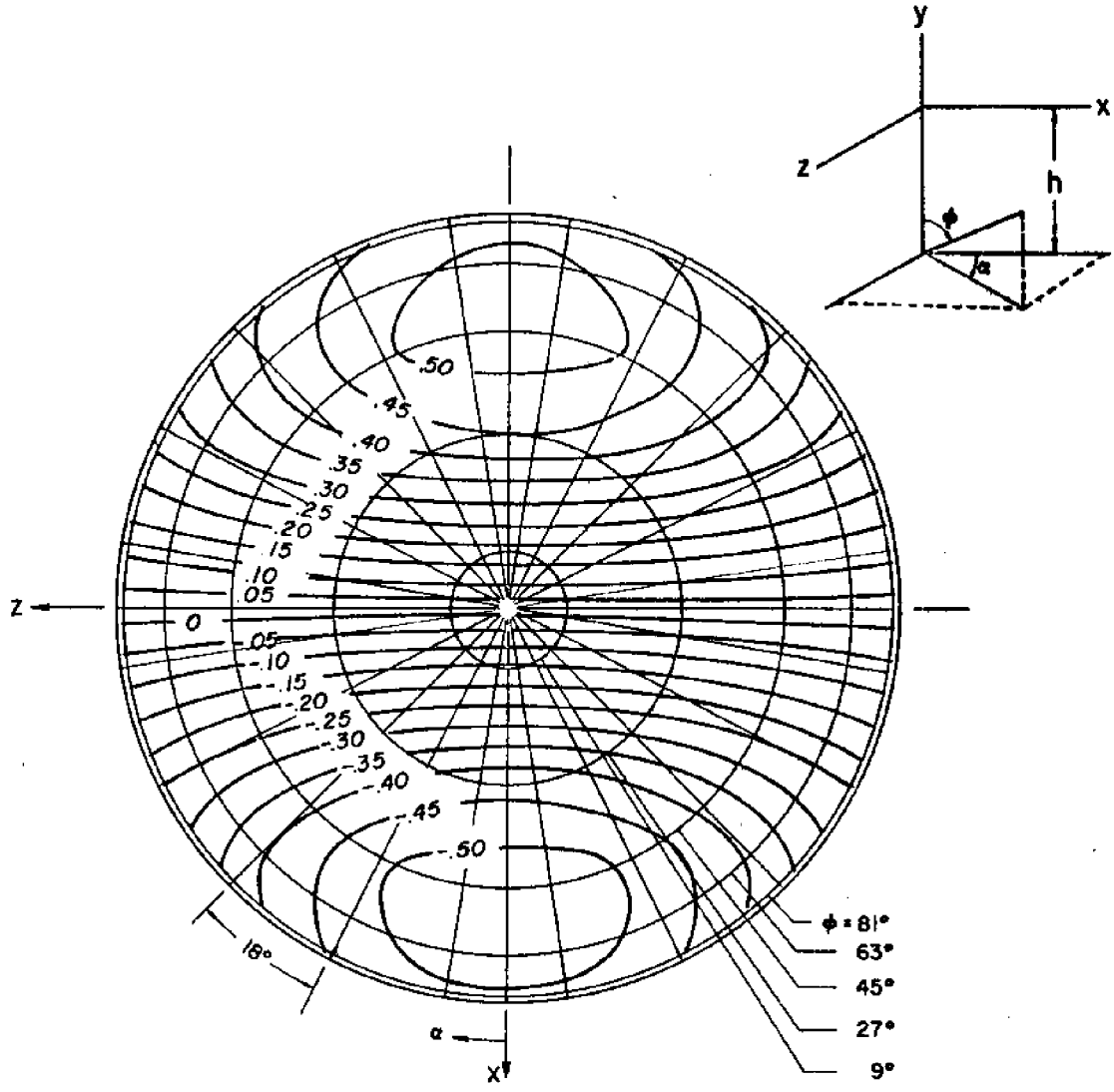

Figure 8. Contours of pressure coefficient at instant of maximum horizontal force for c=1.0, h=1.5 and a=1.07.

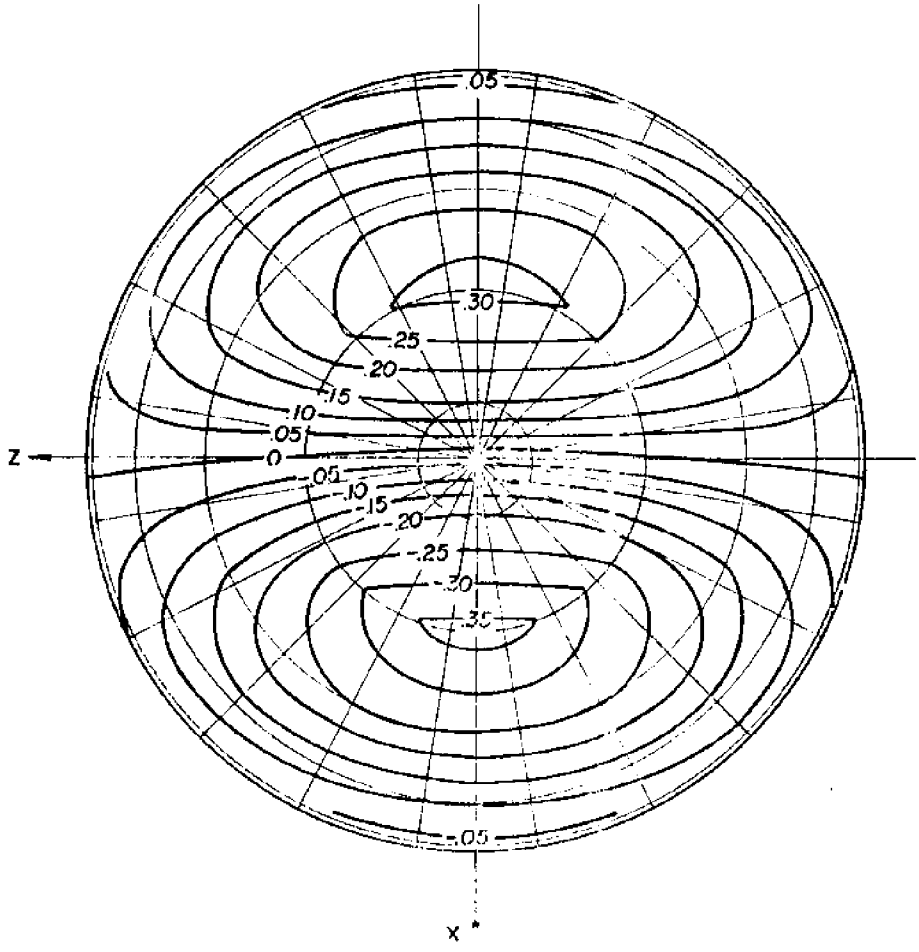

Figure 9. Contours of pressure coefficient at instant of maximum horizontal force for c=1.0, h=1.5 and a=2.29.

which $x < 0$, and the trough portion is overhead of the other half for which $x > 0$. Therefore the pressure distribution is asymmetric about the z-axis. However, from linear wave theory, the magnitudes of the pressures are symmetric. The results of diffraction theory, as presented in figures 8 and 9, are considered next. These figures correspond to $a = 1.07$ and 2.29, respectively. The pressure distribution is asymmetric about the z-axis, as expected. While the magnitudes of the pressures are roughly symmetric about the z-axis for $a = 1.07$, this is however not the situation for $a = 2.29$. The reason could be the greater diffraction effects encountered in the latter case. The two pressure distributions look different partly because, compared to the diameter of the hemisphere, the length of the incident wave is shorter in the latter case.

The condition of maximum vertical force is taken up next. If the incident wave alone were considered, then the vertical force is maximum when the trough portion of the incident wave is directly above the object, such that the pressures on the surface of the object are generally negative and symmetric about the z-axis. Considering now the results of diffraction theory, as presented in figures 10 and 11, and noting that they correspond to different values of a, it is observed that the pressures are indeed almost symmetric about the z-axis and in general negative in both cases. The maximum negative pressure occurs at the highest point on the

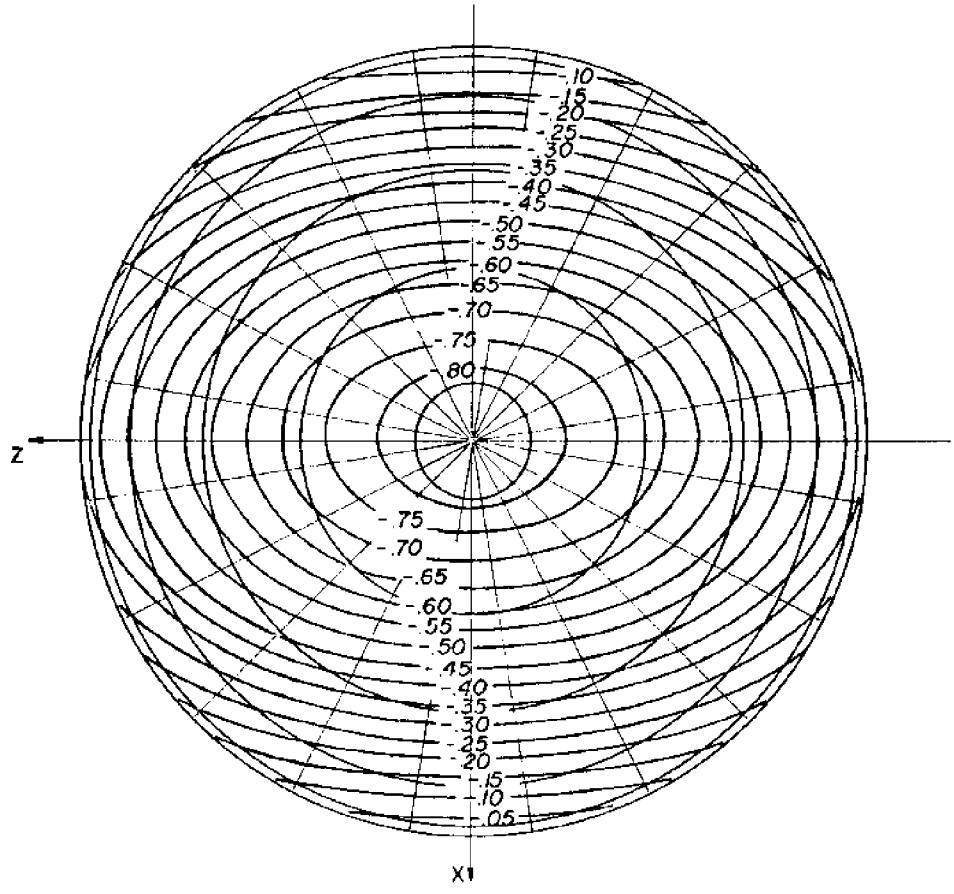

Figure 10. Contours of pressure coefficient at instant of maximum vertical force for c=1.0, h=1.5 and a=1.07.

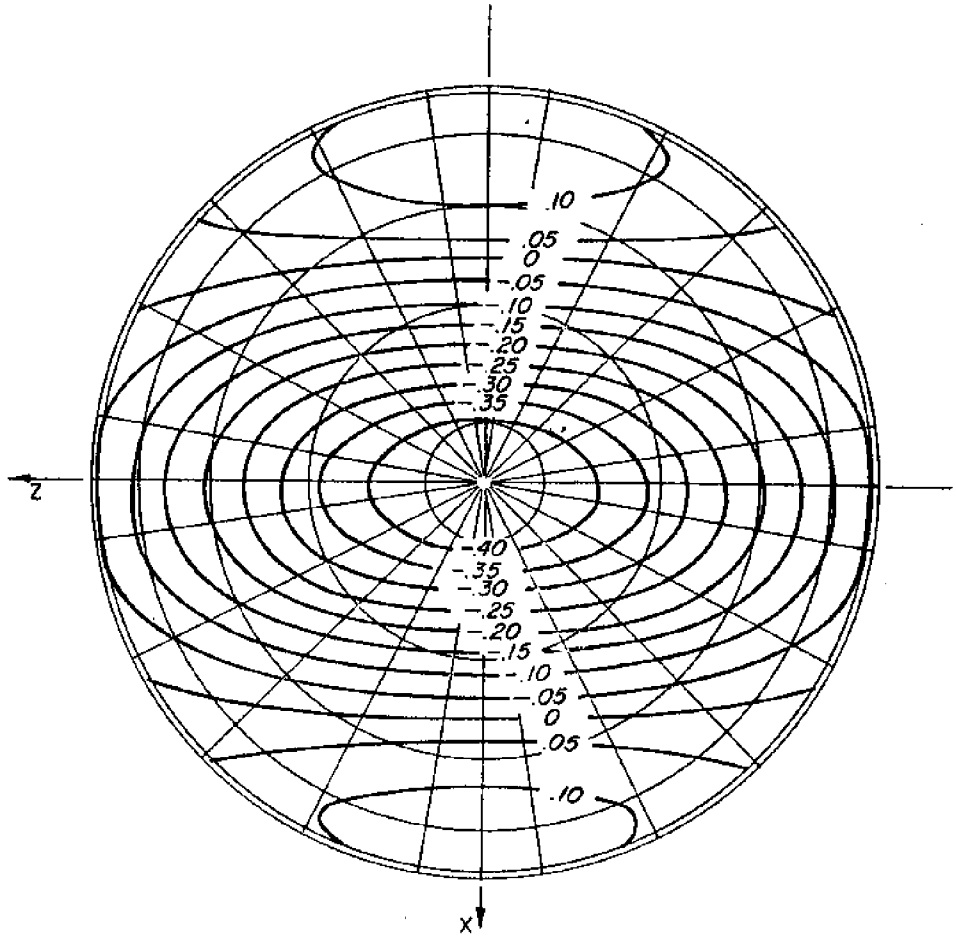

Figure 11. Contours of pressure coefficient at instant of maximum vertical force for c=1.0, h=1.5 and a=2.29.

surface of the object. Again, some of the differences between figures 10 and 11 arise because, relative to the diameter of the hemisphere, the wave length is shorter in the latter case.

The numerical results from diffraction theory for the horizontal and vertical force coefficients and the moment coefficient are presented next in figures 12-29. For a hemisphere, the asymptotic solution and the results of the experiments described in Section 8 are also shown for comparison. For a given h, the results obtained for different values of c are presented in the same figure. In all the figures, solid lines represent diffraction theory, broken lines the asymptotic solution for a hemisphere and circles experimental data for a hemisphere.

Horizontal Force Coefficient, f_x

The results for the horizontal force coefficient are presented in figures 12-18. The figures correspond to the cases h = 1.0, 1.25, 1.5, 2.0, 2.5, 3.0 and 4.0, respectively. The results of the asymptotic solution presented in these figures are obtained from (8.5), by assuming therein a value of $C_m = 0.5$, which corresponds to the case of infinite relative depth h. Note that for the assumed value of C_m equation (8.5) reduces to (8.3).

We consider the results from diffraction theory first. In general the curves for all values of c follow the same trend. They increase with a at first, reach a maximum and then decrease

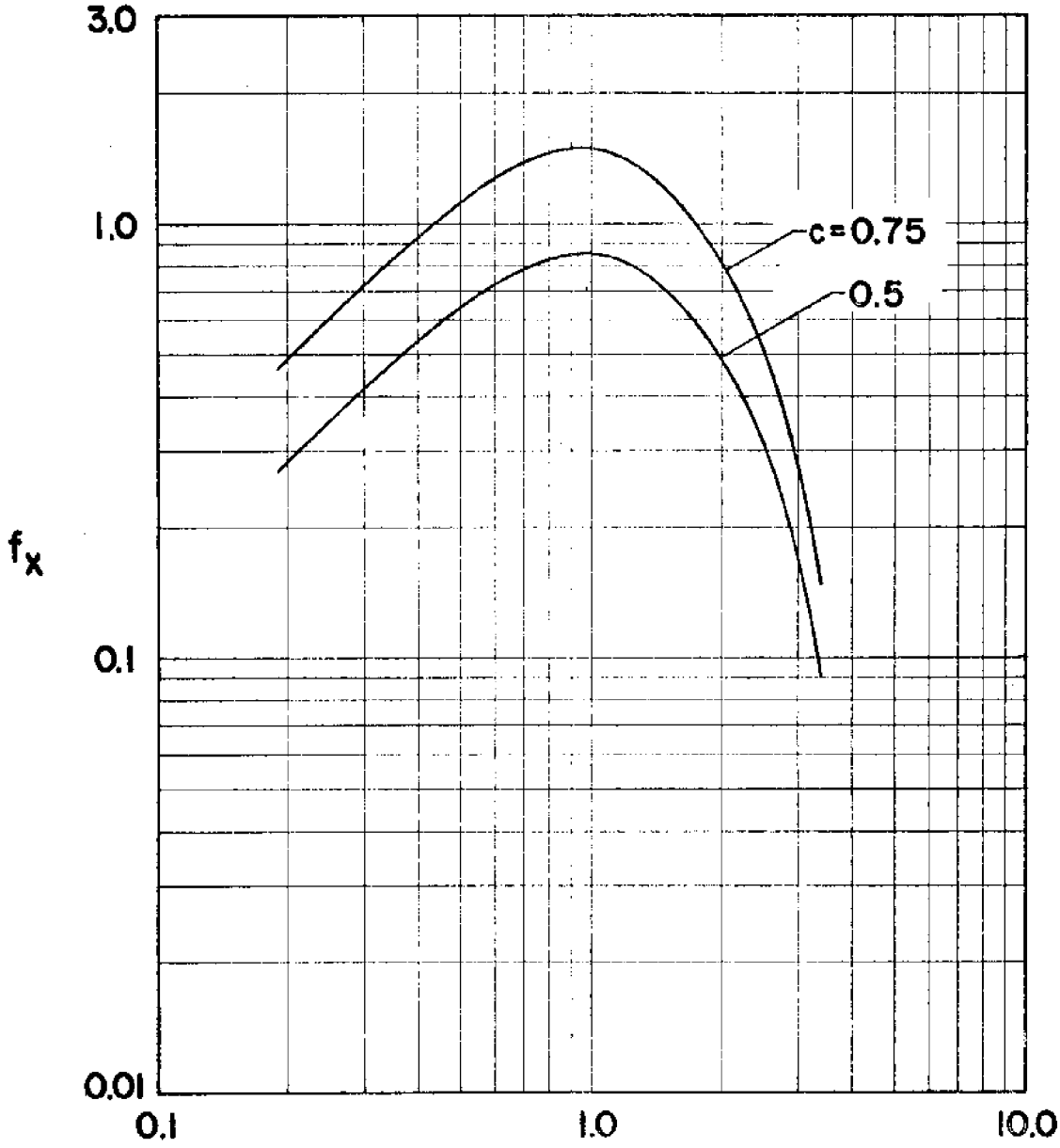

Figure 12. Horizontal force coefficient for h=1.

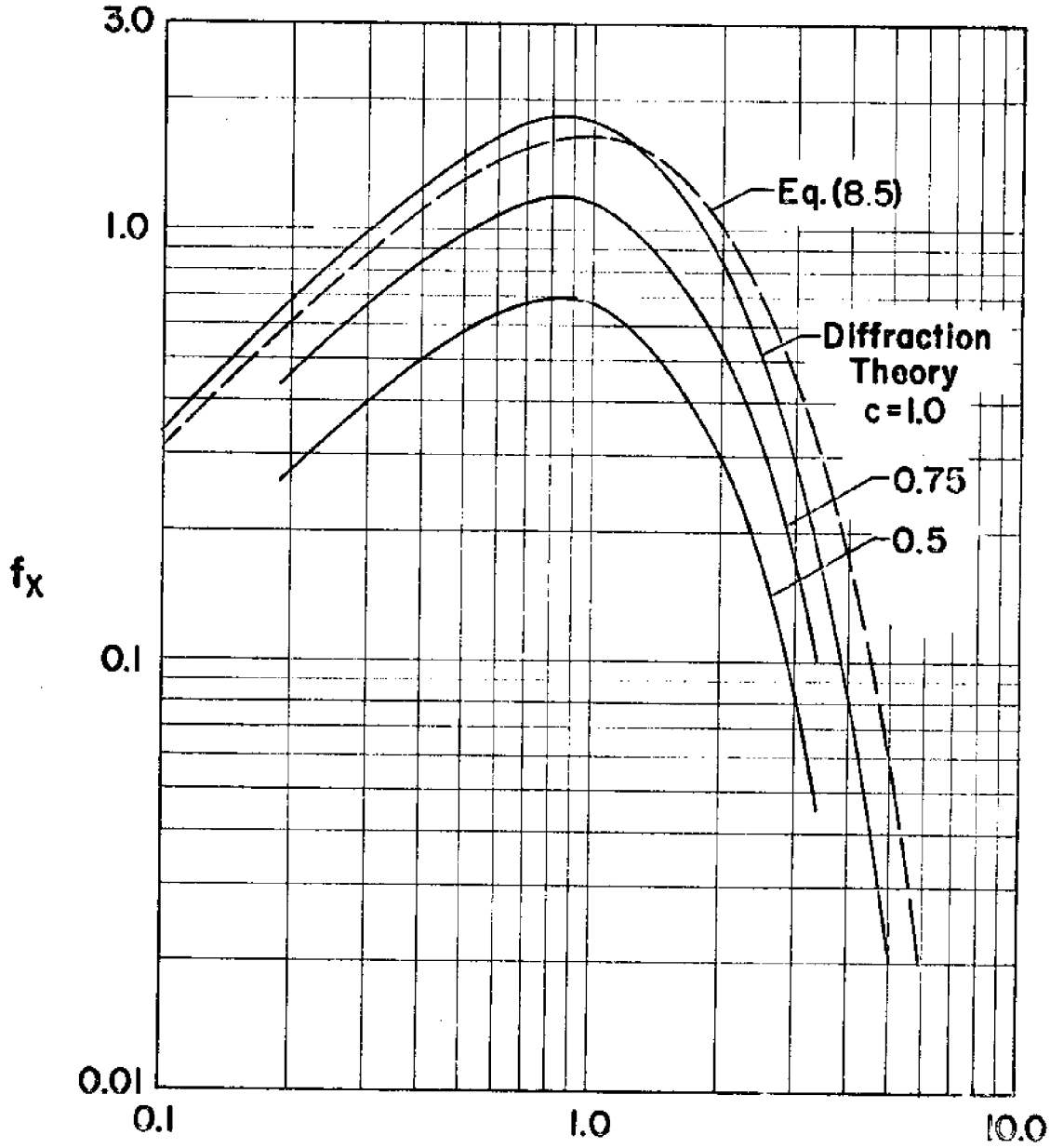

Figure 13. Horizontal force coefficient for h=1.25.

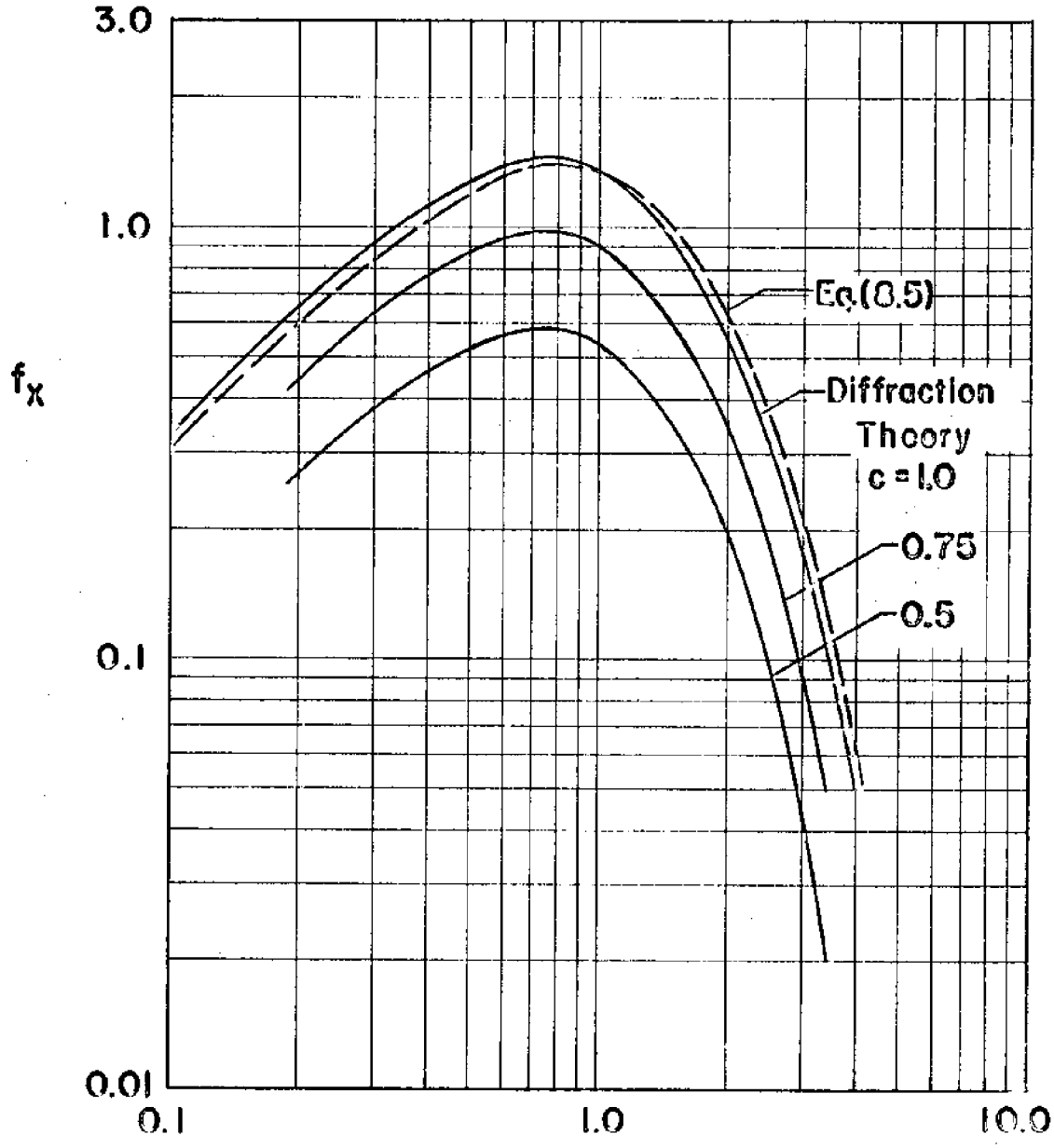

Figure 14. Horizontal force coefficient for h=1.5 .

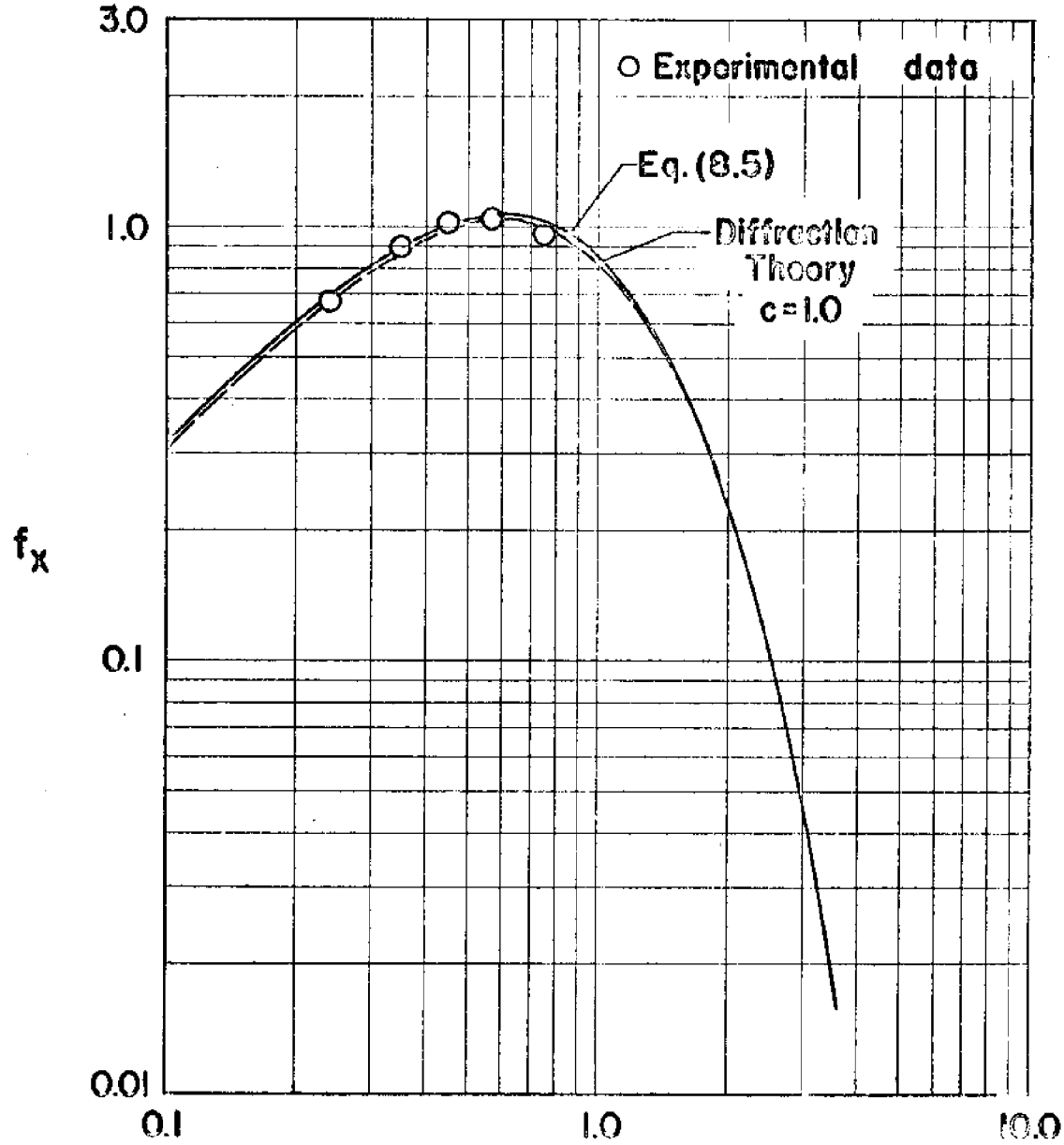

Figure 15. Horizontal force coefficient for h=2 .

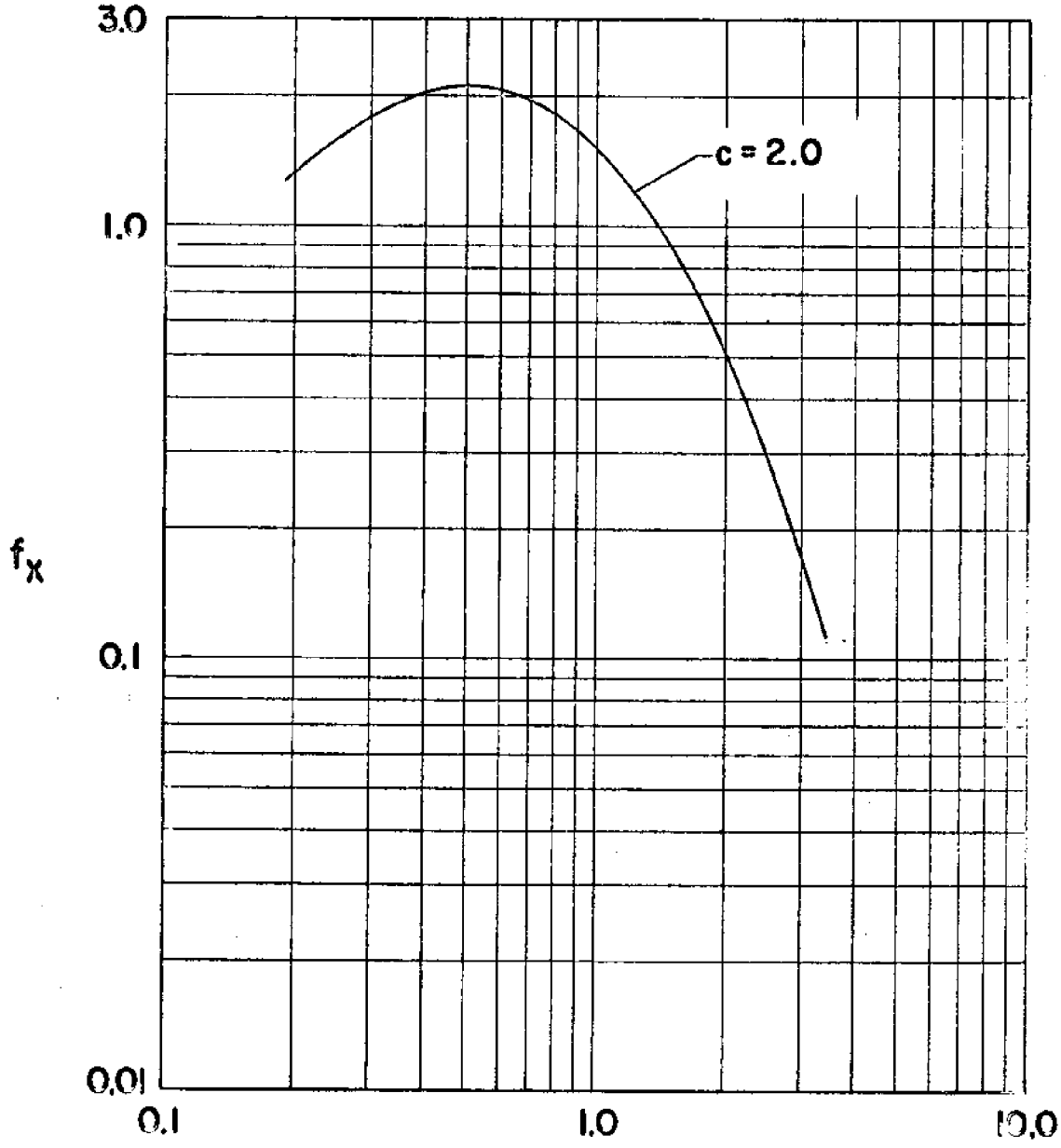

Figure 16. Horizontal force coefficient for h=2.5 .

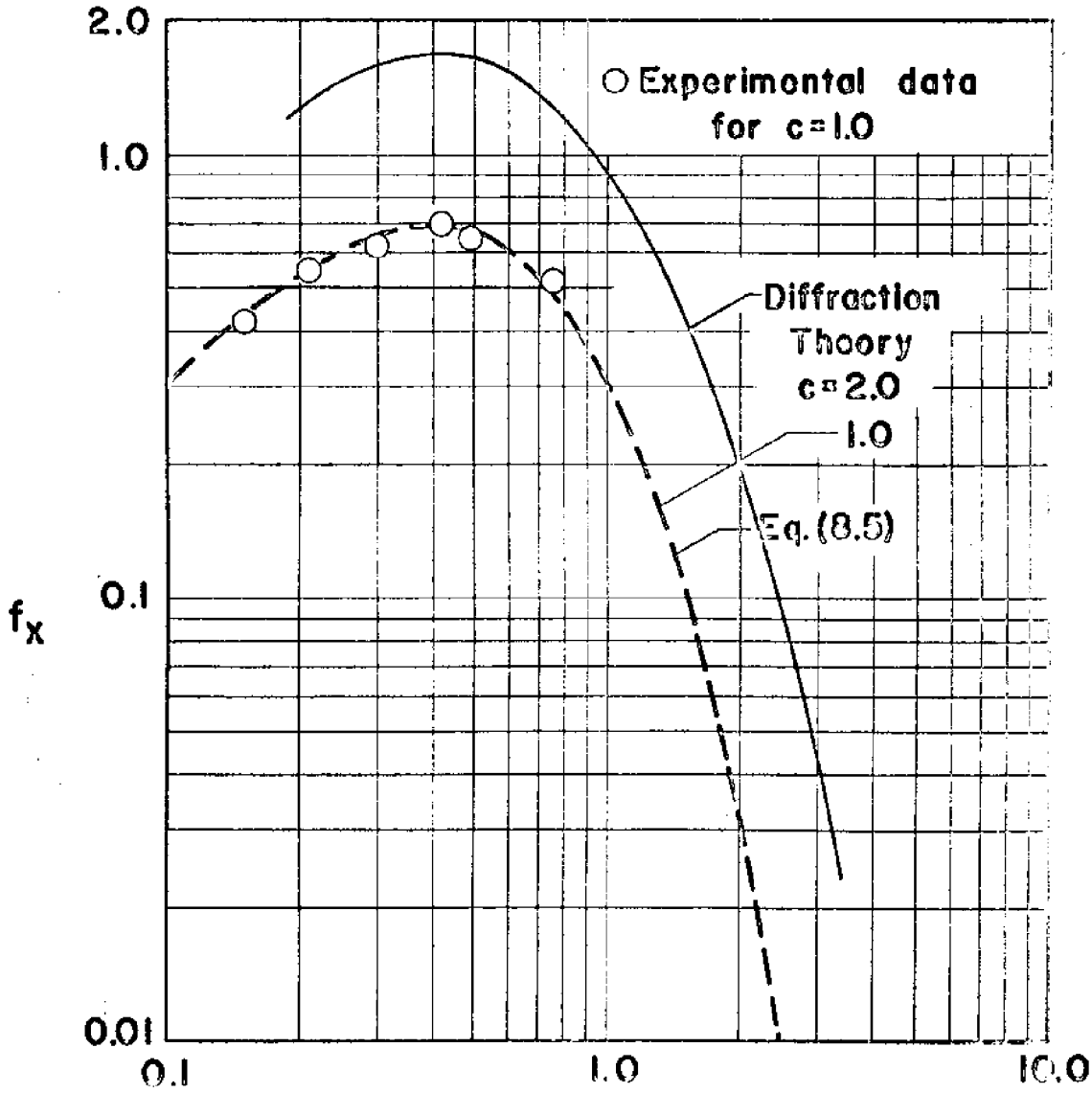

Figure 17. Horizontal force coefficient for h = 3 .

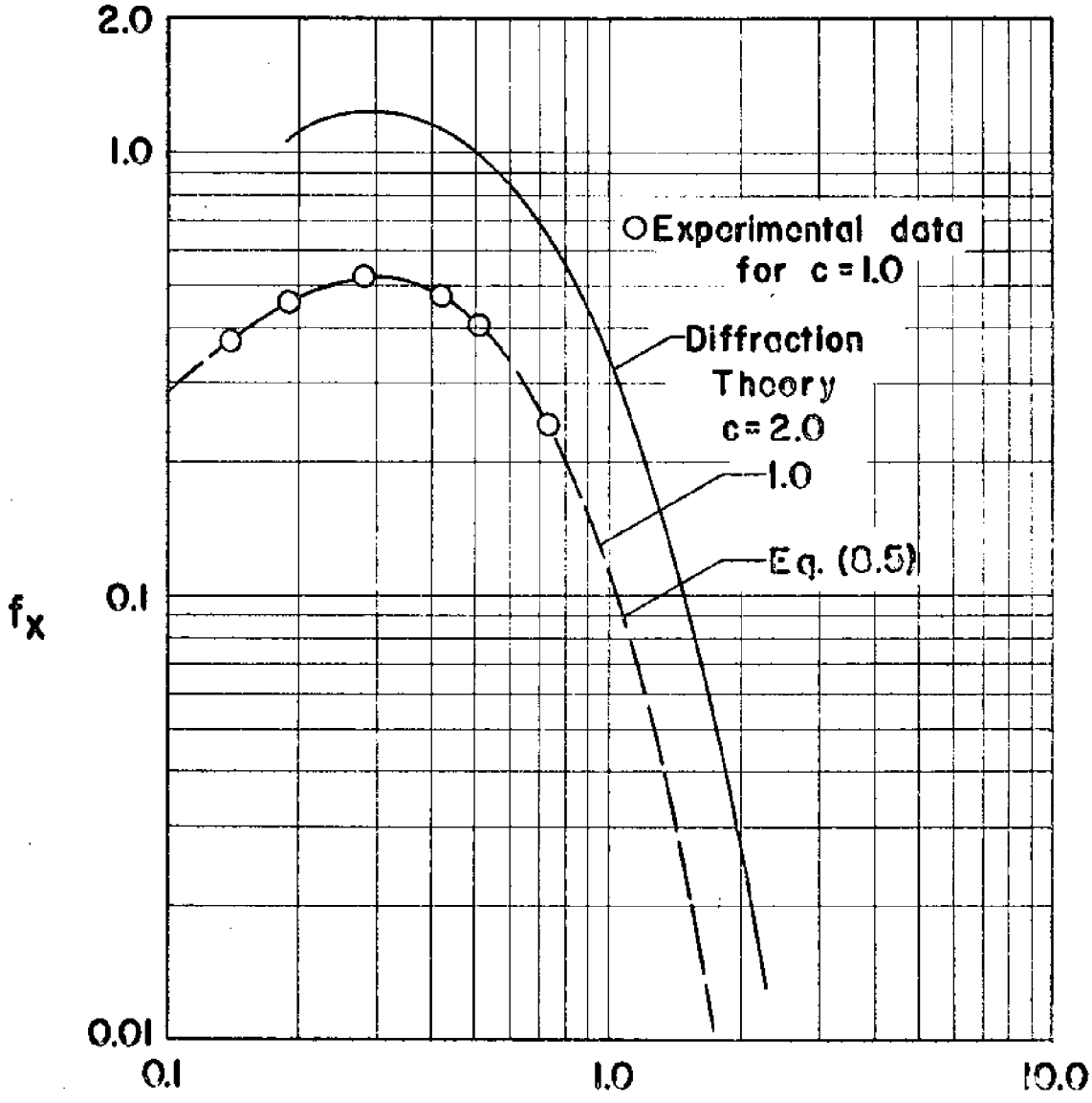

Figure 18. Horizontal force coefficient for h=4 .

rapidly with a. They all exhibit the same asymptotic behaviour for very small a and for large a. They appear to follow a straight line variation for small a, the straight lines having approximately the same slope. The general trends observed may be explained as follows. For a hemisphere it was noted in Section 8 that for small a, $f_x \sim \pi a$, a function represented by a straight line on a log-log plot. As for the behaviour at large a, note that if a were increased, keeping other parameters constant, this means the wavelength is decreasing relative to the liquid depth and the size of the object. Obviously, under such conditions the effect of the wave at the free surface decreases at the bottom where the object is located and so does f_x until they both vanish for $a \to \infty$.

For a given h, the curves for larger relative heights, c, are above those for smaller values of c. This is to be expected since, for a given a, the spheroid with a larger value of c has more vertical projected area to offer and, other parameters being equal, is subjected to a greater horizontal force.

It may be noted from the figures that in general f_x increases as the relative depth h decreases. This is as expected because the free surface is closer to the object for smaller h and therefore the dynamic pressures are greater.

We now compare the asymptotic solution (8.5) with the results from diffraction theory for a hemisphere. In general the two sets of curves follow the same trends. Moreover, they coincide over the

entire range of a considered, for h = 3 and 4. They are quite close even for h = 2. This is very encouraging. The difference between the two solutions increases as the relative depth h decreases, being the maximum for h = 1.25. This is expected since the asymptotic solution assumes $C_m = 0.5$ which corresponds to infinite relative depth.

We note that in the case of the smaller h, for small values of a, the results of equation (8.5) are generally below the results of diffraction theory. In such cases the agreement between the asymptotic solution and diffraction theory can be improved by suitably increasing the value of the added mass coefficient, C_m. For example, in figure 13, the results of (8.5) can be made to agree with diffraction theory for values of a up to approximately 0.7, by increasing the value of C_m used in the equation to 0.7. There is a sound basis for this suggestion. For small values of a, the free surface behaves like a rigid plane boundary. For small h, since this boundary is relatively close to the body, the added mass coefficient, according to potential flow theory, is greater than if the boundary were absent or at an infinite distance.

In figures 13 and 14, for large values of a, the results of the asymptotic solution are higher than those from diffraction theory. The difference increases with a and is quite large. This is to be expected since the asymptotic solution is valid only for

small values of a. Thus in this range of a, the diffraction effects neglected in the asymptotic solution become significant.

A comparison of the experimental results for a hemisphere with the asymptotic solution and diffraction theory in figures 15, 17 and 18 shows good agreement in general. The agreement improves with the relative depth, as one would naturally expect.

Vertical Force Coefficient, f_y

The numerical results for the vertical force coefficient as well as the asymptotic solution (8.4) and the experimental results for a hemisphere are presented in figures 19–25. These figures correspond to relative depths ranging from 1.0 to 4.0, as before.

We consider the results of diffraction theory first. In general the curves for all c tend to π for $a \to 0$. This is indeed the trend predicted by the asymptotic solution (8.4) for c = 1. The value of π represents the effect of the hydrostatic pressures due to the presence of the wave crest or trough of the incident wave alone. As a increases, f_y decreases first gradually and later rapidly. This trend is again predicted by (8.4) for a hemisphere, as evidenced by the figures.

In general, for the same relative depth h, the vertical force coefficient increases with the relative height c. Also, the difference between the curves for two different values of c increases in most cases with the relative size a. This may be

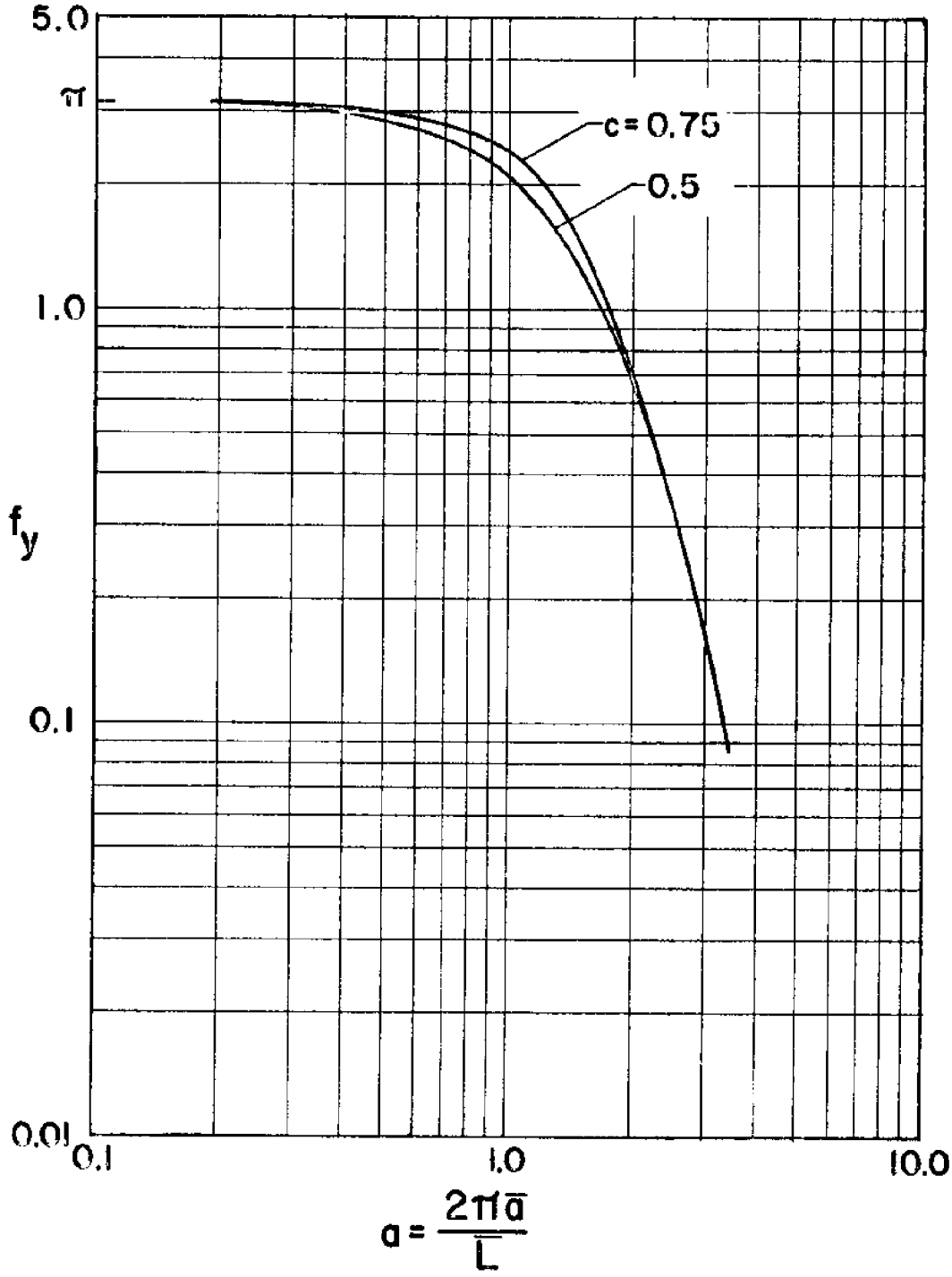

Figure 19. Vertical force coefficient for h = 1 .

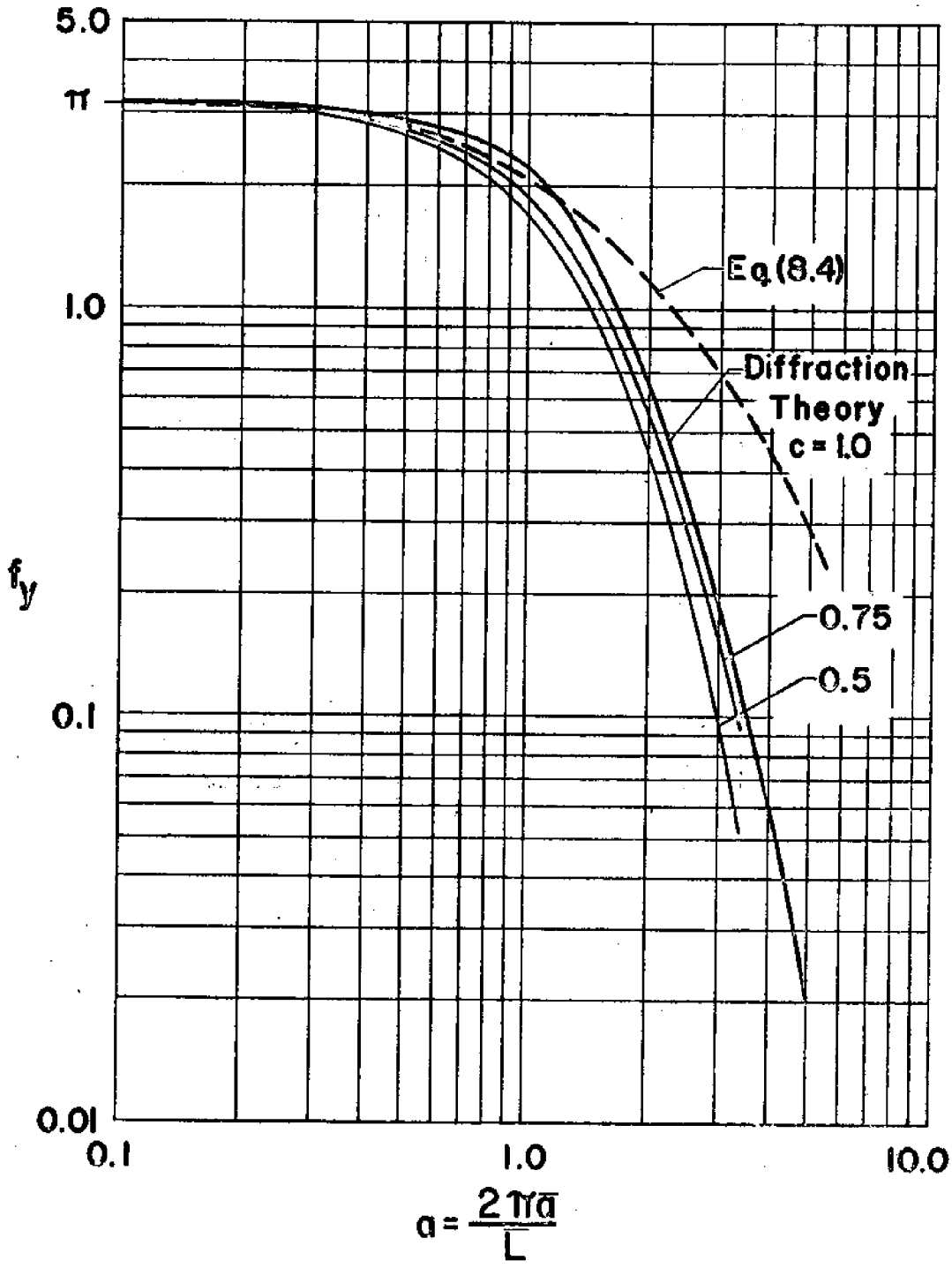

Figure 20. Vertical force coefficient for $h = 1.25$.

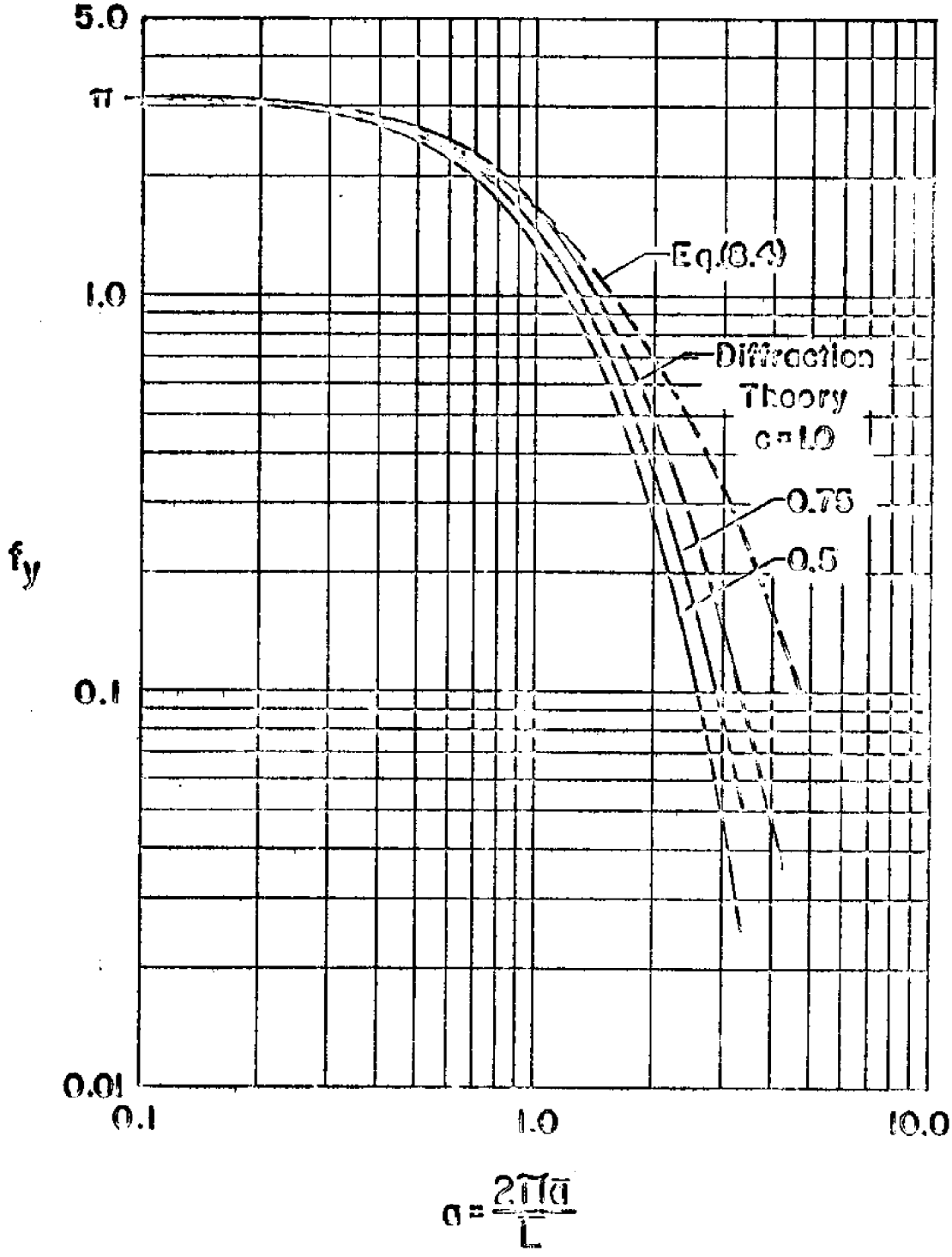

Figure 21. Vertical force coefficient for h = 1.5 .

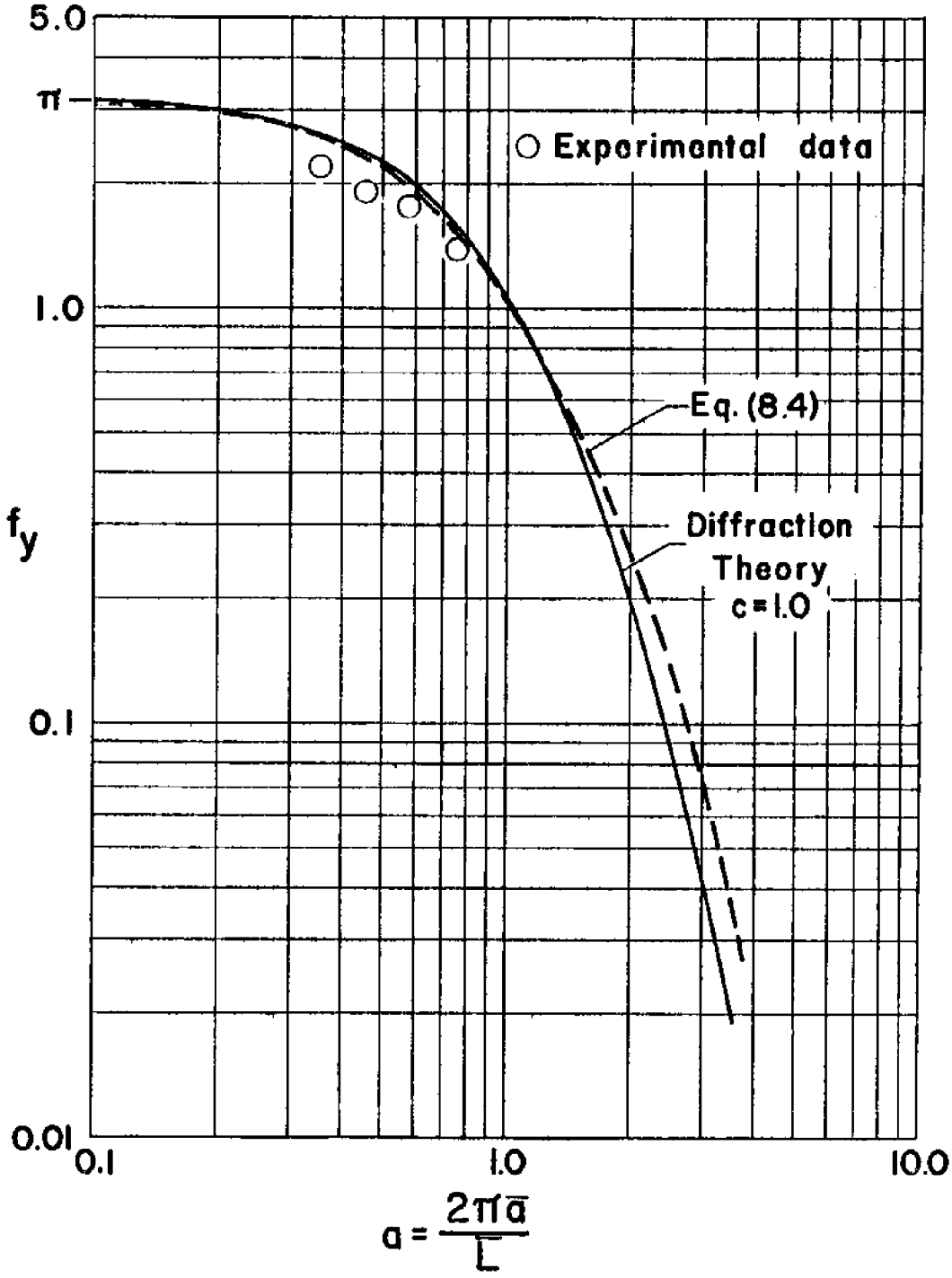

Figure 22. Vertical force coefficient for h = 2 .

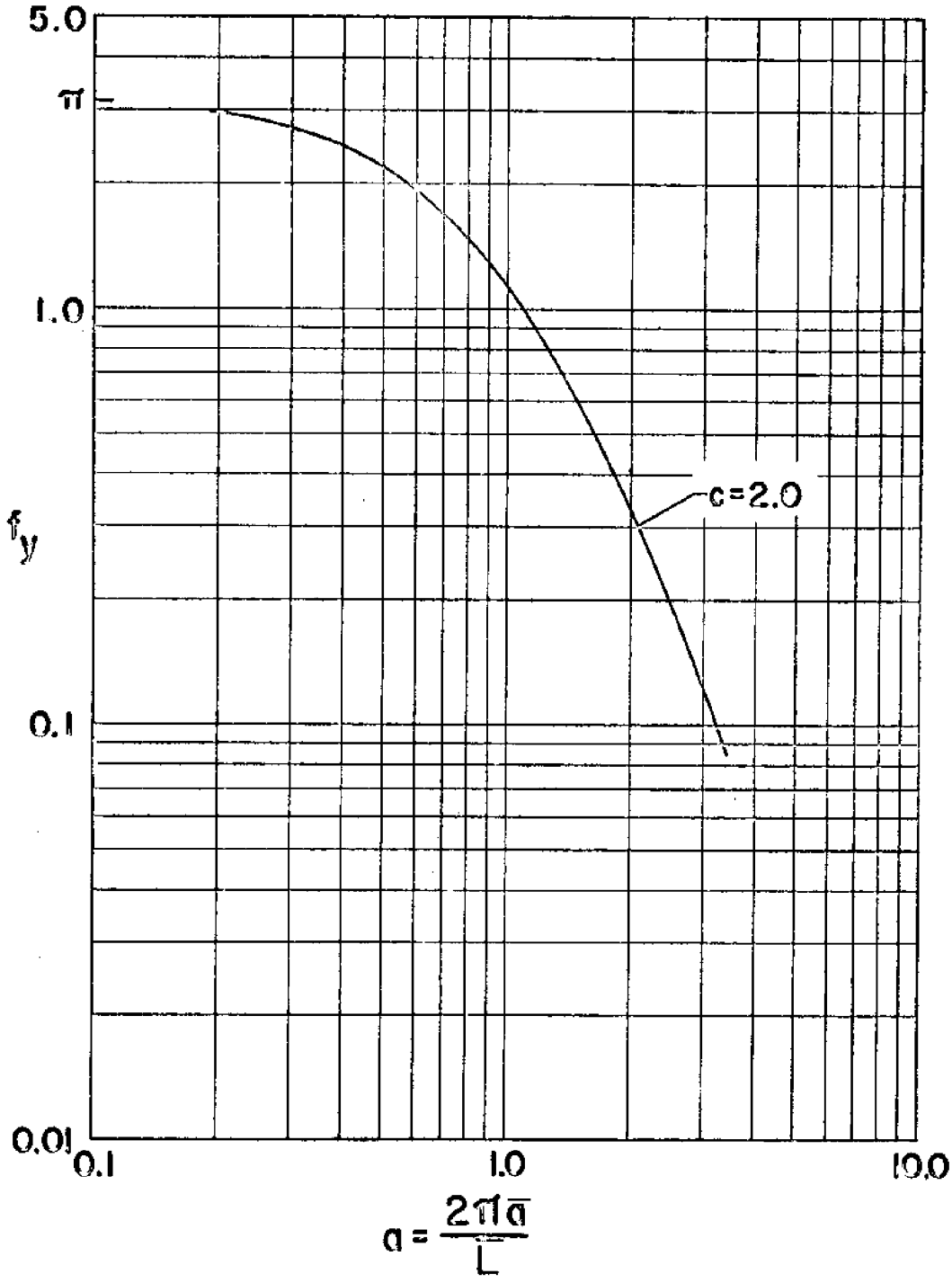

Figure 23. Vertical force coefficient for h = 2.5 .

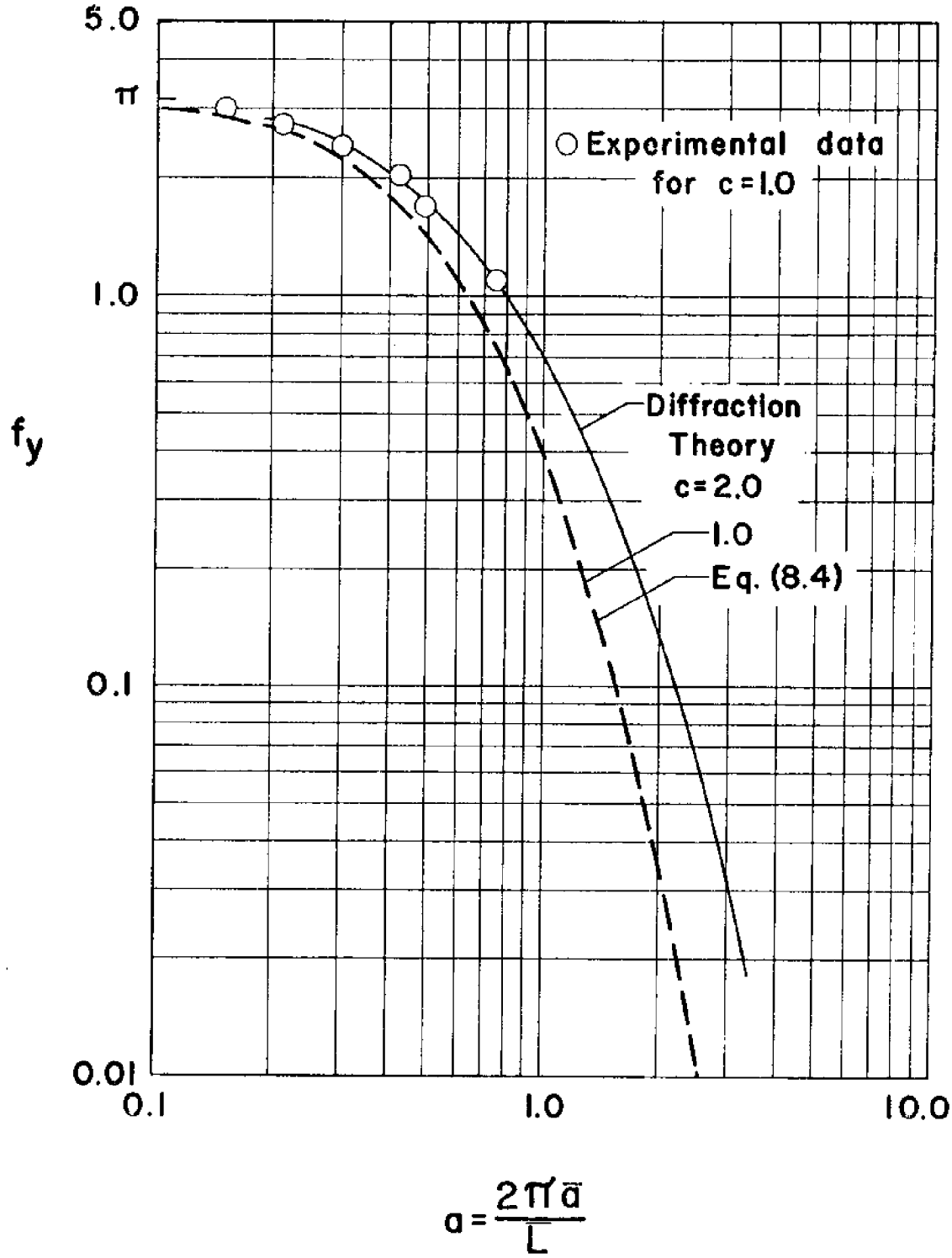

Figure 24. Vertical force coefficient for h = 3 .

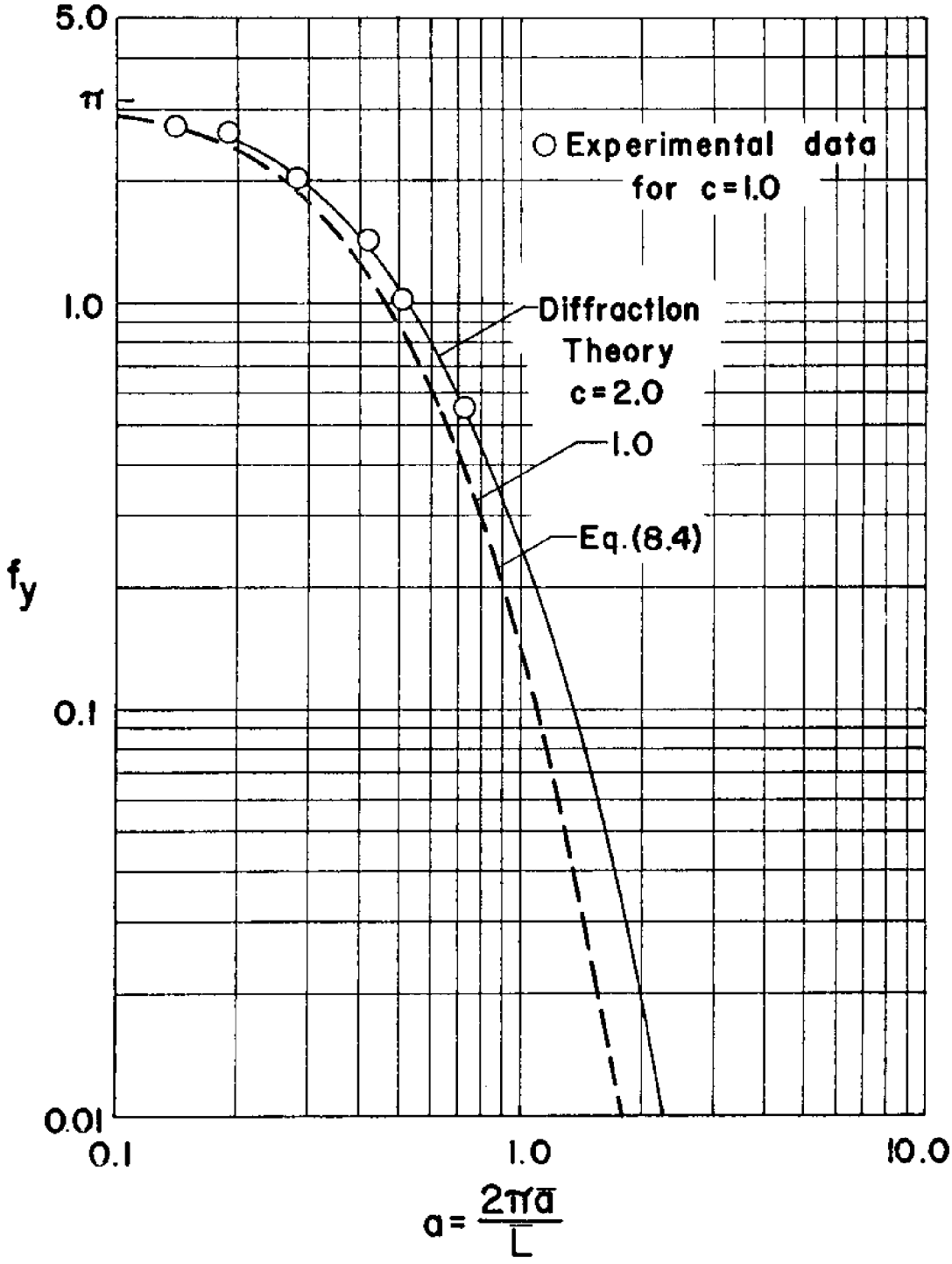

Figure 25. Vertical force coefficient for h = 4 .

explained as follows. The major portion of the vertical force comes from the pressures near the top of the half spheroid. In the case of a spheroid with a larger relative height, the points near the top are closer to the free surface and therefore experience greater dynamic pressures. Hence the total vertical force on a spheroid with a larger relative height is greater than that having a small value of c, even though the two have the same horizontal projected area.

It may be noted from the figures that the vertical force coefficient generally increases as the relative depth h decreases. As in the case of f_x, this may be explained in terms of the proximity of the free surface.

We next compare the asymptotic solution (8.4) with diffraction theory for a hemisphere. As in the case of f_x, the two coincide over the whole range of a, for h = 3 and 4. As h is reduced, they begin to diverge, the difference being greatest for h = 1.25. This is to be expected since the asymptotic solution is valid only for large values of h. In general the asymptotic solution gives results that are lower than those from diffraction theory for small values of a, and higher than those from diffraction theory for large values of a. Even for the smaller relative depths, the agreement is quite good for small values of a up to approximately a = 1.0. This is unlike the case for f_x. It may be explained by the fact that there is no added mass coefficient in (8.4).

In the case of small h, for large values of a, the asymptotic solution for f_y differs from diffraction theory by an order of magnitude sometimes, considering that the scales of the plots are logarithmic. In general if figures 13-15 for the horizontal force coefficient are compared with the corresponding figures 20-22 for the vertical force coefficient in the range of large a, it is observed that the difference between the asymptotic solution and the exact theory is larger for the vertical force coefficient. This may be explained by the fact that the major portion of the horizontal force arises due to pressures at the bottom of the hemisphere, whereas the pressures at the top of the hemisphere contribute most of the vertical force. Since the pressures at the top are more strongly influenced by free surface effects, the vertical force coefficient shows more diffraction effects. Thus diffraction effects which are neglected in the asymptotic solution become very important in the case of f_y for large values of a, when the relative depth is small.

A comparison of the experimental results for a hemisphere with the asymptotic solution and diffraction theory in figures 22, 24 and 25 shows that the agreement is not as good as for f_x. The reason is not known. However it is noted that unlike the horizontal force, the vertical force was measured in the experiments by using the readings of the pressure transducer as well as the

strain gages. It is therefore believed that this more complicated arrangement led to greater experimental errors in the case of f_y.

Moment Coefficient, m_z,

The results for the moment coefficient obtained from diffraction theory are shown in figures 26-29. These correspond to relative depths of h = 1.0, 1.25, 1.5, 2.5, 3.0 and 4.0. We note that the moment coefficients for c = 2.0 for the relative depths of h = 2.5, 3.0 and 4.0 are all plotted on the same figure, namely figure 29. As previously indicated, the moment coefficient is zero for a hemisphere (c = 1.0).

In general m_z, follows the same trend with variation of a, as f_x did. Thus it increases at first, reaches a peak and then decreases fairly rapidly. This is not surprising since the horizontal force and the moment about the z'-axis have their maximum values simultaneously, and are both the result of the same pressure distribution on the object. Note also that, for the same c, the peak of the m_z, curve moves to the left as the relative depth h is increased. The same trend was observed for f_x.

If we consider the effect of variation of c, for a given h, it is apparent from the figures that, in the range $c < 1.0$, the moment coefficient decreases as c increases until m_z, is zero for $c = 1.0$. On the other hand, in the range $c > 1.0$, the moment

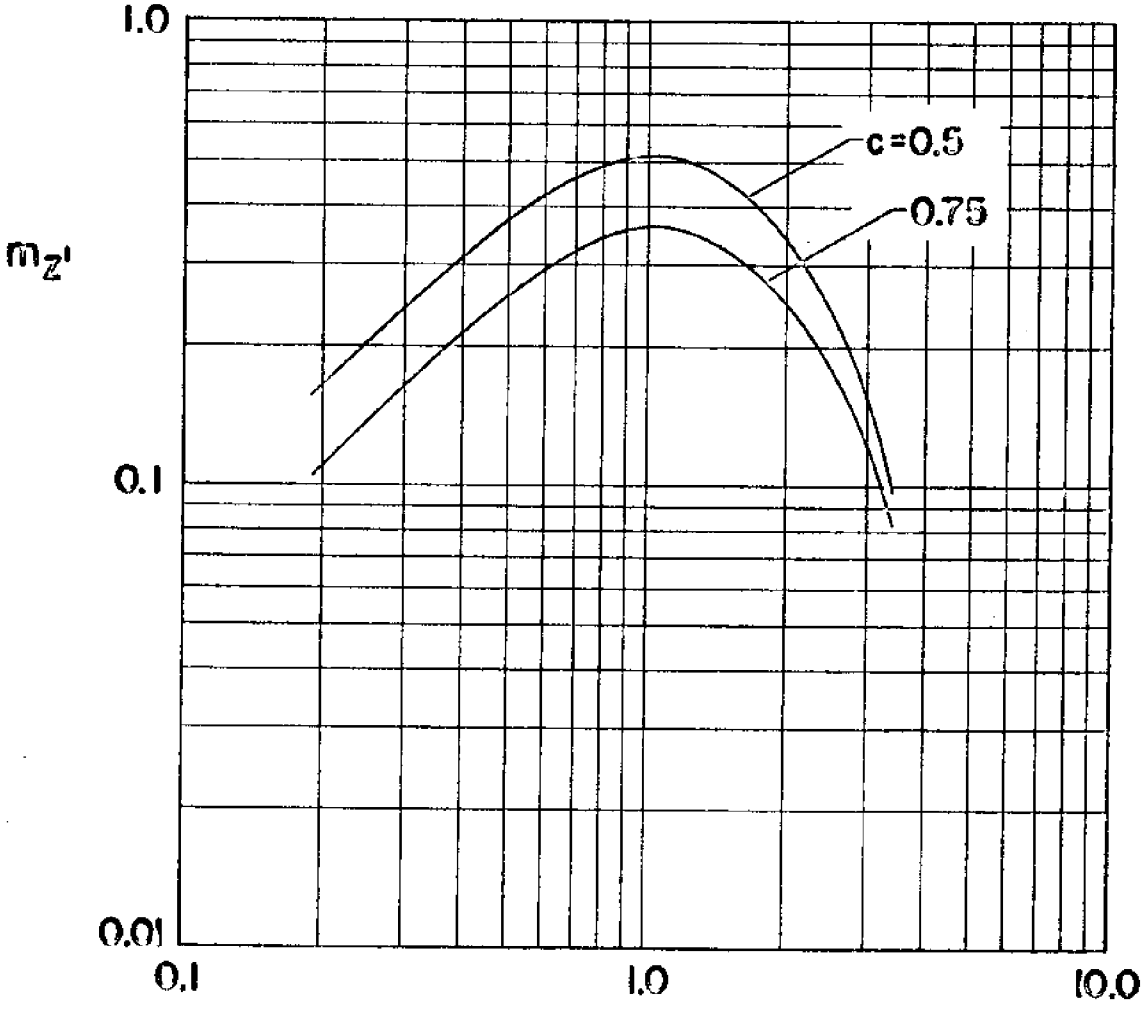

$$a = \frac{2\pi\bar{a}}{L}$$

Figure 26. Moment coefficient for h=1 .

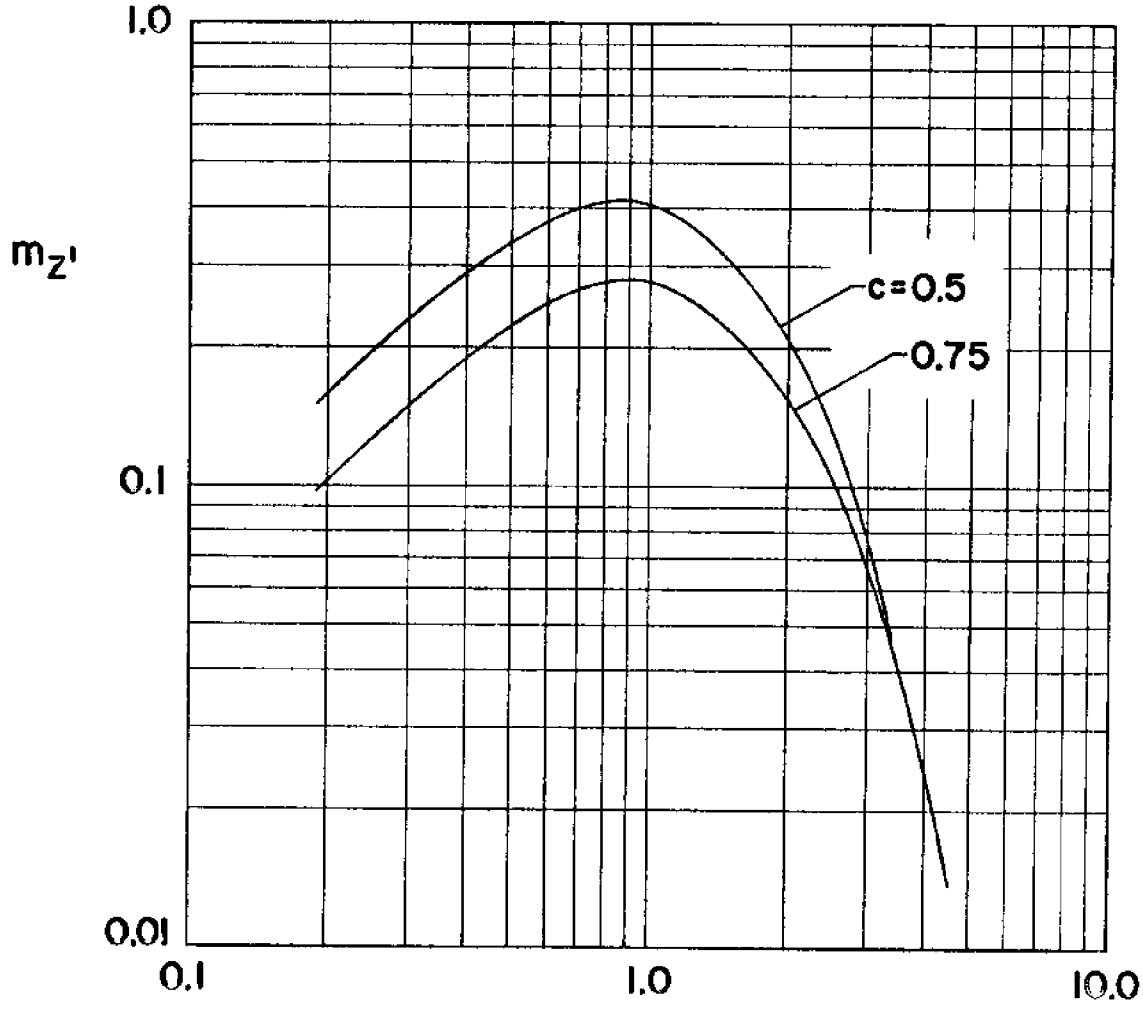

Figure 27. Moment coefficient for h=1.25 .

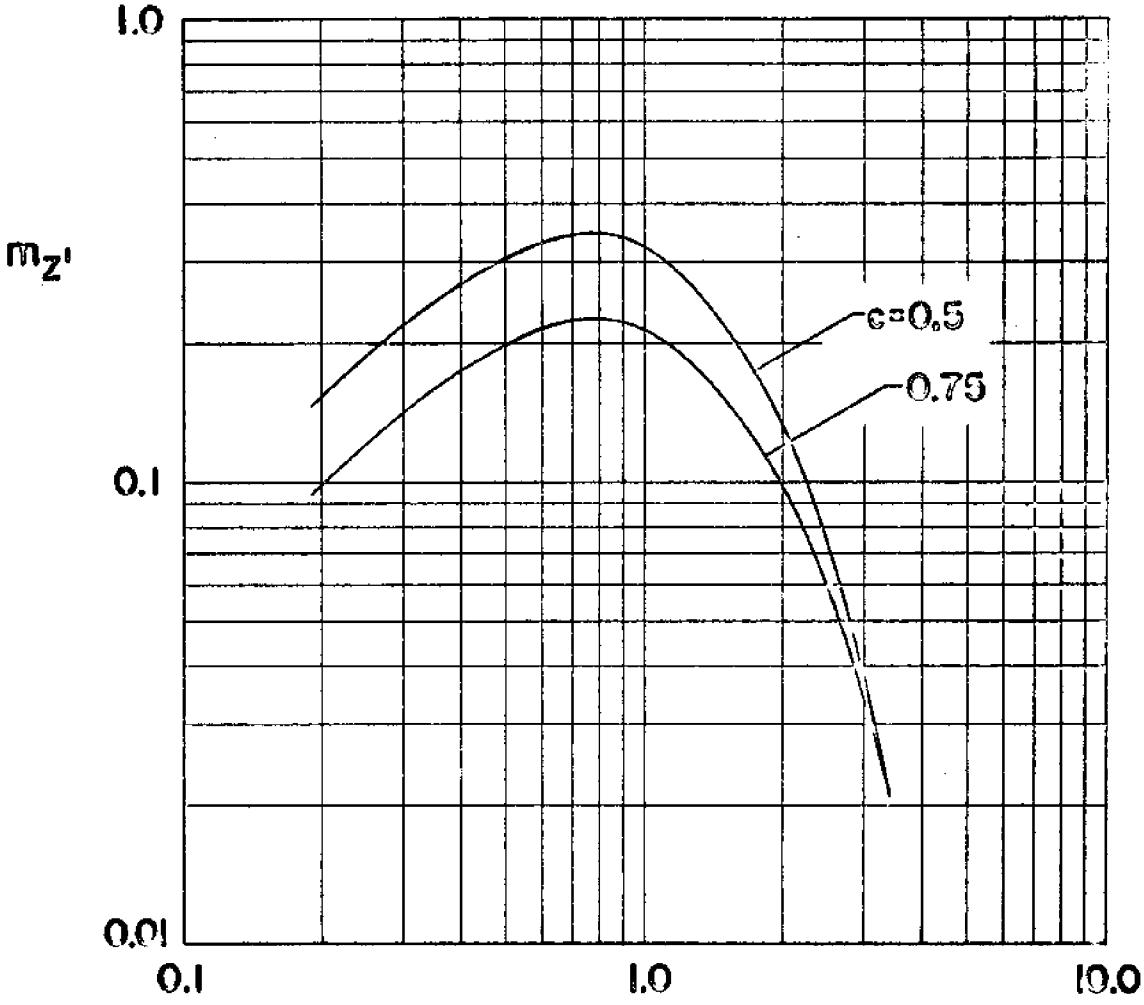

$$a = \frac{2\pi\bar{a}}{L}$$

Figure 20. Moment coefficient for h=1.5 .

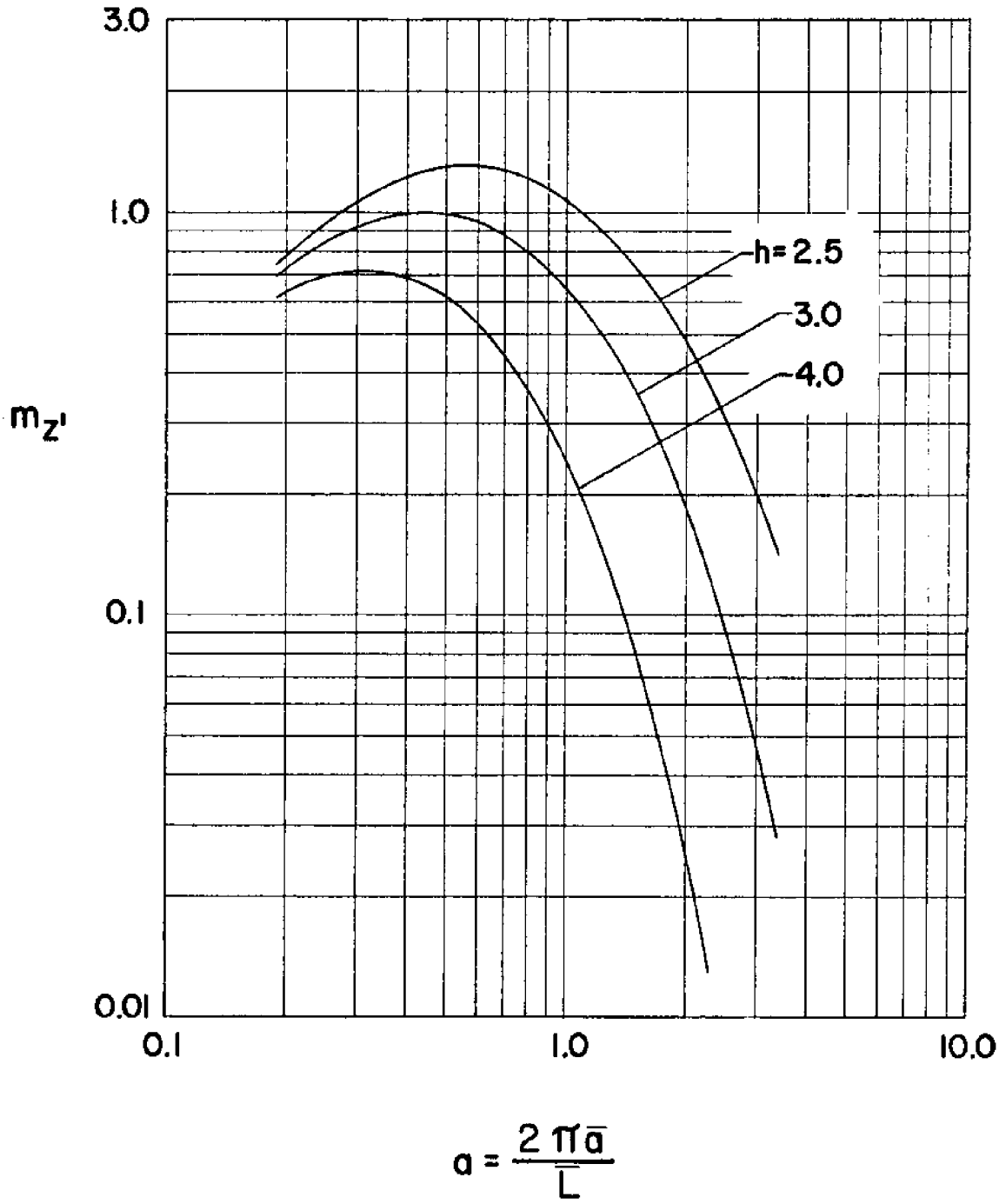

Figure 29. Moment coefficient for c=2.0 .

coefficient increases with c. Such a peculiar trend results partly, if not wholly, due to a factor $|1 - c^2|$ in the expression for $m_{z'}$.

The figures show that the moment coefficient decreases as the relative depth increases. This is again in keeping with the trend observed for f_x and results for the same reasons.

Phase Shifts, δ_x, δ_y and δ_m

We now consider the phase shifts of the horizontal and vertical forces and the moment, obtained from diffraction theory. These results are presented in figures 30-33. The figures show the results for c = 0.5, 0.75, 1.0 and 2.0, respectively. For a given c, the results for various relative depths are shown in the same figure.

It must be noted that in the general case of a spheroid, the phase shift for the horizontal force, δ_x, is exactly identical to that for the moment, δ_m.

For $a \to 0$, the phase shifts δ_x and δ_m tend to the limit $-\pi/2$ and the phase shift δ_y to the limit $-\pi$, which values may be predicted by considering the incident wave alone. This means that the horizontal force and the moment lag the incident wave at the origin by $\pi/2$, and are in phase with the horizontal particle acceleration due to the wave. Similarly the vertical force lags the incident wave at the origin by π and its maximum value occurs when the wave trough is directly above the z'-axis.

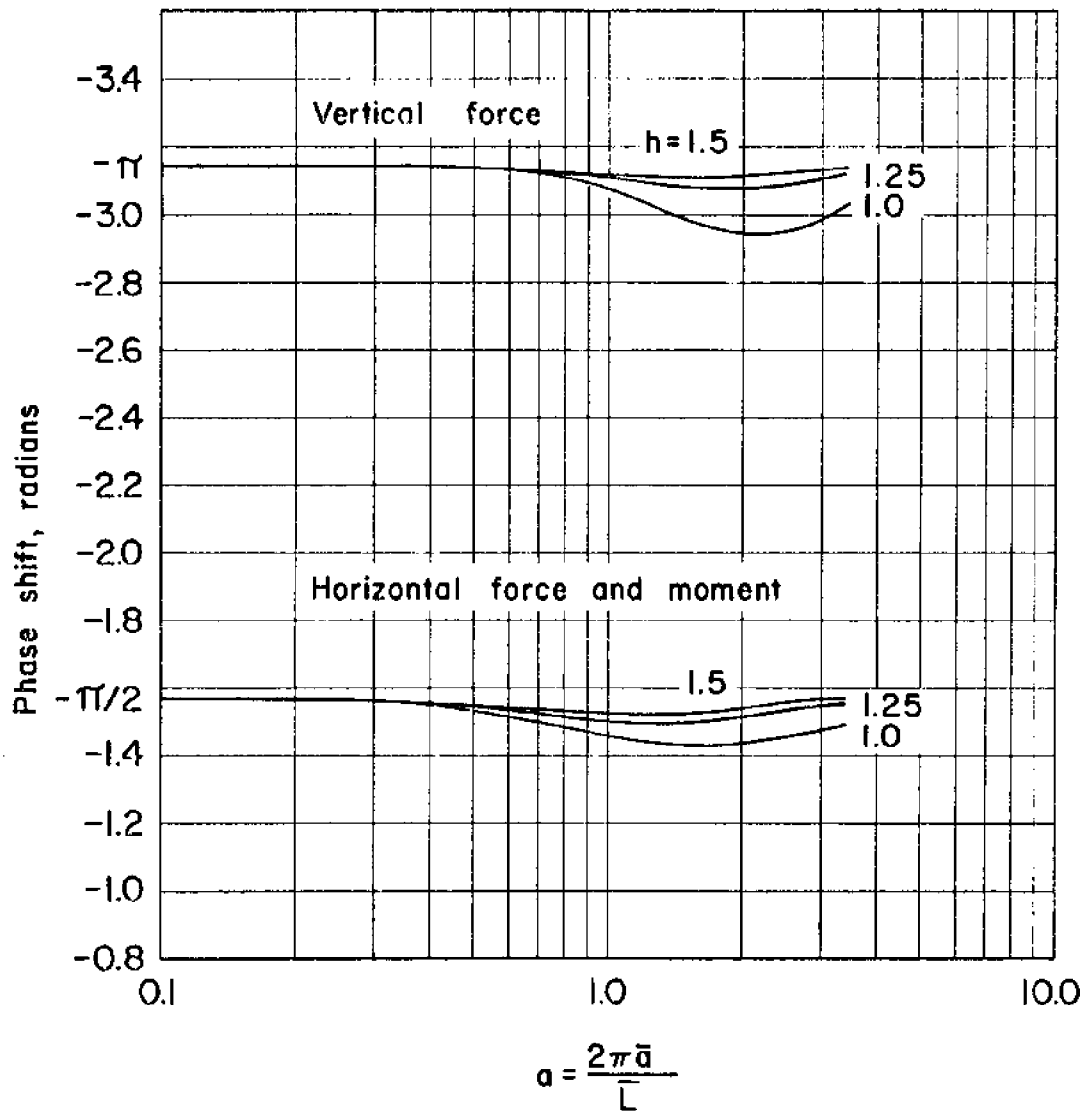

Figure 30. Phase shifts of forces and moment relative to incident wave for c=0.5 .

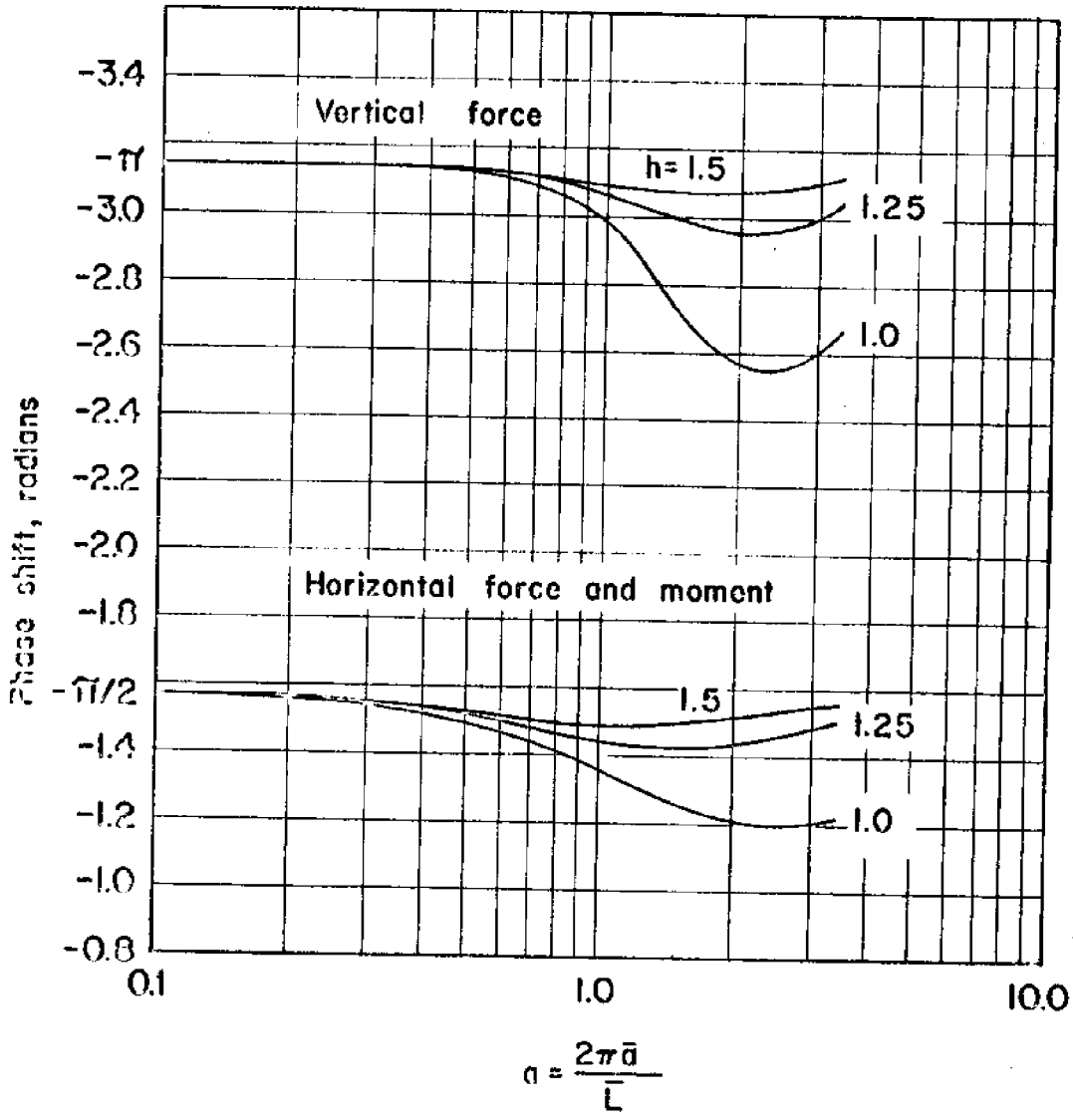

Figure 31. Phase shifts of forces and moment relative to incident wave for c=0.75.

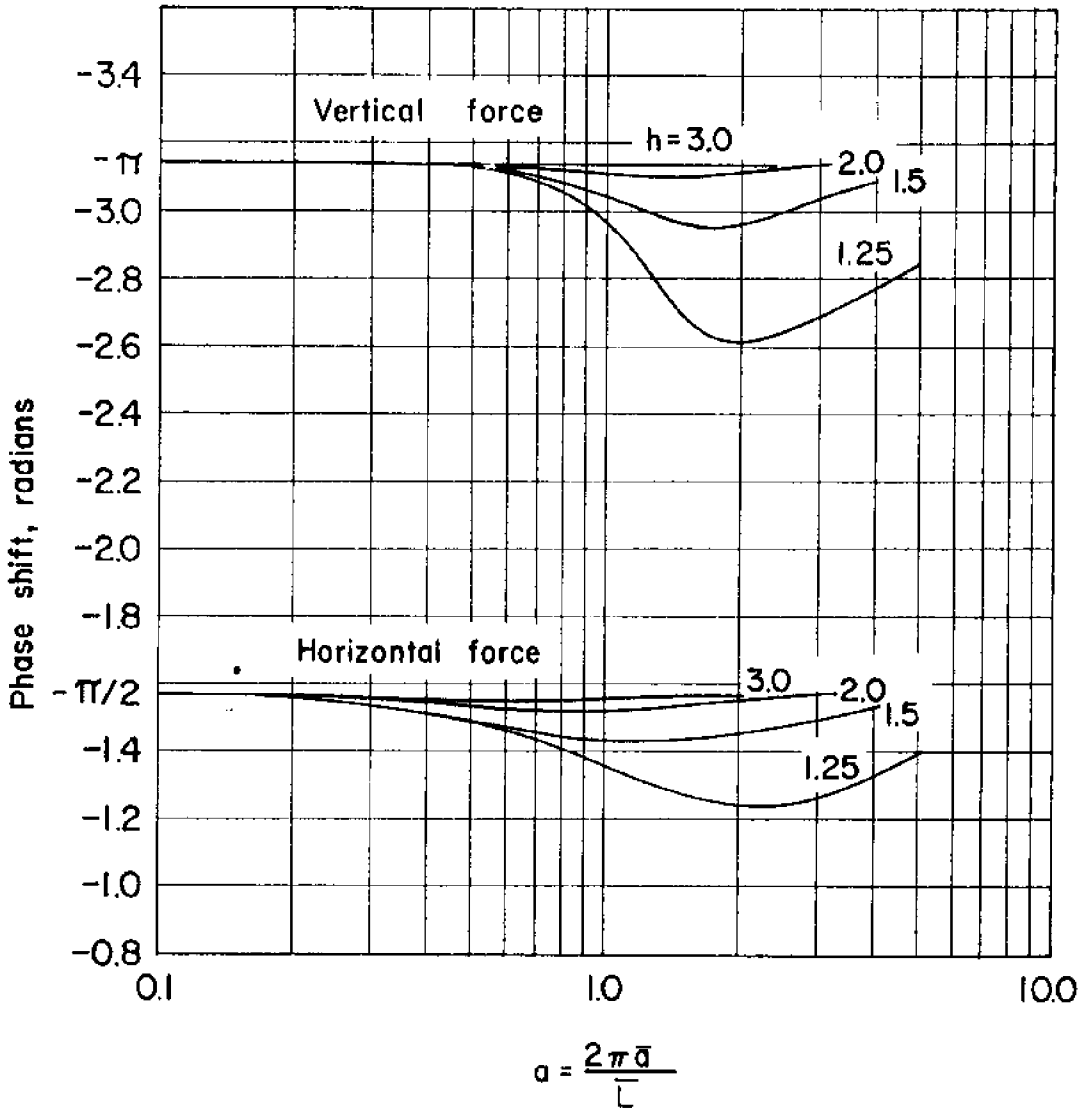

Figure 32. Phase shifts of forces relative to incident wave for c=1.0.

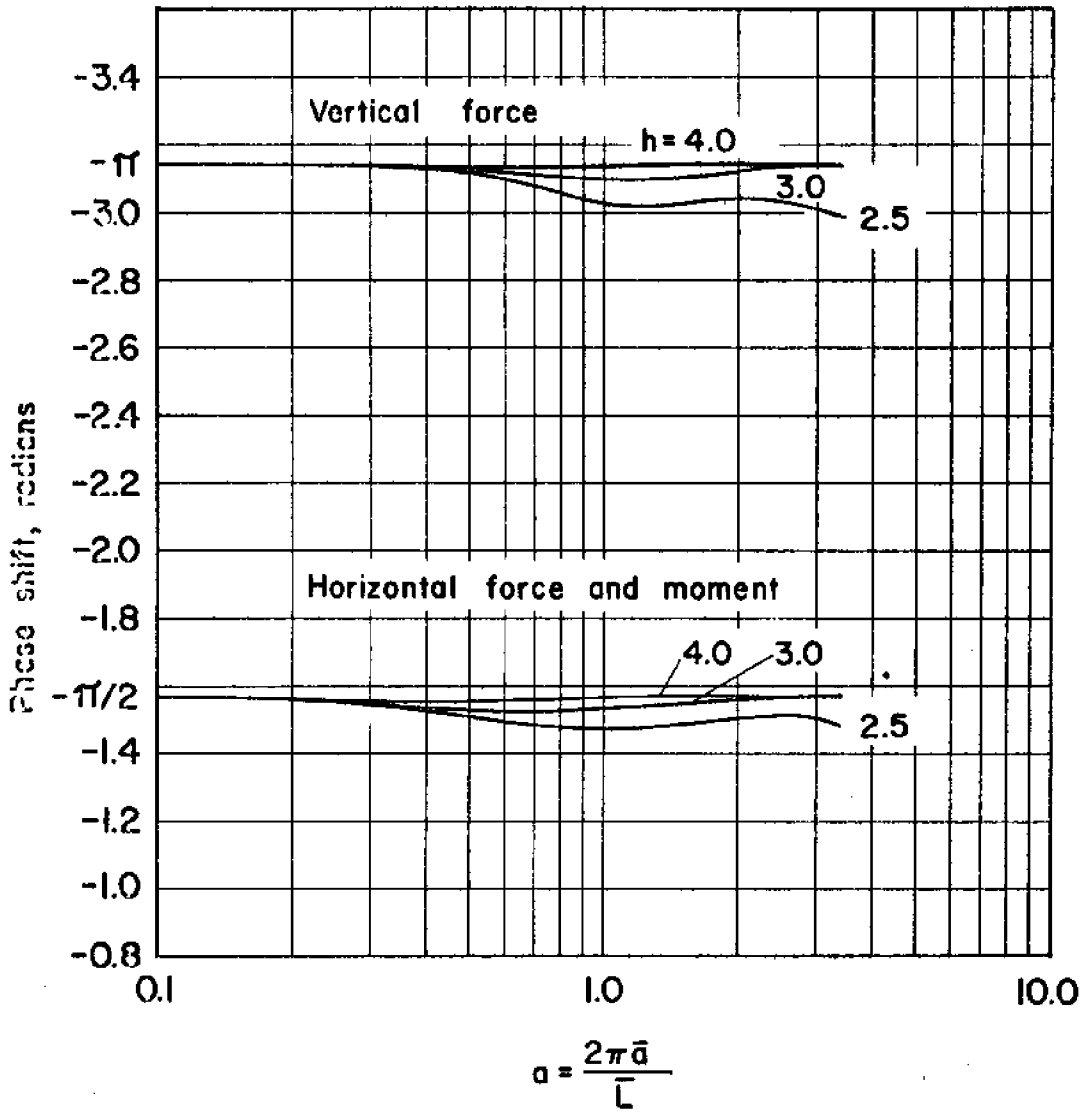

Figure 33. Phase shifts of forces and moment relative to incident wave for c=2.0.

In general the magnitudes of the phase shifts decrease as a increases, up to a point. Thereafter they increase with a, but not indefinitely. They may be expected to fluctuate with a in the range of higher values of a.

The figures show that for a given spheroid, the phase shifts for large relative depths agree closely with the values of $-\pi/2$ and $-\pi$ throughout the range of a considered. Thus in the case of a hemisphere, the curves for δ_x and δ_y are almost horizontal straight lines for h = 3. The results for h = 4 were not presented for this case since they could not be distinguished from the values of $-\pi/2$ and $-\pi$. In general as the relative depth decreases, the deviation of the phase shifts from the asymptotic values increases. It can be seen that it is quite large for h = 1.0 corresponding to c = 0.75, and for h = 1.25 corresponding to c = 1.0. These deviations can be attributed to diffraction effects, and naturally increase as the relative depth h is decreased.

If the phase shift curves for different relative heights, c, are compared for the same h, it is observed that the results for smaller values of c show less diffraction effects. This is to be expected since, for lesser c values, the spheroids are more deeply submerged and therefore less influenced by the free surface.

10. CONCLUSIONS

In this dissertation the diffraction problem which involves the action of small amplitude surface gravity waves on a rigid submerged object in finite depth of water was formulated by using the Green's function approach. Simultaneously, the radiation problem of a submerged object oscillating in otherwise still water was also formulated in order to check the solution for the diffraction problem. The detailed theory and numerical scheme were worked out for a semiellipsoid. Finally, in order to reduce the computation time, numerical results were obtained only for the case of a half spheroid, which was circular in plan.

The numerical results presented in this dissertation were checked in different ways for their validity and accuracy. These checks included the use of Haskind's relations for the diffraction problem, the energy check for the radiation problem and comparison, in the case of a hemisphere, with results from an asymptotic solution, valid for large relative depths and small relative sizes of object. For a hemisphere, comparisons were also made with experimental data obtained in a "two-dimensional" wave channel. All of these checks and comparisons were successful and therefore it appears, on the basis of the limited evidence available, that the present method yields accurate results.

On the basis of the dimensionless results presented in Section 9 and the discussion that followed, the following conclusions appear justified for a half spheroid:

Horizontal Force Coefficient, f_x

1. The horizontal force coefficient increases with the relative size, a, at first, reaches a peak and later decreases rapidly as a increases.
2. It increases with the relative height of the spheroid, c.
3. It increases as the relative depth of water, h, is decreased.
4. The asymptotic solution (8.5) coincides with diffraction theory over the entire range of a tested for large relative depths. Even in the case of smaller relative depths, the agreement can be improved for small relative sizes, a, by increasing the added mass coefficient, C_m, suitably to account for the effect due to the free surface.
5. The experimental results available for comparison agree excellently with diffraction theory.

Vertical Force Coefficient, f_y

1. The vertical force coefficient starts with a value of π corresponding to zero relative size and decreases at first slowly and later rapidly, as a is increased.
2. It increases with the relative height, c, of the spheroid.

3. It increases with a decrease in the relative depth, h.
4. The asymptotic solution (8.4) for a hemisphere coincides with diffraction theory over the entire range of the relative size tested, for large relative depths. Even for small relative depths, the agreement is quite good for small values of a up to about 1.0 approximately.
5. In general the vertical force coefficient shows more diffraction effects than the horizontal force coefficient.

Moment Coefficient, m_z,

1. The moment coefficient shows the same general trend of variation with relative size, a, as the horizontal force coefficient.
2. It decreases with an increase in the relative height, c, in the range $c < 1$ and increases with c in the range $c > 1$.
3. It increases as the relative depth, h, is decreased.

Phase Shifts, δ_x, δ_y and δ_m

1. The phase shifts for the horizontal force and the moment are exactly equal.
2. For $a \to 0$, the phase shifts δ_x and δ_m approach the asymptotic value of $-\pi/2$ and δ_y approaches $-\pi$.
3. The magnitudes of the phase shifts generally decrease at first as the relative size increases, and later increase with a in the range of relative sizes tested.

4. For large relative depths, the magnitudes of the phase shifts are equal to the asymptotic values of $\pi/2$ and π over the entire range of a, and as the relative depth is decreased, they deviate more and more from these values.
5. For a given relative depth, h, the phase shifts deviate more from the asymptotic values, as the relative height, c, is increased.

Finally it is noted that diffraction effects are quite significant in the range of small relative depths of water and large relative sizes. In this range diffraction theory comes to its own and becomes necessary. Since some of the engineering structures contemplated for the near future will be both relatively large and built in shallow waters, it is recommended that diffraction theory be used in this range inspite of its greater complexity.

Recommendations for Future Research

1. Numerical results may be obtained for the general case of a semiellipsoid, by using the theory presented up to Section 7. In order to do this within reasonable computer time, the form of the Green's function given in (3.19) may be used only when the source (ξ,η,ζ) is close to the point (x,y,z). For other cases, the series form of the Green's function given in (C.26) in Appendix C may be employed, since it converges more rapidly and takes less computer time.

2. The work reported here may be extended to the two-dimensional case of semielliptic cylinders resting in finite depth of water and acted on by waves.

REFERENCES

Barakat, R. 1962 Vertical motion of a floating sphere in a sine-wave sea. J. Fluid Mech. 13, 540-56.

Beckmann, H. & Thibodeaux, M. H. 1962 Wave force coefficients for offshore pipelines, Proc. ASCE, J. Waterways and Harbors Div. 88, 125-38.

Dean, R. G. & Ursell, F. 1959 Interaction of a fixed semi-immersed circular cylinder with a train of surface waves. Tech. Rep. no. 37, Hydrody. Lab., M.I.T.

Garrison, C. J. 1969 On the interaction of an infinite shallow draft cylinder oscillating at the free surface with a train of oblique waves. J. Fluid Mech. 39, 227-55.

Garrison, C. J. & Snider, R. H. 1970 Wave forces on large submerged tanks. Sea Grant Publ. no. 210. Texas A&M Univ.

Garrison, C. J., Seetharama Rao, V. & Snider, R. H. 1970 Wave interaction with large submerged objects. Proc. Second Offshore Technology Conf., Houston. Paper no. OTC 1278.

Garrison, C. J. & Seetharama Rao, V. 1971 Interaction of waves with submerged objects. Proc. ASCE, J. Waterways, Harbors and Coastal Engrg. Div. (accepted for publication in May issue).

Grace, R. A. & Casciano, F. M. 1969 Ocean wave forces on subsurface sphere. Proc. ASCE, J. Waterways and Harbors Div. 95, 291-317.

Havelock, T. 1955 Waves due to a floating sphere making periodic heaving oscillations. Proc. Roy. Soc. A, 231, 1-7.

John, F. 1949 On the motion of floating bodies. I. Comm. Pure Appl. Math. 2, 13-57.

John, F. 1950 On the motion of floating bodies. II. Comm. Pure Appl. Math. 3, 45-101.

Kim, W. D. 1964a On oscillating ships in waves. Tech. Memorandum, no. 25. Flight Sciences Lab., Boeing Sci. Res. Lab.

Kim, W. D. 1964b On the harmonic oscillation of a rigid body on a free surface. Tech. Rep., no. 91. Flight Sciences Lab., Boeing Sci. Res. Lab.

Kim, W. D. 1965 On the harmonic oscillations of a rigid body on a free surface. J. Fluid Mech. 21, 427-51.

Landweber, L. & Macagno, M. 1960 Added mass of a rigid prolate spheroid oscillating horizontally in a free surface. J. Ship Res. 3, 30-36.

Macagno, E. O. & Landweber, L. 1958 Irrotational motion of the liquid surrounding a vibrating ellipsoid of revolution, J. Ship Res. 2, 37-49.

MacCamy, R. C. & Fuchs, R. A. 1954 Wave forces on piles: a diffraction theory. Tech. Memorandum, no. 69, Beach Erosion Board.

Monacella, V. J. 1966 The disturbance due to a slender ship oscillating in waves in a fluid of finite depth. J. Ship Res. 10, no. 4, 242-52.

Morison, J. R., et al. 1950 The force exerted by surface waves on piles. Petroleum Trans., AIME, 189, 149-54.

Newman, J. N. 1962 The exciting forces on fixed bodies in waves. J. Ship Res. 6, 10-17.

Porter, W. R. 1960 Pressure distribution, added-mass and damping coefficients for cylinders oscillating in a free surface. Tech. Rep., series 82, issue 16, Inst. Engr. Res., Univ. California, Berkeley.

Sarpkaya, T. & Garrison, C. J. 1963 Vortex formation and resistance in unsteady flow. Trans. ASME, J. Appl. Mech. 30, 16-24.

Stoker, J. J. 1957 Water Waves. Interscience Publishers, New York.

Ursell, F. 1949a On the heaving motion of a circular cylinder on the surface of a fluid. Quart. J. Mech. Appl. Math. 2, 218-31.

Ursell, F. 1949b On the rolling motion of cylinders in the surface of a fluid. Quart. J. Mech. Appl. Math. 2, 335-53.

Wehausen, J. V. & Laitone, E. V. 1960 Surface waves. Encycl. Phys. 9, 446-778.

Yu, Y. S. & Ursell, F. 1961 Surface waves generated by an oscillating circular cylinder on water of finite depth: theory and experiment. J. Fluid Mech. 11, 529-51.

APPENDIX A

DERIVATION OF THE FUNCTIONS, $\bar{h}_j(\bar{x},\bar{y},\bar{z})$

In this section the functions $\bar{h}_j$ used in connection with the kinematic condition on the surface of the oscillating object are derived.

Consider the linear motion of the rigid object in surge. From (2.2-a), for j=1, the velocity of the surface normal to itself is given by

$$\hat{i}\,\dot{\bar{X}}_1 \cdot \hat{n} = Re\,[-i\sigma\,\bar{X}_1^o\,n_x\,e^{-i\sigma t}]\ . \tag{A.1}$$

Application of the kinematic boundary condition on the surface S gives

$$\frac{\partial \Phi_1}{\partial \bar{n}} = Re\,[-i\sigma\,\bar{X}_1^o\,n_x\,e^{-i\sigma t}]\ . \tag{A.2}$$

Substituting for Φ_1 from (2.3) and simplifying yields

$$\frac{\partial V_1}{\partial \bar{n}}(\bar{x},\bar{y},\bar{z}) = -\,i\sigma\,\bar{X}_1^o\,n_x \tag{A.3}$$

or

$$\bar{h}_1(\bar{x},\bar{y},\bar{z}) = -\,i\sigma\,\bar{X}_1^o\,n_x \text{ on } S\ . \tag{A.4}$$

The functions $\bar{h}_2$ and $\bar{h}_3$ can be derived similarly.

Consider next the angular motion of the object in roll. From (2.2-b), for j=4, the velocity of the surface is given by

$$\hat{i}' \dot{\theta}_4 \times \vec{\bar{r}} = \hat{i}' [Re(-i\sigma\theta_4^o e^{-i\sigma t})] \times [\hat{i}'\bar{x}' + \hat{j}'\bar{y}' + \hat{k}'\bar{z}']$$

$$= [Re(-i\sigma\theta_4^o e^{-i\sigma t})] [-\hat{j}'\bar{z}' + \hat{k}'\bar{y}'] . \qquad (A.5)$$

The velocity of the surface normal to itself is hence given by

$$(\hat{i}' \dot{\theta}_4 \times \vec{\bar{r}}) \cdot \hat{n} = [Re(-i\sigma\theta_4^o e^{-i\sigma t})] [\bar{y}'n_z - \bar{z}'n_y] . \qquad (A.6)$$

Noting that $\bar{y}' = \bar{y}+\bar{h}$ and $\bar{z}' = \bar{z}$, and applying the kinematic boundary condition on S, we have

$$\frac{\partial \Phi_4}{\partial \bar{n}} = [Re(-i\sigma\theta_4^o e^{-i\sigma t}) \{(\bar{y}+\bar{h}) n_z - \bar{z} n_y\}] . \qquad (A.7)$$

Substituting for Φ_4 from (2.3) and simplifying gives

$$\frac{\partial V_4}{\partial \bar{n}}(\bar{x},\bar{y},\bar{z}) = - i\sigma\theta_4^o [(\bar{y}+\bar{h}) n_z - \bar{z} n_y] \qquad (A.8)$$

or

$$\bar{h}_4(\bar{x},\bar{y},\bar{z}) = - i\sigma\theta_4^o [(\bar{y}+\bar{h}) n_z - \bar{z} n_y] . \qquad (A.9)$$

The functions $\bar{h}_5$ and $\bar{h}_6$ are similarly obtained.

APPENDIX B

EFFECT OF THE SINGULARITY

In this appendix, it is shown that the extra term $-f_j(x,y,z)/2$ in (3.26) arises at a point (x,y,z) on the surface because of the singularity located there.

In view of the representation (3.17), at any point (x,y,z) on the surface S

$$\frac{\partial u_j}{\partial n}(x,y,z) = \frac{\partial}{\partial n}\left[\frac{1}{4\pi} \int\int_S f_j(\xi,\eta,\zeta)\ G(x,y,z;\xi,\eta,\zeta)\ dS \right]. \qquad (B.1)$$

However as the point (ξ,η,ζ) approaches (x,y,z), the normal derivative of the Green's function becomes singular because of the $1/R$ term so that the region of the surface S surrounding the point (x,y,z) must be treated in a special way. Therefore, for carrying out the surface integration in (B.1) the surface S is divided into two parts. One of these is a small area Σ, which is bounded by the intersection of S and the surface of an imaginary circular cylinder of radius r_0, the cylinder's axis being normal to S at (x,y,z). The area Σ is shown in figure 34. The second part is given by the remainder of the surface S. Therefore (B.1) may be rewritten as

$$\frac{\partial u_j}{\partial n}(x,y,z) = \frac{1}{4\pi} \int\int_{\Sigma} f_j(\xi,\eta,\zeta) \frac{\partial}{\partial n} G(x,y,z;\xi,\eta,\zeta)\ dS$$

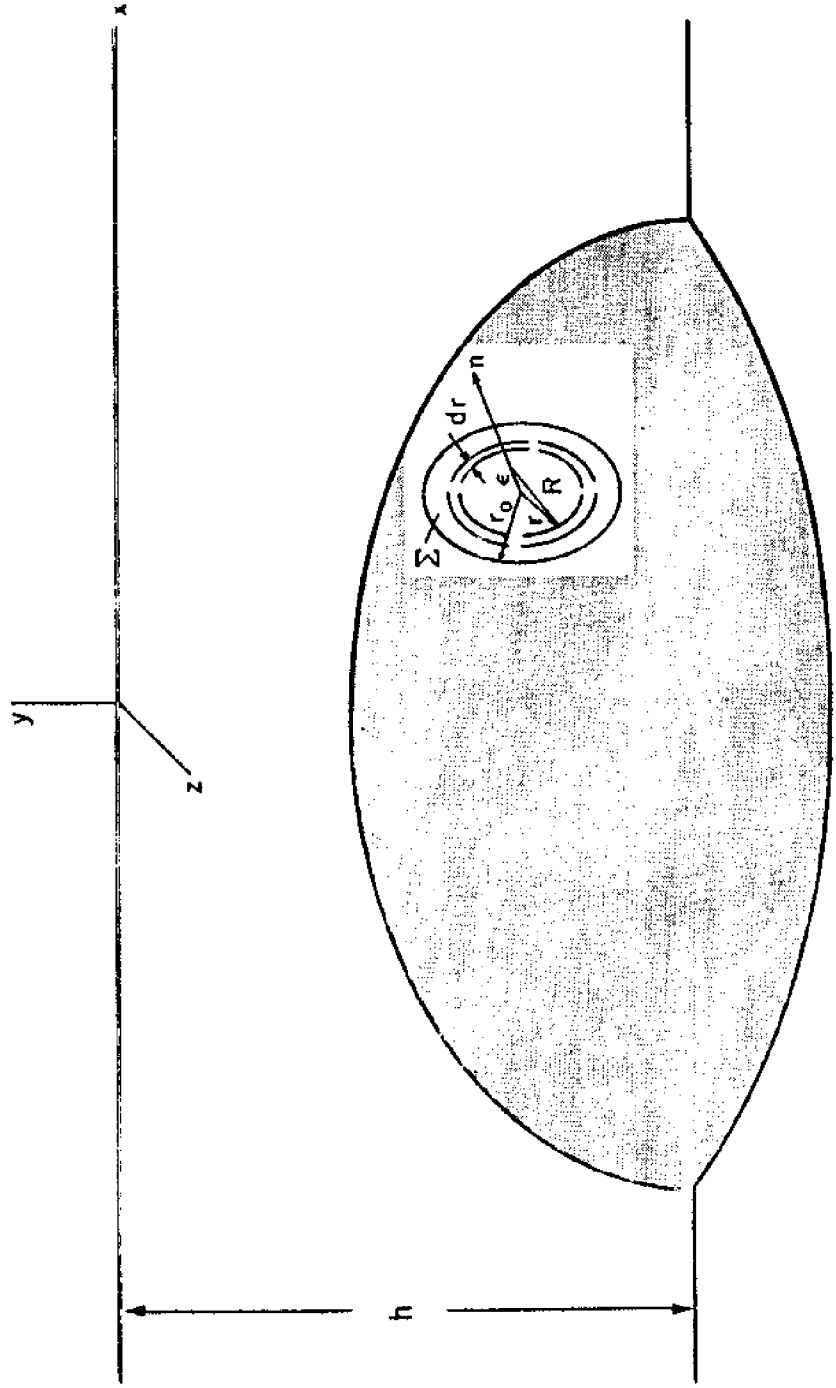

Figure 34. Determination of $\partial u/\partial n$.

$$+ \frac{1}{4\pi} \int\int_{S-\Sigma} f_j(\xi,\eta,\zeta) \frac{\partial}{\partial n} G(x,y,z;\xi,\eta,\zeta)\, dS \ . \qquad (B.2)$$

Writing G in the form given in (3.24) and noting that $f(\xi,\eta,\zeta)$ is a well-behaved function, we may take the limiting condition as Σ, or equivalently r_0, tends to zero to obtain

$$\frac{\partial u_j}{\partial n}(x,y,z) = \lim_{\Sigma\to 0} \frac{f_j(x,y,z)}{4\pi} \int\int_{\Sigma} \frac{\partial}{\partial n} \left(\frac{1}{R}\right) dS$$

$$+ \lim_{\Sigma\to 0} \frac{f_j(x,y,z)}{4\pi} \int\int_{\Sigma} \frac{\partial}{\partial n} G^*(x,y,z;\xi,\eta,\zeta)\, dS$$

$$+ \lim_{\Sigma\to 0} \frac{1}{4\pi} \int\int_{S-\Sigma} f_j(\xi,\eta,\zeta) \frac{\partial G}{\partial n}(x,y,z;\xi,\eta,\zeta)\, dS \ . \qquad (B.3)$$

Assuming the point (x,y,z) lies along the normal at an infinitesimal distance ε from the surface S as indicated in figure 34, and noting that for small r_0 the surface area Σ may be considered to be plane, the first integral in (B.3) can be written as

$$\lim_{\Sigma\to 0} \frac{f_j(x,y,z)}{4\pi} \int\int_{\Sigma} \frac{\partial}{\partial n} \left(\frac{1}{R}\right) dS$$

$$= \lim_{\substack{r_0\to 0 \\ \varepsilon\to 0}} \frac{f_j(x,y,z)}{4\pi} \frac{\partial}{\partial \varepsilon} \int_0^{r_0} \frac{2\pi r}{(r^2+\varepsilon^2)^{1/2}}\, dr$$

$$= \lim_{\substack{r_0 \to 0 \\ \varepsilon \to 0}} \frac{f_j(x,y,z)}{2} \frac{\partial}{\partial \varepsilon} \left[(r_0^2 + \varepsilon^2)^{1/2} - \varepsilon \right]$$

$$= \lim_{\substack{r_0 \to 0 \\ \varepsilon \to 0}} \frac{f_j(x,y,z)}{2} \left[\frac{\varepsilon}{(r_0^2 + \varepsilon^2)^{1/2}} - 1 \right]$$

$$= - \frac{f_j(x,y,z)}{2} \quad . \tag{B.4}$$

Further since $\partial G^*/\partial n$ occurring in the second integral of (B.3) is regular, that integral vanishes in the limit as $\Sigma \to 0$, giving the desired result

$$\frac{\partial u_j}{\partial n}(x,y,z) = - \frac{f_j(x,y,z)}{2} + \frac{1}{4\pi} \iint_S f_j(\xi,\eta,\zeta) \frac{\partial G}{\partial n}(x,y,z;\xi,\eta,\zeta) \, dS \, . \tag{3.26}$$

Note that in (3.26) the surface integration is to be carried out over the surface of the object with the singularity (x,y,z) excluded.

APPENDIX C

HASKIND'S RELATIONS AND ENERGY CHECK

Haskind's Relations

In the case of the diffraction problem, the dimensionless wave force and moment components, $F_i'(t)$, on an object of arbitrary shape are given by (4.18). Substituting for the functions $h_i(x,y,z)$ from (2.25-D), equation (4.18) may be rewritten as

$$F_i'(t) = Re\left[a \iint_S (u_7+u_0) \frac{\partial u_i}{\partial n} dS \; e^{-i\sigma t} \right] , \; i=1,2,3,\ldots,6, \tag{C.1}$$

where u_i are the radiation potentials.

We now eliminate the scatter potential u_7 from (C.1) by applying Green's theorem to the functions u_7 and u_i in the region R, as shown in figure 3 in Section 3. Since both u_7 and u_i satisfy the Laplace equation in the region R,

$$\iint_{S+S_f+S_b+S_\infty} (u_i \frac{\partial u_7}{\partial n} - u_7 \frac{\partial u_i}{\partial n}) \; dS = 0 . \tag{C.2}$$

Also since both u_7 and u_i satisfy the free surface and bottom boundary conditions, and the radiation condition at infinity, it can be shown as in Section 3 that the contributions to the surface integral in (C.2) from the surfaces S_f, S_b and S_∞ vanish. Further, from (2.25-D) and (4.4)

$$\frac{\partial u_7}{\partial n} = - \frac{\partial u_0}{\partial n} \quad \text{on } S. \tag{C.3}$$

Hence equation (C.2) yields the result

$$\int\int_S u_7 \frac{\partial u_i}{\partial n} \, dS = - \int\int_S u_i \frac{\partial u_0}{\partial n} \, dS \tag{C.4}$$

which may be rewritten as

$$\int\int_S (u_7+u_0) \frac{\partial u_i}{\partial n} \, dS = \int\int_S (u_0 \frac{\partial u_i}{\partial n} - u_i \frac{\partial u_0}{\partial n}) \, dS \, . \tag{C.5}$$

We next replace the surface integral on the right hand side of (C.5) by an integral on S_∞, by applying Green's theorem to u_0 and u_i in the region R. Since both u_0 and u_i satisfy the Laplace equation and the free surface and bottom boundary conditions,

$$\int\int_{S+S_\infty} (u_0 \frac{\partial u_i}{\partial n} - u_i \frac{\partial u_0}{\partial n}) \, dS = 0 \, . \tag{C.6}$$

Hence

$$\int\int_S (u_0 \frac{\partial u_i}{\partial n} - u_i \frac{\partial u_0}{\partial n}) \, dS = - \int\int_{S_\infty} (u_0 \frac{\partial u_i}{\partial n} - u_i \frac{\partial u_0}{\partial n}) \, dS. \tag{C.7}$$

Since by convention n is the direction of the normal to a surface drawn into the fluid, $\partial/\partial n = -\partial/\partial r$ on S_∞. Moreover, using the radiation condition (2.25-E) for u_i, we can show that

$$\frac{\partial u_i}{\partial r} = ia\, u_i - \frac{1}{2}\frac{u_i}{r} \quad \text{on } S_\infty . \tag{C.8}$$

Since $x = r\cos\theta$, it can be shown from the expression for u_0 given in (4.4) that

$$\frac{\partial u_0}{\partial r} = ia\, u_0 \cos\theta . \tag{C.9}$$

Therefore

$$\int\int_{S_\infty} \left(u_0 \frac{\partial u_i}{\partial n} - u_i \frac{\partial u_0}{\partial n}\right) dS = - \int\int_{S_\infty} u_0 u_i \left[ia(1-\cos\theta) - \frac{1}{2r}\right] dS . \tag{C.10}$$

Substituting for u_0 and u_i on the right hand side of (C.10)

$$\int\int_{S_\infty} \left(u_0 \frac{\partial u_i}{\partial n} - u_i \frac{\partial u_0}{\partial n}\right) dS = - \int_{y=-h}^{0}\int_{\theta=0}^{2\pi} \frac{A_i(\theta)}{a} \frac{\cosh^2 a(h+y)}{\cosh^2 ah}$$

$$r^{-1/2}\, e^{iar(1+\cos\theta)} \left[\frac{1}{2r} - ia(1-\cos\theta)\right]$$

$$r\, d\theta\, dy$$

$$= - \frac{1}{a\cosh^2 ah} \left[\frac{\sinh 2ah}{4a} + \frac{h}{2}\right] e^{iar}$$

$$\int_{\theta=0}^{2\pi} A_i(\theta)\, r^{-1/2} \left[\frac{1}{2} - iar(1-\cos\theta)\right]$$

$$e^{iar\cos\theta}\, d\theta . \tag{C.11}$$

Since $r \to \infty$ and $e^{iar \cos \theta}$ is a fluctuating quantity,

$$\int_{\theta=0}^{2\pi} \frac{A_i(\theta)}{2} r^{-1/2} e^{iar \cos \theta} d\theta = 0 \text{ on } S_\infty . \qquad (C.12)$$

We next rewrite the remaining part of the original integral as

$$-\int_{\theta=0}^{2\pi} A_i(\theta) \, iar^{1/2} (1-\cos \theta) e^{iar \cos \theta} d\theta$$

$$= - iar^{1/2} e^{iar} \int_{\theta=0}^{2\pi} A_i(\theta) (1-\cos \theta) e^{-iar(1-\cos \theta)} d\theta . \qquad (C.13)$$

Since $ar >> 1$, the solution to the integral on the right hand side of (C.13) may be obtained by the method of stationary phase (refer, for example, Stoker (1957), Sec. 6.5 and 6.8). Thus

$$\int_{\substack{\theta=0 \\ ar \to \infty}}^{2\pi} A_i(\theta) (1-\cos \theta) e^{-iar(1-\cos \theta)} d\theta$$

$$= \left(\frac{2\pi}{ar}\right)^{1/2} \left\{ e^{-\pi i/4} [A_i(\theta) (1-\cos \theta)] \Big|_{\theta=0} \right.$$

$$\left. + e^{i(\frac{\pi}{4} - 2ar)} [A_i(\theta) (1-\cos \theta)] \Big|_{\theta=0} \right\}$$

$$= 2\left(\frac{2\pi}{ar}\right)^{1/2} e^{i(\frac{\pi}{4} - 2 ar)} A_i(\pi) . \qquad (C.14)$$

Hence, after some simplification, we can show that

$$\iint_{S_\infty} \left(u_0 \frac{\partial u_i}{\partial n} - u_i \frac{\partial u_0}{\partial n}\right) dS = i\left(\frac{2\pi}{a}\right)^{1/2} \frac{1}{\cosh^2 ah}$$

$$\left[\frac{\sinh 2ah}{2a} + h\right] e^{i\pi/4} \; A_i(\pi) \; . \qquad \text{(C.15)}$$

From (C.1), (C.5), (C.7) and (C.15), simplifying, we have

$$F_i'(t) = Re\left[- \frac{i(2\pi a)^{1/2}}{\cosh^2 ah} \left[\frac{\sinh 2ah}{2a} + h\right] e^{i\left(\frac{\pi}{4} - \sigma t\right)} \; A_i(\pi) \right] . \qquad \text{(C.16)}$$

Taking the modulus on both sides gives the desired result

$$f_i' = \frac{(2\pi a)^{1/2}}{\cosh^2 ah} \left[\frac{\sinh 2ah}{2a} + h\right] \left|A_i(\pi)\right| \; , \; i=1,2,3,\ldots,6 \; . \qquad \text{(C.17)}$$

Equation (C.17) really represents six different equations, corresponding to the different values of the index i. These equations are known as "Haskind's relations." They relate the force and moment components in the case of the diffraction problem to the asymptotic velocity potentials for the corresponding radiation problem. They are very valuable because the asymptotic potentials mentioned are much easier to obtain than the "near field" scatter potential.

Energy Check

In the case of the radiation problem, the dimensional force (or moment) component, in the i-th direction, on the oscillating object due to oscillations in the i-th mode may be obtained from (4.12) by

setting j=i. The forces and moments exerted by the body on the fluid are equal and opposite to these components so that the energy, E_i, transmitted by the body to the surrounding fluid over one period is given by

$$E_i = - \int_{t=0}^{T} (\bar{a} \text{ or } 1)\, F_{ii}(t)\, \dot{X}_i(t)\, dt \qquad (C.18)$$

where $X_i(t) = \ddot{X}_i(t)/\bar{a}$ for i=1,2,3 and $X_i(t) = \theta_i(t)$ for i=4,5,6. In (C.18) the coefficient $\bar{a}$ is to be used for a force (i=1,2,3) and the factor 1 for a moment (i=4,5,6). On substituting for $F_{ii}(t)$ from (4.12), for the damping coefficient $\bar{N}_{ii}$ from (4.15) and (4.16), and for $X_i(t)$ from (2.2), and simplifying and carrying out the integration, equation (C.18) may be rewritten as

$$E_i = \pi\rho\sigma^2\, \bar{a}^5\, X_i^{o2}\, N_{ii} \quad i=1,2,3,\ldots,6 \; . \qquad (C.19)$$

If we consider the fluid region R shown in figure 3, then by conservation of energy, since the energy in the interior of the region does not change, the above input of energy must be equal to the energy flux across the surface S_∞ over one period due to outgoing progressive waves.

If $\bar{\eta}_i^o$ is the amplitude of the outgoing progressive waves at S_∞ due to the oscillation of the body in the i-th mode, then by applying the dynamic free surface boundary condition, we can relate $\bar{\eta}_i^o$ to the asymptotic velocity potential u_i. Thus

$$\bar{\eta}_i^o(r,\theta) = \bar{a}\, X_i^o \tanh(k\bar{h})\; a\left|u_i(r,\theta,0)\right| \quad . \tag{C.20}$$

The energy, dE_i, transmitted across S_∞ per unit length of crest over one period is given from linear wave theory as

$$dE_i = \frac{\rho g\, \bar{\eta}^{o\,2}}{4}\, \bar{L}\, \left[1 + \frac{2k\bar{h}}{\sinh\, 2k\bar{h}}\right] \quad . \tag{C.21}$$

Therefore the total energy transmitted across S_∞ over one period is given by

$$E_i = \lim_{\bar{r}\to\infty} \frac{\rho g\, \bar{L}}{4}\left[1 + \frac{2k\bar{h}}{\sinh\, 2k\bar{h}}\right] \int_{\theta=0}^{2\pi} \bar{\eta}_i^{o\,2}\, \bar{r}\, d\theta \quad . \tag{C.22}$$

Substituting for $\bar{\eta}_i^o$ from (C.20), and simplifying,

$$E_i = \lim_{\bar{r}\to\infty} \frac{\rho\bar{L}}{4}\left[1 + \frac{2k\bar{h}}{\sinh\, 2k\bar{h}}\right] \frac{\bar{a}^4\, \sigma^4}{g}\, X_i^{o\,2}\, \bar{r}$$

$$\int_{\theta=0}^{2\pi} \left|u_i(r,\theta,0)\right|^2\, d\theta \quad , \quad i=1,2,3,\ldots,6 \quad . \tag{C.23}$$

By comparing (C.19) and (C.23), a relation may be written for the damping coefficients N_{ii} in terms of the asymptotic velocity potentials u_i. Thus, after simplification, we have the relationship

$$N_{ii} = \lim_{r\to\infty} \frac{1}{2}\tanh(ah)\, \left[1 + \frac{2ah}{\sinh\, 2ah}\right] r$$

$$\int_{\theta=0}^{2\pi} \left|u_i(r,\theta,0)\right|^2\, d\theta \quad , \quad i=1,2,3,\ldots,6 \quad . \tag{C.24}$$

Substituting for u_i from the radiation condition (2.25-E), we have the alternate form

$$N_{ii} = \frac{\tanh ah}{2}\left[1 + \frac{2ah}{\sinh 2ah}\right] \int_{\theta=0}^{2\pi} |A_i(\theta)|^2 \, d\theta \ ,$$

$$i=1,2,3,\ldots,6 \ . \qquad \text{(C.25)}$$

Equation (C.24) or (C.25) represents the energy check for the radiation problem. It relates the damping coefficients N_{ii} for the object (which are dependent on the near field characteristics of the problem) to the asymptotic velocity potentials u_i which are dependent on the far field characteristics of the problem.

We note also a certain similarity in the relations (C.17) and (C.25). Thus under certain conditions, it is possible to relate f_i' directly to N_{ii}. Newman (1962) obtained such relations for the case of a submerged spheroid.

Numerical Evaluation of Haskind's Relations and Energy Check for a Half Spheroid

For a spheroid symmetric about the vertical axis, the only cases of interest are those pertaining to i=1,2 and 6.

The left hand sides of (C.17) and (C.24) may be obtained from the numerical solution to the corresponding diffraction and radiation problems by numerical quadrature on the surface of the object, using the relations given in Section 4. As for the right hand

sides, these involve the asymptotic velocity potentials u_i. These potentials are computed numerically from (3.17). For this purpose the distribution functions f_i obtained from the numerical solution of the radiation problem are used. As for the Green's function G, since the form given in (3.19) is quite complicated, it is natural to look for a simpler asymptotic form valid for large r_1. An infinite series form for the Green's function is given by John (1950) and when made dimensionless in our variables appears as follows:

$$G(x,y,z;\xi,\eta,\zeta) = \frac{2\pi(\nu^2-a^2)}{a^2h-\nu^2h+\nu} \cosh[a(y+h)]\ \cosh[a(\eta+h)]$$

$$[Y_0(ar_1) - i\ J_0(ar_1)] + 4\pi \sum_{k=1}^{\infty} \frac{(\mu_k^2+\nu^2)}{\mu_k^2\ h+\nu^2 h-\nu}$$

$$\cos[\mu_k(y+h)]\ \cos[\mu_k(\eta+h)]\ K_0(\mu_k r_1) \qquad \text{(C.26)}$$

where μ_k are the positive real roots of the equation

$$\mu\ \tan(\mu h) + \nu = 0\ ,$$

and Y_0 and K_0 are respectively the Bessel function, and modified Bessel function, of the second kind of order zero.

For $r_1 \to \infty$, considerable simplification is possible in the above expression for G and for y=0, the asymptotic form may be written as

$$G(x,0,z;\xi,\eta,\zeta) \underset{r_1\to\infty}{=} -\frac{2\pi i(\nu^2-a^2)}{a^2h-\nu^2h+\nu}\cosh ah\,\cosh[a(\eta+h)]$$

$$\left(\frac{2}{\pi a r_1}\right)^{1/2} e^{i\left(ar_1-\frac{\pi}{4}\right)} \quad . \tag{C.27}$$

Substituting for G from (C.27), we may write the asymptotic potential u_i as

$$u_i(r,\theta,0) = -\frac{i}{2}\left(\frac{2}{\pi a}\right)^{1/2}\frac{(\nu^2-a^2)\cosh ah}{a^2h-\nu^2h+\nu}$$

$$\int\int_S f_i(\xi,\eta,\zeta)\cosh[a(\eta+h)]\, r_1^{-1/2}\, e^{i\left(ar_1-\frac{\pi}{4}\right)}\, dS \quad . \tag{C.28}$$

Since r_1 is large, it may be replaced by r and taken outside the integral. Moreover, we note from figure 35 that for large r

$$r_1 = r-\rho_1\cos(\beta-\theta) \tag{C.29}$$

where $\rho_1 = (\xi^2+\zeta^2)^{1/2}$ and β has the usual notation.

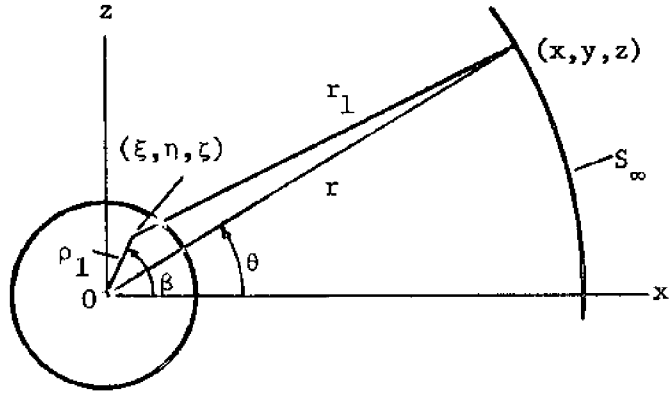

Figure 35. Plan view of the spheroid.

Therefore u_i may be rewritten as

$$u_i(r,\theta,0) = -i(2\pi a)^{-1/2} \frac{(\nu^2-a^2)\cosh ah}{a^2h-\nu^2h+\nu} r^{-1/2} e^{i(ar-\frac{\pi}{4})}$$

$$\int\int_S f_i(\xi,\eta,\zeta) \cosh a(\eta+h) e^{-ia\rho_1 \cos(\beta-\theta)} dS . \qquad (C.30)$$

Once $f_i(\xi,\eta,\zeta)$ is known, $u_i(r,\theta,0)$ is computed for any (r,θ) by numerical integration over the surface, S, of the object, using also the symmetry of the distribution function.

As far as Haskind's relations (C.17) are concerned, we make use of the radiation condition (2.25-E) to obtain $A_i(\pi)$, once $u_i(r,\pi,0)$ is known. Thus

$$A_i(\pi) = u_i(r,\pi,0)\ r^{1/2}\ e^{-iar} . \qquad (C.31)$$

Hence

$$f_i' = \frac{1}{\cosh ah}\left[\frac{\sinh 2ah}{2a} + h\right]\left|\frac{(\nu^2-a^2)}{a^2h-\nu^2h+\nu}\int\int_S f_i(\xi,\eta,\zeta)\right.$$

$$\left.\cosh a(\eta+h)\ e^{-ia\rho_1 \cos(\beta-\pi)}\ dS\right|, \quad i=1,2,6. \qquad (C.32)$$

The energy check (C.24) involves integration from $\theta = 0$ to 2π. In this case, we observe that for a spheroid because of symmetry of the asymptotic velocity potentials u_i, it is necessary to integrate only over one quadrant and multiply the result by a factor of 4. In the case of heave (i=2), it can be shown from physical

considerations that $u_1(r,\theta,0)$ is independent of θ. So it is necessary to evaluate the integrand for only one value of θ, say $\theta=\pi$, and multiply it by 2π to get the integral.